Concentration Polarization, Nanophotonic Flux Enhancement and the Mitigation of Concentration Polarization in Pervaporation Desalination

by

Stewart Mann

A Dissertation Presented in Partial Fulfillment
of the Requirements for the Degree
Doctor of Philosophy

Approved July 2019 by the
Graduate Supervisory Committee:

Mary Laura Lind, Chair
Matthew Green
Shane Walker
Erica Forzani
Heather Emady

ARIZONA STATE UNIVERSITY

August 2019

ABSTRACT

Membrane based technology is one of the principal methods currently in widespread use to address the global water shortage. Pervaporation desalination is a membrane technology for water purification currently under investigation as a method for processing reverse osmosis concentrates or for stand-alone applications. Concentration polarization is a potential problem in any membrane separation. In desalination concentration polarization can lead to reduced water flux, increased propensity for membrane scaling, and decreased quality of the product water. Quantifying concentration polarization is important because reducing concentration polarization requires increased capital and operating costs in the form of feed spacers and high feed flow velocities. The prevalent methods for quantifying concentration polarization are based on the steady state thin film boundary layer theory. Baker's method, previously used for pervaporation volatile organic compound separations but not desalination, was successfully applied to data from five previously published pervaporation desalination studies. Further investigation suggests that Baker's method may not have wide applicability in desalination. Instead, the limitations of the steady state assumption were exposed. Additionally, preliminary results of nanophotonic enhancement of pervaporation membranes were found to produce significant flux enhancement. A novel theory on the mitigation of concentration polarization by the photothermal effect was discussed.

DEDICATION

To my wife Candice, my two sons Matthew and Gabriel, my two grandchildren Milo and Delaney

ACKNOWLEDGMENTS

My dissertation advisor Professor Mary Laura Lind

Members of my dissertation committee: Professor Matthew Green, Professor Shane Walker, Professor Erica Forzani, Professor Heather Emady

Pinar Cay Durgan, Elisabeth Thomas, Huidin Yin, Tianmiao Lai, Afsaneh Khosravi, Anjali Mulchandani, Douglas Rice, Mitch Durbin, Fred Rivers, Fred Pena

TABLE OF CONTENTS

Page

LIST OF TABLES vi

LIST OF FIGURES viii

CHAPTER

1 INTRODUCTION 1

Motivation 1

Review of Processes for RO Concentrate Management 1

Pervaporation Desalination Compared with Membrane Distillation 4

Brief History of Pervaporation and Industrial Applications 6

Transport Models for Pervaporation 8

Comparing Pervaporation Performance 22

Materials for Pervaporation Desalination Membranes 24

2 CONCENTRATION POLARIZATION IN PERVAPORATION DESALINATION 35

Introduction to Concentration Polarization 35

Introduction to Methods for Quantifying Concentration Polarization 38

TFBLT, 3 Methods for Determining C' 42

Baker Method Applied to Data from Previous Studies 61

Concentration Polarization in Membrane Distillation 72

Results and Discussion:Baker Method Applied to Previous Studies 74

Comparison of Baker Method to Sherwood Correlations 75

CHAPTER Page

Factors Affectin C' using Baker Method 79

Evaluation of Experimental Data using Baker Method..... 86

Excel Modeling of Concentration Polarization 99

Conclusions for Chapter 2..... 119

3 NANOPHOTONIC FLUX ENHANCEMENT IN PERVAPORATION DESALINATION 124

Temperature Polarization..... 124

The Nanophotonic Photothermal Effect in MD and Pervaporation 131

Making and Testing Nanophotonic Pervaporation Membranes..... 135

Results of Testing Nanophotonic Pervaporation Membranes..... 137

Conclusions for Chapter 3..... 141

4 THE MITIGATION OF CONCENTRATION POLARIZATION BY THE NANOPHOTONIC PHOTOTHERMAL EFFECT AND CONCLUSIONS.. 142

REFERENCES 149

LIST OF TABLES

Table		Page
1.	Pervaporation Performance Of Membrane	31
2.	Summary Of Semiquantitative Analysis	49
3.	Membrane Permeance As Function Of Assumed C’	53
4.	Input Values For Equation (64) Pervaporation Desalination Studies	63
5.	$V'\delta/D_i$ And Concentration Polarization In MD	74
6.	$V'\delta/D_i$ And Concentration Polarization In Pervaporation Desalination	75
7.	DC1 Room Temperature	89
8.	DC1 30 ℃	90
9.	DC1 40 ℃	91
10.	DC1 60 ℃	91
11.	DC1 70 ℃	92
12.	DC1 80 ℃	92
13.	DC1 90 ℃	93
14.	“6/22/17” 40 ℃	95
15.	“6/22/17” 60 ℃	96
16.	“6/22/17” 70 ℃	96
17.	“6/22/17” 80 ℃	97
18.	“6/22/17” 90 ℃	97
19.	Process Variables For First Stage RO	102
20.	RO Membrane Properties	102
21.	Adjustable Process Variables	103

Table Page

22. Recovery and Rejection 112

23. Pervaporation C' values 115

LIST OF FIGURES

Figure		Page
1.	Mitsui Pervaporation Ethanol Dehydration Plant	7
2.	Pervaporation Process And Transport	9
3.	Nacl Saturation Pressure As Function Of Temperature	17
4.	Salt Content Profiles M-S Model	18
5.	Water Content Profiles M-S Model	19
6.	Support Resistance In Pervaporation	20
7.	LTA (Naa) Framework	25
8.	GO Nanosheet Structure	29
9.	Effect Of Feed Concentration On GO/PAN Membrane	30
10.	Membrane Separation Results In Boundary Layer	36
11.	Boundary Layer Volume	37
12.	Solute Flux To And From Membrane	39
13.	Pervaporation VOC Separation From Water	48
14.	Pervaporation VOC Separation From Water	50
15.	Pervaporation Desalination	52
16.	TCE Enrichment	58
17.	Baker's Method An Data	65
18.	Baker's Method Drobek Data	66
19.	Baker's Method Drobek Data	67
20.	Baker's Method Lin Data	68
21.	Baker's Method Malekpour Data	69

Figure Page

22. Baker's Method Malekpour Data 70
23. Baker's Method Malekpour Data 70
24. Baker's Method Naim Data..... 72
25. C' As Function Of Exp(Pe)..... 82
26. Lab Pervaporation Setup..... 87
27. Top View Of Pervaporation Cell..... 88
28. Baker's Method Data For DC1 94
29. Baker's Method Data For "6/22/17"..... 98
30. MWH Model Increment..... 100
31. Stages Of RO/Pervaporation Hybrid Model..... 100
32. Number Of Elements Per Stage..... 101
33. Number Of Increments Per Element..... 101
34. Recovery And Rejection As Function Of Feed Pressure RO..... 113
35. Rejection As Function Of Feed Pressure RO 114
36. Maximum C' As Function Of Re Number At Various Temperatures..... 116
37. Recovery And Rejection As Function Of Temperature, Re = 0.27..... 117
38. Recovery And Rejection As Function Of Temperature, Re = 0.29..... 117
39. Recovery And Rejection As Function Of Temperature, Re = 0.3..... 118
40. Recovery And Rejection As Function Of Temperature, Re = 0.31..... 118
41. Recovery And Rejection As Function Of Temperature, Re = 0.33..... 119
42. Reversal Of Temperature Polarization..... 130
43. Boundary Layer Temperature Profile 135

Figure Page

44. CB Coated And Uncoated Deltamem Membranes 136

45. Pervaporation Setup For Simulated Solar Irradiation..... 137

46. Pervaporation 3.2 Wt % Nacl Nanophotonic Coated/Uncoated 138

47. Pervaporation Simulated BGNDRF Water Nanophotonic Coated/Uncoated ... 139

48. Pervaporation Simulated Buckeye Water Nanophotonic Coated/Uncoated 140

49. Heat And Mass Flow Away From Membrane..... 144

50. Thinning Of Boundary Layer 145

51. Hypothetical Plot Equation (64) Enhanced/Nonenhanced Membranes 146

CHAPTER 1

INTRODUCTION

1.1 Motivation

The motivation for this research stems from the scarcity of fresh water. About 1 billion people experience shortages in fresh drinking water. [1] Fresh water scarcity has led to the development of desalination techniques which can be divided into membrane based and thermal based (Multistage Flash Distillation and Multi Effect Distillation). Reverse osmosis is the primary membrane based desalination technology. In his discussion of desalination plants in the Mediterranean region Fritzmann states that RO has become more prevalent than the thermal based processes. [2] Managing the concentrated waste produced through desalination (including minimization, treatment, and disposal solutions) is an ongoing critical challenge to inland brackish water desalination. .

Researchers have investigated various combinations of separation technologies for minimizing the concentrate volume of inland brackish water desalination. Attempts have even been made to turn the concentrate into a valuable resource. These include treating the concentrate from inland brackish water RO further with pressure driven membrane processes, thermal processes, electrical-potential driven membranes, and emerging technologies.

1.2 Review of Processes for RO Concentrate Management

Pressure driven and miscellaneous processes include: [1]

1. Intermediate chemical softening
2. Pellet reactors

3. Electrocoagulation
4. Intermediate biological reduction
5. High efficiency RO
6. Advanced reject recovery of water
7. Seeded slurry precipitation and recycle
8. Disc tube filtration
9. Oxidation-based technologies

In the above list only high efficiency RO and disc tube filtration are primary membrane processes; the other processes listed are feed treatments designed to increase RO recovery. Pressure driven membrane processes are limited by the solute concentration within the feedwaters (e.g., < 60,000 milligrams per liter [mg/L]) and are not suited to high concentrations because of both scaling and pressure limitations.

Thermal-based technologies include: [1]

1. Multi-effect distillation and mechanical vapor compression
2. Brine concentrators and crystallizers
3. Wind-aided intensified evaporation
4. Spray dryers

Thermal membrane-based processes have the key advantage of robustly dealing with waters with very high salt concentrations (e.g., > 100,000 mg/L)—much higher than the capacity of osmotic processes. Our investigations have shown that scaling propensity is lower when chemical activities instead of concentrations are used as a predictor and depend more on kinetic (residence

time) than thermodynamic constraints. However, conventional thermal processes are considered to be energy intensive.

Electrical potential driven membrane processes include: [1]

1. Electrodialysis
2. Electrodialysis reversal
3. Electrodialysis metathesis

Electrical potential driven membrane processes are not cost efficient compared to thermal processes when the feed to be processes has a TDS greater than 15 g/L. [1]

Emerging technologies include: [1]

1. Forward osmosis
2. Membrane distillation
3. Thermo-ionic processes
4. Eutectic freeze crystallization

The advantages of membrane distillation (MD) are that there is a high limit on the TDS of the feed water, and that there are no feed pressure requirements. [1]

Membrane distillation (MD) is driven by the temperature-dependent differences in vapor pressure of the components being separated. [3] MD uses porous hydrophobic membranes whose sole purpose is to provide a barrier between the liquid and vapor phases. The MD membrane does not exhibit selectivity for any specific dissolved component.

There are four types of membrane distillation: [4]

1. Direct contact membrane distillation (DCMD)
2. Sweep gas membrane distillation (SGMD)

3. Air gap membrane distillation (AGMD)
4. Vacuum membrane distillation (VMD)

1.3 Pervaporation Desalination Compared with Membrane Distillation

A separation similar to MD using dense polymeric or microporous inorganic (e.g. zeolite) hydrophilic membranes is commonly referred to as pervaporation desalination. [3, 5-24] Salt water feeds in that separation can be regarded as a "pseudo-liquid" mixture. [23, 24] On the other hand pervaporation has been described as a process that separates true liquid mixtures.[25, 26] For example, Baker states that pervaporation is thermodynamically equivalent to vapor permeation, where the components to be separated are present in the vapor phase on the feed side.[25] Pervaporation desalination can be considered as an alternative to MD.

Pervaporation desalination has almost identical energy requirements as VMD on the lab scale. For example, both processes require heating the feed and supplying the energy for the vacuum pump on the permeate side. [3] A significant problem for VMD is that the hydrophobic membrane can become wet from applying the vacuum allowing the feed to contaminate the product water. [4] Therefore, VMD is not being widely investigated for desalination applications, although it is the most energy efficient type of membrane distillation. [4, 27]

Direct contact membrane distillation (DCMD) is a more widely investigated form of MD for desalination than VMD. In DCMD, both the feed and permeate side of the membrane are in contact with liquid water, and the feed side is maintained at a higher temperature. [4] A major problem with DCMD is that significant conductive heat

(energy) loss can occur across the membrane from the water contact on both sides of the membrane. [28, 29] This makes DCMD less energy efficient than VMD or pervaporation desalination. [27, 28]

Some researchers maintain that, in general, conventional MD can achieve higher water flux than conventional pervaporation desalination. This conclusion should be taken as preliminary because there are so few published studies on pervaporation desalination. Conventional pervaporation may be superior to conventional DCMD when membranes having improved flux are developed. Subramani and Jacangelo state that there is a lack of long term performance data for MD due to issues relating to wetting of the porous hydrophobic membranes used. [24] Membrane wetting is not a problem in pervaporation desalination.

One advantage of using a hydrophilic membrane is that type of membrane will separate water preferentially over volatile organic compounds (VOCs) that may be present in the feed. DCMD can be used for separating VOCs but in that case VOCs are permeated preferentially over water. Therefore if a salt water feed contains VOCs, two DCMD processes are needed to separate the components to obtain fresh water. Because MD and pervaporation are thermally driven, flux is increased by heating the feed. One way of increasing performance in both processes is by using solar energy to heat the feed. This has been done both in pervaporation and DCMD.[30, 31] In DCMD, solar heating of the feed was accomplished by embedding nanophotonic particles in the membrane. [30] Nanophotonic heating may be more efficient in pervaporation desalination than DCMD because there is no conductive heat loss to the permeate side of the membrane.

These considerations form the motivation for this study of pervaporation as a means of desalination.

1.4 Brief History of Pervaporation and Industrial Applications

According to Baker, pervaporation originated in the 19th century and the term was coined by Kober in 1917 [32]: The species in the feed permeate through the membrane and evaporate on the permeate side. The process was first studied in systematic fashion in the 1950s by American Oil. By the 1980s advances in membrane technology made it possible to prepare economically viable pervaporation systems. [25] The most important current industrial application of pervaporation is the removal of water from organic solvents, most importantly ethanol. Pervaporative dehydration of ethanol typically produces a product containing less than 1 wt% water from a feed containing 10 wt% water. It is not possible to achieve this by simple distillation since ethanol and water form an azeotrope at about 95% ethanol. According to Baker, "One of the industrial leaders in applying pervaporation technology is Sulzer Chemtech (GFT membranes). They have installed about 200 small plants mostly to remove water from ethanol and isopropyl alcohol streams for the pharmaceutical and fine chemical industries."[25]

As a blend for gasoline, the water content for ethanol must be reduced to 2000 ppm, for ethyl tertiary butyl ether production the water content of ethanol must be <500 ppm. The hydrophilic NaA (**LTA** structure) zeolite (crystalline microporous) membrane is extremely selective in the pervaporation separation of water from ethanol and can achieve purity in the order of 500 ppm.[33] (Figure 1) Mitsui Engineering and

Shipbuilding Co. pioneered the field in 2000, and together with its subsidiary BNRI has about 100 pervaporation units in operation. [34]

Baker also lists other industrial applications of pervaporation including volatile organic compound (VOC) separation from water and organic-organic separations. [25] An important future industrial application of pervaporation is the dehydration of bioethanol. [25, 35] In 2010 13 billion gallons of fuel bioethanol were produced from corn using distillation to separate water from ethanol.[25] However, pervaporation will be more energy efficient in that process than distillation, although not yet adopted by industry. [35]

Figure 1: Mitsui Pervaporation Ethanol Dehydration Plant (NaA zeolite membrane) (from Mitsui E & S website)

1.5 Transport Models for Pervaporation

In pervaporation, the feed is a liquid and the permeate is a vapor.[25] Transport from the feed through the membrane is most often described by the solution-diffusion model. [25, 36]

The solution diffusion model:[25, 36, 37]

In 1748 Nollet reported that a pig bladder was more permeable to water than ethanol. In 1831 Mitchel conducted a series of experiments showing that different gases permeated at different rates through balloons made of natural rubber (cis-poly-isoprene). Fick's laws of diffusion, based on Fourier's law of heat conduction and Ohm's law, provided a description of mass transport across dense membranes. And in 1866 Sir Thomas Graham published one of the first descriptions of the solution-diffusion model.[38] Figure 2 shows (a), the basics of a lab scale pervaporation setup, and (b), the solution and diffusion of a species through a pervaporation membrane.

The following description of the solution diffusion model (equation (1) – equation (27)) is given by Baker.[25]

The solution diffusion model is based on the following assumptions:

1. The driving force causing species transport across the membrane is the chemical potential difference of the species between the feed/membrane interface and the permeate/membrane interface. The driving force can be equivalently expressed as a concentration difference or a partial pressure difference.
2. The liquid at the feed/membrane interface is in equilibrium with the membrane at the feed/membrane interface, and the vapor at the permeate/membrane interface is in equilibrium with the membrane at the permeate/membrane interface.

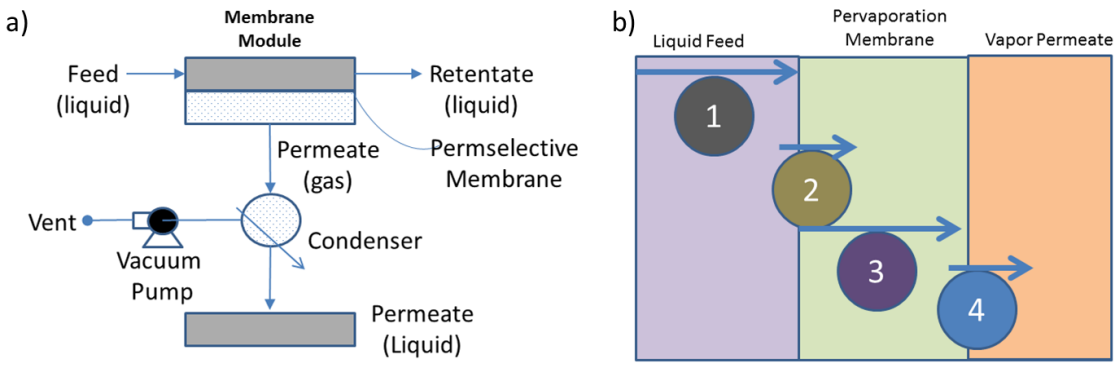

Figure 2: a) Schematic of pervaporation process. (b)Schematic of details of transport within pervaporation process—step (1) transfer of the main permeating species from the bulk feed to the membrane surface, governed by the concentration gradient that exists between the bulk feed and the membrane surface (step 2) sorption of the permeating species onto the membrane surface; (step 3) is the diffusion of the main permeating species through nonporous membrane; (step 4) transfer of the main permeating species from the membrane surface on the permeate side to the bulk permeate.

The second assumption results in equations (1) and (5). Equation (1) states that the chemical potential of species *i* in the feed liquid at the liquid solution/membrane interface is equivalent to the chemical potential of species *i* in the membrane at the feed liquid solution/membrane interface.

$$\mu_i^0 + RTln(\gamma_{i0}x_{i0}) + v_i(p_0 - p_{isat}) = \mu_i^0 + RTln\left(\gamma_{i0(m)}n_{i0(m)}\right) + v_i(p_0 - p_{isat}) \quad (1)$$

In equation(1), μ_i^0 [J mol^{-1}] is the standard state chemical potential of species *i*, *R* [J mol^{-1} K^{-1}] is the gas constant, T is the temperature [K], γ_{i0} [-] is the activity coefficient of species *i* in the feed liquid at the liquid solution/membrane feed interface, x_{i0} [-] is the mole fraction of species *i* in the feed liquid at the liquid solution/membrane feed

interface, v_i [m^3 mol^{-1}] is the molar volume of species *i*, p_0 [bar] is the pressure of the fluid on the feed side at the liquid feed/membrane interface, p_{isat} [bar] is the saturation pressure of species *i*, $\gamma_{i0(m)}$ [-] is the activity coefficient of species *i* in the membrane at the liquid solution/membrane feed interface, and $n_{i0(m)}$ [-] is the mole fraction of species *i* in the membrane at the liquid solution/membrane feed interface.

Equation (2) results from equation (1) since the first and third terms on both sides of equation (1) are identical.

$$n_{i0(m)} = \frac{\gamma_{i0} x_{i0}}{\gamma_{i0(m)}} \quad (2)$$

$$n_{i0(m)} = K_i n_{i0} \quad (3)$$

Equation (3) is based on the following definition of the liquid phase sorption coefficient:

$$K_i = \frac{\gamma_{i0}}{\gamma_{i0(m)}} \quad (4)$$

$$\mathrm{K_i} = \text{liquid phase sorption coefficient, i } [-]$$

Equation (5) states that the chemical potential of species *i* in the permeate vapor at the permeate vapor/membrane interface is equivalent to the chemical potential of species *i* in the membrane at the permeate vapor/membrane interface.

$$\mu_i^0 + RTln(\gamma_{ip} y_{ip}) + RTln\frac{p_p}{p_{isat}} = \mu_i^0 + RTln(\gamma_{ip(m)} n_{ip(m)}) + v_i(p_0 - p_{isat}) \quad (5)$$

In equation (5), μ_i^0 [J mol^{-1}] is the standard state chemical potential of species *i*, *R* [J mol^{-1} K^{-1}] is the gas constant, T is the temperature [K], γ_{ip} [-] is the activity coefficient of species *i*, in the permeate vapor at the permeate vapor/membrane interface, y_{ip} [-] is the mole fraction of species *i*, in the permeate vapor at the permeate vapor/membrane interface, p_p [bar] is the gas pressure of the permeate at the permeate/membrane

interface, p_{isat} [bar] is the saturation pressure of species *i*, $\gamma_{ip(m)}$ [-] is the activity coefficient of species *i*, in the membrane at the permeate vapor/membrane interface, $n_{ip(m)}$ [-] is the mole fraction of species *i*, in the membrane at the permeate vapor/membrane interface, v_i [m^3 mol^{-1}] is the molar volume of species *i*, and p_0 [bar] is the pressure of the fluid on the feed side at the liquid feed/membrane interface.

Equation (5) can be rearranged to equation (6) by eliminating the standard state chemical potential terms on both sides of equation (5):

$$n_{ip(m)} = \frac{\gamma_{ip}}{\gamma_{ip(m)}} \frac{p_p}{p_{isat}} y_{ip} \exp\left(\frac{-v_i(p_0 - p_{isat})}{RT}\right) \quad (6)$$

The exponent in equation (6) is close to 1:

$$exp\left(\frac{-v_i(p_0 - p_{isat})}{RT}\right) \cong 1 \quad (7)$$

Then equation (6) can be simplified to equation (8)

$$n_{ip(m)} = \frac{\gamma_{ip}}{\gamma_{ip(m)}} \frac{p_p}{p_{isat}} y_{ip} \quad (8)$$

Equation (9) states that the partial pressure of species *i* in the permeate vapor is equal to the product of the mole fraction of species *i* in the permeate vapor at the permeate vapor/membrane interface and the total pressure of the permeate vapor at the permeate vapor/membrane interface.

$$y_{ip} p_p = p_{ip} \quad (9)$$

In equation (9), y_{ip} [-] is the mole fraction of species *i*, in the permeate vapor at the permeate vapor/membrane interface, p_p [bar] is the gas pressure of the permeate at the permeate/membrane interface, and p_{ip} [bar] is the partial pressure of species *i*, in the permeate vapor at the permeate vapor/membrane interface.

The gas phase sorption coefficient is defined by equation (10)

$$\frac{\gamma_{ip}}{\gamma_{ip(m)}p_{isat}} = K_{i,n}^{G} \quad (10)$$

$$K_{i.n}^{G} = mole\ fraction\ gas\ phase\ sorption\ coefficient, i\ [bar^{-1}]$$

Substituting equations (9) and (10) into equation (10) results in equation (11)

$$n_{ip(m)} = K_{i,n}^{G} p_{ip} \quad (11)$$

The purpose of equations (12) – (17) is to show $n_{i0(m)}$ is a function of the gas phase sorption coefficient $K_{i,n}^{G}$.

Equation (12) states that the liquid at the liquid feed/membrane interface is in equilibrium with a hypothetical vapor:

$$\mu_i^0 + RTln(\gamma_{i0}^{L} x_{i0}^{L}) + v_i(p_0 - p_{isat}) = \mu_i^0 + RTln\left(\gamma_{i0}^{G} y_{i0}^{G}\right) + RTln\frac{p_0}{p_{isat}} \quad (12)$$

In equation (12), μ_i^0 [J mol^{-1}] is the standard state chemical potential of species *i*, *R* [J mol^{-1} K^{-1}] is the gas constant, T is the temperature [K], γ_{i0}^{L} [-] is the activity coefficient of species *i* in the feed liquid at the liquid solution/membrane feed interface, x_{i0}^{L} [-] is the mole fraction of species *i* in the feed liquid at the liquid solution/membrane feed interface, v_i [m^3 mol^{-1}] is the molar volume of species *i*, p_0 [bar] is the pressure of the fluid on the feed side at the liquid feed/membrane interface, p_{isat} [bar] is the saturation pressure of species *i*, γ_{i0}^{G} [-] is the activity coefficient of species *i* in the hypothetical vapor at the liquid solution/membrane feed interface, and y_{i0}^{G} [-] is the mole fraction of species *i* in the hypothetical vapor at the liquid solution/membrane feed interface. The LHS of equation (1) is identical to the LHS of equation (12). This results in equations

(13) and (14) (an exponential term similar to that appearing in equation (6) is assumed to be equal to 1).

$$x_{i0}^{L} = x_{i0} \quad (13)$$

$$x_{i0} = \frac{\gamma_{i0}^{G}}{\gamma_{i0}^{L} p_{isat}} p_{i0} \quad (14)$$

In equation (14) p_{i0} [bar] is the partial pressure of species *i* in the hypothetical vapor at the liquid solution/membrane feed interface.

Henry's law coefficient [bar] is defined by equation (15):

$$\frac{\gamma_{i0}^{L} p_{isat}}{\gamma_{i0}^{G}} = H_i \quad (15)$$

Substitute equation (14) into equation (2) results in equations (16) and (17):

$$n_{i0(m)} = \frac{\gamma_{i0}^{G}}{\gamma_{i0(m)}} \frac{p_{i0}}{p_{isat}} \quad (16)$$

$$n_{i0(m)} = K_{i,n}^{G} p_{i0} \quad (17)$$

Comparison of equations (16) and (17) with equation (10) results in:

$$\frac{\gamma_{i0}^{G}}{\gamma_{i0}^{L}} = \frac{\gamma_{ip}}{\gamma_{ip(m)}} \quad (18)$$

Substitute equations (11) and (17) into Fick's law (allowing for the conversion of concentrations to mole fractions) results in equation (19):

$$J_{i,v} = \frac{P_{i,n}^{G}}{l} \left(p_{i0} - p_{ip} \right) \quad (19)$$

In equation (19) $J_{i,v}$ is volumetric flux [m s^{-1}] or [m^3 m^{-2} s^{-1}], $P_{i,n}^{G}$ [m^2 bar^{-1} s^{-1}] is the mole fraction gas phase permeability coefficient of species *i*, l [m] is the membrane thickness, p_{i0} [bar] is the partial pressure of species *i* in the hypothetical vapor at the liquid

solution/membrane feed interface, and p_{ip} [bar] is the partial pressure of species *i*, in the permeate vapor at the permeate vapor/membrane interface.

The gas phase permeability coefficient is defined as the product of the gas phase sorption coefficient and the diffusion coefficient (equation (20)):

$$P_{i,n}^{G} = K_{i,n}^{G} D_i \quad (20)$$

In equation (20), $P_{i,n}^{G}$ [m^2 bar^{-1} s^{-1}] is the mole fraction gas phase permeability coefficient of species *i*, $K_{i,n}^{G}$ [bar^{-1}] is the mole fraction gas phase sorption coefficient of species *i*, and D_i [m^2 s^{-1}] is the diffusion coefficient of species *i*.

Equation (19) can be written for mass flux by converting mole fraction to concentration:

$$c_i = mw_i \rho_i n_i \qquad (21)$$

In equation (21), c_i [g L^{-1}] is the concentration of species *i*, mw_i [g mol^{-1}] is the molecular weight of species *i*, ρ_i [mol L^{-1}] is the density of species *i*, and n_i [-] is the mole fraction of species *i*.

The gas phase sorption coefficient becomes:

$$K_i^{G} = mw_i \rho_i \frac{\gamma_{ip}}{\gamma_{ip(m)} p_{isat}} \qquad (22)$$

In equation (22), K_i^{G} [kg m^{-3} bar^{-1}] is the gas phase sorption coefficient of species *i*, mw_i [kg mol^{-1}] is the molecular weight of species *i*, ρ_i [mol m^{-3}] is the molar density of species *i*, γ_{ip} [-] is the activity coefficient of species *i* in the permeate vapor at the permeate vapor/membrane interface, p_{isat} [bar] is the saturation pressure of species *i*, $\gamma_{ip(m)}$ [-] is the activity coefficient of species *i*, in the membrane at the permeate vapor/membrane interface.

The gas phase permeability coefficient becomes:

$$P_i^G = K_i^G D_i \quad (23)$$

In equation (23), P_i^G [km m m^{-2} s^{-1}] is the gas phase permeability coefficient of species *i*, K_i^G [kg m^{-3} bar^{-1}] is the gas phase sorption coefficient of species *i*, and D_i [m^2 s^{-1}] is the diffusion coefficient of species *i*.

The mass flux is given by equation (24):

$$J_i = \frac{P_i^G}{l}\left(p_{i0} - p_{ip}\right) \quad (24)$$

In equation (24), J_i [kg m^{-2} s^{-1}] is the mass flux of species *i*, P_i^G [km m m^{-2} s^{-1}] is the gas phase permeability coefficient of species *i*, l [m] is the membrane thickness, p_{i0} [bar] is the partial pressure of species *i* in the hypothetical vapor at the liquid solution/membrane feed interface, and p_{ip} [bar] is the partial pressure of species *i*, in the permeate vapor at the permeate vapor/membrane interface.

It is practical to use modified Raoult's law to represent p_{i0} (bar)[39]:

$$x_{i0}\gamma_{i0}p_{isat} = p_{i0} \quad (25)$$

In equation (25), γ_{i0} [-] is the activity coefficient of species *i* in the feed liquid at the liquid solution/membrane feed interface, x_{i0} [-] is the mole fraction of species *i* in the feed liquid at the liquid solution/membrane feed interface, p_{isat} is the saturation pressure of species *i*, p_{i0} [bar] is the partial pressure of species *i* in the hypothetical vapor at the liquid solution/membrane feed interface. Equation (25) represents equivalent fugacities of the liquid and (in this case) hypothetical vapor phase. An excellent discussion of this can be found in Wijmans and Baker. [37]

The liquid mole fractions at the feed/membrane interface are not known so that equation (25) is usually modified by using the bulk feed mole fraction, activity coefficient and partial pressure:

$$x_i \gamma_i p_{isat} = p_i \qquad (26)$$

In equation (26) x_i [-] is the bulk feed liquid mole fraction of species i, γ_i [-] is the bulk feed activity coefficient of species i, and p_i [bar] is the partial pressure of species i in the hypothetical vapor at the liquid solution/membrane feed interface.

Substituting equation (26) into equation (24) results in:

$$J_i = \frac{P_i^G}{l}\left(x_i \gamma_i p_{isat} - p_{ip}\right) \qquad (27)$$

Equation (27) is used ubiquitously in the MD and pervaporation literature. [3, 4, 6, 9, 15, 25, 28, 36, 37, 40]

As already suggested, the term "pervaporation" may not be appropriate for feed solutions containing inorganic salts, e.g. sodium chloride. The underlying assumption of equation (12) is not met because, for example in the case of sodium chloride, the saturation pressure is negligible at temperatures typically used in pervaporation, as shown in Figure 3. Similarly, equation (27) is not applicable.

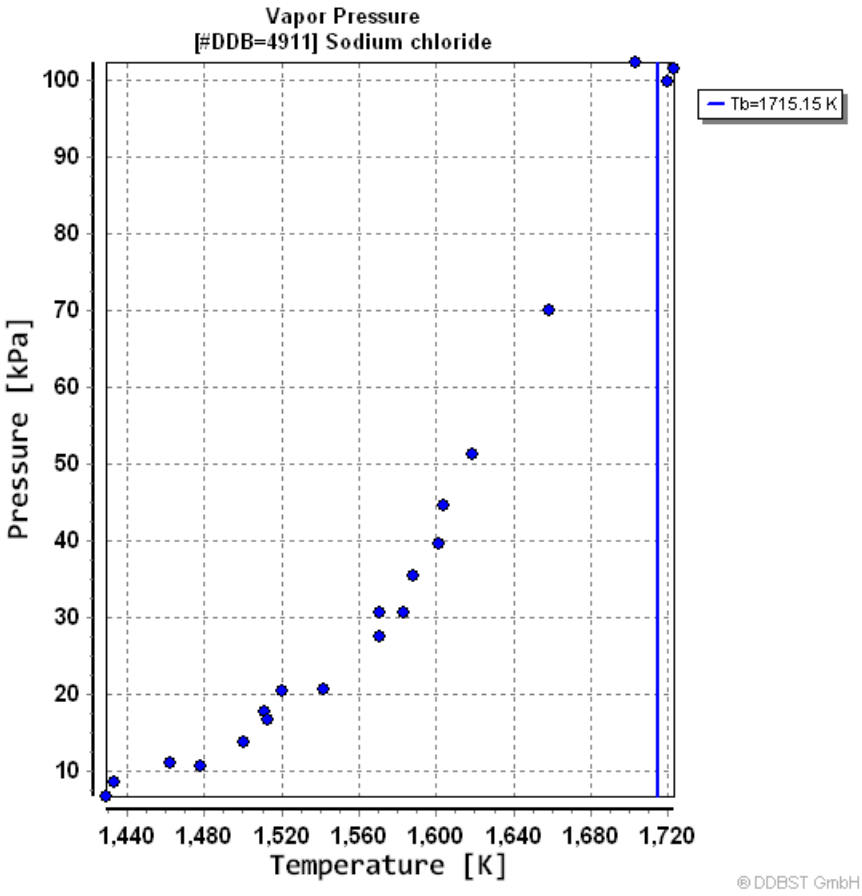

Figure 3: Sodium Chloride saturation pressure as a function of temperature. [41]

Models other than the solution diffusion model have been used to describe transport through pervaporation membranes. A number of simulation techniques have been used and sometimes combined to describe mixture transport through dense polymer and zeolite membranes, i.e. the active layer of pervaporation membranes. These include Monte-Carlo, molecular dynamics, transition-state theory, Fick and Onsager formulations, and the Maxwell-Stefan model. [42] It is generally accepted that the generalized Maxwell-Stefan formulation offers the most convenient and nearest quantitative prediction of multicomponent adsorption and diffusion through dense

polymer and zeolite membranes. [43, 44] No literature examples where the Maxwell-Stephan model was used to describe aqueous sodium chloride and water transport through pervaporation membranes were found, although it is possible to derive adsorption isotherms for sodium chloride on zeolite.[45] Costa-Corredor et al. found the results of Maxwell-Stefan modelling (see Figure 4 and Figure 5) were comparable to experimental results in examination of the transport of aqueous sodium chloride in dried sausage.[46]

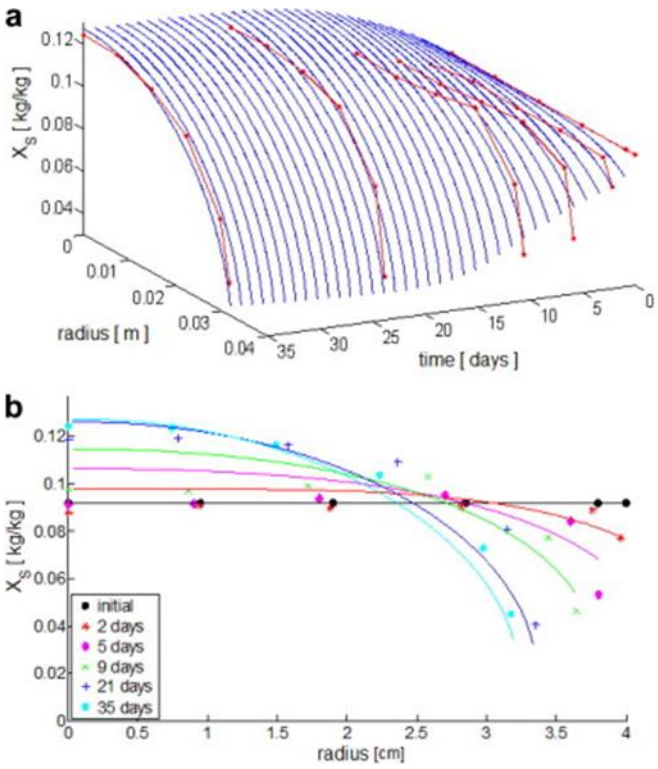

Figure 4: Experimental (points) and computed (lines) salt content profiles, (a) in 3D and (b) 2D. [46]

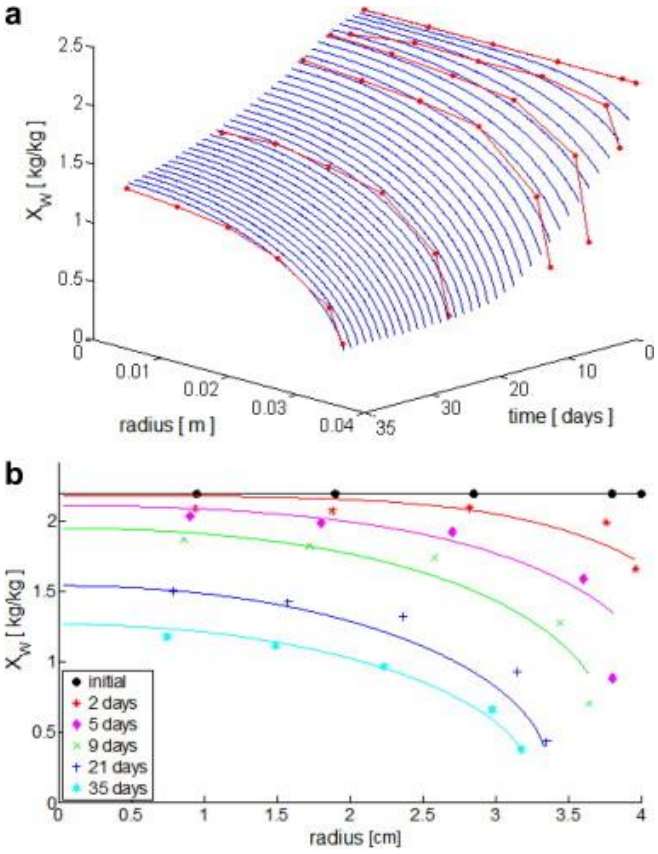

Figure 5: Experimental (points) and computed (lines) water content profiles (a) in 3D and (b) 2D [46]

To analyze the zeolite layer in conjunction with the support requires coupling with a second model for flux through the support such as the dusty gas model.[47] A simpler support model has been proposed by de Bruijn [48]: This model uses the assumption of a single permeating species and is intended to show the role of support resistance to flux. [42, 48]

Using this model requires the following input data: [48]

1. Total flux through the composite zeolite-support membrane
2. Separation factor
3. Feed pressure of the permeating species

4. Permeate pressure of the permeating species
5. Pore diameter of the support
6. Thickness of the support
7. Viscosity of the permeating species

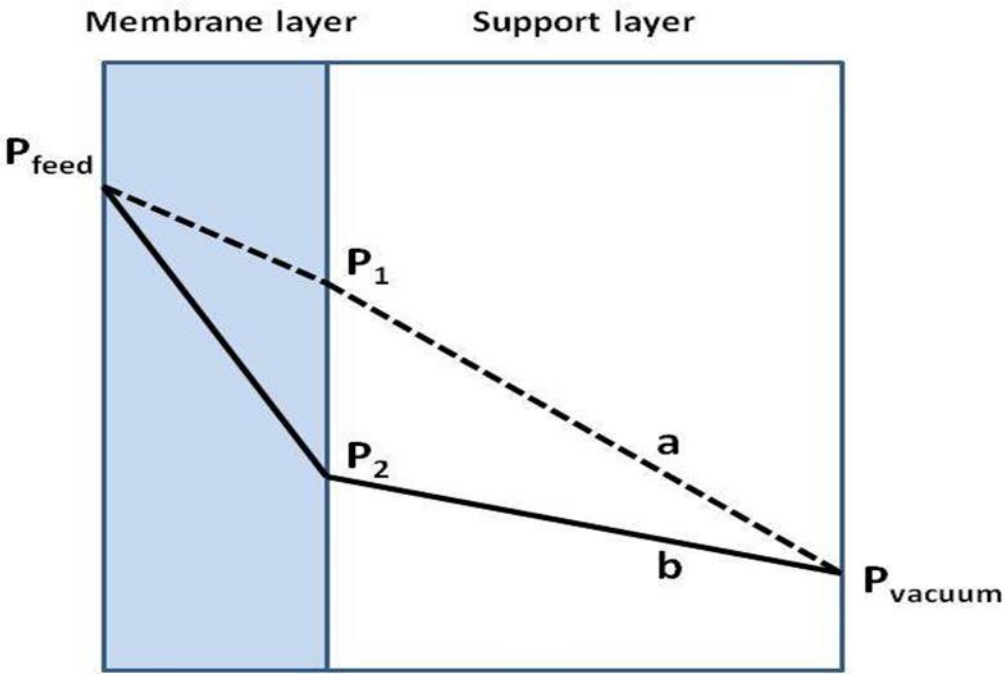

Figure 6: P_1 and P_2 represent high and low interfacial pressures. Curve (a) represents high support resistance, curve (b) low support resistance [42]

Figure 6 illustrates the case of high support resistance and low support resistance. The de Bruijn study included a large retrospective review of the pervaporation literature. Pervaporation separations were broken down to two groups: dehydration of organics, and organics separations. Dehydration separations utilized a hydrophilic zeolite membrane while organic separations utilized an organophilic (hydrophobic) zeolite membrane. Fluxes and separation factors were high for the dehydration of organics and

support resistance to mass transfer was found to be significant in that group. Fluxes and separation factors were significantly lower in the organic separations. However support resistance to mass transfer was found to be significant for several cases within the second group, included ethanol separation from water using a silicalite-1 membrane. They also determined that Knudsen flow dominated over viscous flow in the support, well over 90% in systems where the flux was < 5 $\frac{kg}{m^2 h}$, with pore diameters up to 5μ. [42, 48]

A significant limitation of the de Bruijn model is that it requires the input of support properties ε, τ, and pore diameter that may be difficult to obtain. 14 of 18 of the studies evaluated in the de Bruijn study were examined [49-66] [19, 30-46]. Values for ε and τ were not provided in any of the 14. De Bruijn had to use estimates. Similarly, pore diameter of the support was usually not measured, the value provided by the industrial supplier of the support was often used. Another limitation is that the "resistance to mass transfer" does not provide how much flux was lost relative to the theoretical flux of the stand- alone zeolite layer. Also, an analysis of the relation of "resistance to mass transfer" to selectivity was not provided.

The de Bruijn model shows that two properties are important when choosing a support:

1. Material compatibility with the active layer
2. Resistance to flux

The purpose of briefly discussing other transport models is to illustrate that the solution diffusion model has limitations. However the solution diffusion model is relatively simple and easy to use.

1.6 Comparing Pervaporation Performance

Permeance is pressure normalized flux. It is also a rough measure of the cost of the flux since the driving force (heat the feed, power the vacuum, etc.) has to be paid for. The following equation is used to calculate the permeance:

$$water\ permeance = \frac{water\ flux}{P^{sat}_{water,feed} - P^{sat}_{water,permeate}} \qquad (28)$$

In equation (28) the assumptions for the RHS denominator is that the water mole fraction and activity coefficient both equal 1. These assumptions impart about a 1% error. Once the permeance value has been calculated for the pervaporation and MD membranes they can be compared. Rearranging equation (28):

$$water\ flux = (water\ permeance)\left(P^{sat}_{water,feed} - P^{sat}_{water,permeate}\right) \quad (29)$$

Equation (29) says that for a given driving force, the membrane with the larger permeance will deliver the larger flux. For example if a MD membrane has a lower permeance than a pervaporation membrane, then under identical operating conditions, the pervaporation membrane will deliver a larger flux. Permeance to answer the question of which membrane delivers the largest amount of quality water under identical operating conditions. When using equation (45) it is usually assumed that permeance is stable, for thermally driven separations, over a range of feed temperatures.

Permeability is permeance normalized for membrane thickness. The following equation is used to calculate permeability (note the Darcy equation can also be used):

$$Water\ permeability = (water\ permeance)(l) \quad (30)$$

In equation (30), l is membrane thickness. The general concept behind the use of equation (30) is that, given the membranes are of similar porosity and material, a thinner membrane will have greater (not less as suggested by the equation) permeability because the permeance goes up disproportionately to the decrease in membrane thickness. This is because thinner membranes have lower resistance (the reciprocal of permeance in a resistance in series model). Note that in this comparison it is most useful to compare membranes operating under the same driving force; otherwise we are dealing with two variables, driving force and membrane thickness.

Comparing water permeabilities of pervaporation and MD membranes does not provide an answer as to which type of membrane can deliver the larger amount of quality water. For one thing, these membranes are of different materials (e.g. pervaporation membranes are hydrophilic and MD membranes are hydrophobic) and porosity. It does not make sense to use the Darcy equation for polymeric pervaporation membranes since they are dense not porous. In order to obtain the useful metric for comparing membrane performance, equation (30) can be rearranged:

$$Water\ permeance = \frac{water\ permeability}{l} \qquad (31)$$

Equation (31) informs us that although pervaporation membranes have lower permeability, they have higher permeance than MD membranes because they are thinner. As already discussed, water permeance is the useful metric to decide which membrane can deliver the most water under identical operating conditions.

Since the following chapters include experimental results of pervaporation membranes having zeolite, silica, or polymer active layers, a brief description of these is given.

1.7 Materials for Pervaporation Desalination Membranes

Zeolites are aluminosilicate framework crystalline structures which can be represented by the formula: $M_{2/n}O.Al_2O_3.xSiO_2.yH_2O$ where n is the cation valence. The basic structural unit in zeolites is a TO 4 regular tetrahedron formed of a tetrahedrally ccoordinated atom (the "T" atom, often silicon) located at the center of four oxygen atoms which form the vertices of the tetrahedron. The tetrahedra are corner linked by oxygen bridges containing 8, 10, or 12 oxygen atoms to form periodic frameworks, usually displaying channels (pores) in one or more dimensions. The number of oxygen atoms in the bridge determines the pore size of the zeolite. Each framework type is uniquely defined by the way the comprising tetrahedra are linked. There are currently over 200 zeolite topologies recognized to exist as real materials by the Structure Commission of the International Zeolite Association (IZA). Each of the known framework types is assigned a boldface three letter code by the IZA that defines the structure but not necessarily the type of material. In some cases, the code is derived from the name of the first material found to exhibit the framework topology. An example of the description of one framework type found on the IZA website (LTA framework, the framework for NaA) is seen in Figure 7. Many types of materials are represented within the 200+ framework types. About 20% of the framework types have been synthesized as pure silicates. Silicon atoms are often replaced by aluminum, germanium, phosphorous, or boron atoms, among others. When a trivalent atom replaces silicon, other extra-framework cations are required to preserve electroneutrality. One significant consequence of this type of substitution is that the hydrophilicity of the zeolite changes,

zeolites with high silicon content being relatively hydrophobic (organophilic). Details of each zeolite structure can be found on the official IZA website. [67] [42]

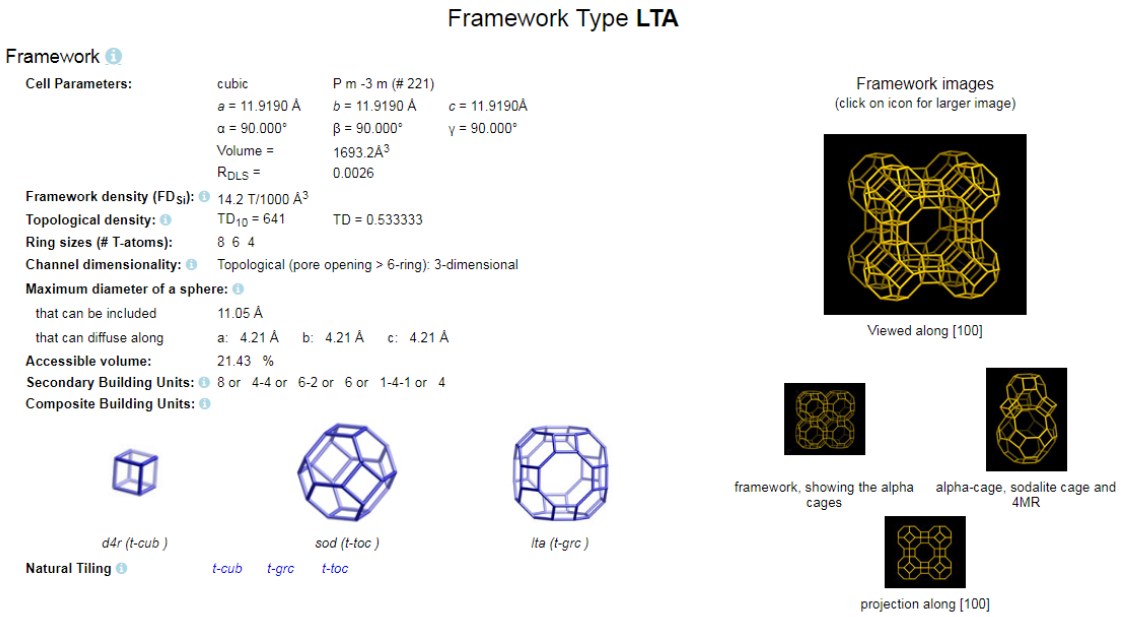

Figure 7: Information on LTA (NaA) framework from IZA website [68]

For industrial applications, zeolite membranes must provide high flux and selectivity. Highly selective membranes are often thick so as to minimize intercrystalline defects, while flux is inversely related to membrane thickness. [34] According to Pina et al., it is difficult to use zeolite membranes industrially because of the cost and because of the difficulty of reproducing defect free zeolite membranes. [34] Pina et al. suggest these difficulties are minimized when small membranes are required, for example in micro-reactors, sensors, and rapid adsorption screening; it is also possible to omit using a support for small applications.[34]

Drobek et al. tested the use of MFI zeolite membranes for pervaporation desalination. [6] They tested two types of MFI zeolite membranes: Silicalite-1 and ZSM-5. As discussed, silicalite-1 is the most hydrophobic zeolite due to its low aluminum content. They noted that NaA membranes are more hydrophillic and could be expected to yield higher water flux. Both zeolite types have pore sizes under 6.6 Å and therefore sieve water molecules from hydrated ions. They prepared there membranes by secondary growth because this growth method produced more selective membranes with better salt rejection as described by Duke et al. [14] The support was tubular α-alumina. Details of the synthetic method can be found in Drobek et al. [6] The testing of the membranes included SEM images showing a 6 μm thickness for the silicalite-1membrane and 3.3 μm for the ZSM-5 membrane. One significant finding in the Drobek et al. study was that ZSM-5 was not stable in salt solutions. The membranes were tested with feeds ranging from 0.3 to 15 wt% NaCl at 21-75 ℃. The silicalite-1 membrane achieved a flux of about 12 kg m^{-2} h^{-1} using a 0.3 wt% NaCl feed at 75℃. Further details of this study will be given in the chapter on concentration polarization.

An et al. tested a naturally occurring zeolite, clinoptilolite as a composite with $MgKPO_4$. [5] They observe that phosphate cement is a ceramic material used in dental treatments and synthetic bones. [5]These membranes were prepared dry pressing a mixture of clinoptilolite, MgO, and monopotassium phosphate. They obtained a disc which was then mounted on a ceramic support and then steam autoclaved. One of the advantages of clinoptilolite is that the cost is low. The authors describe the difficulty in obtaining support materials for synthetic zeolite membranes. They suggest that the supports have fall within a certain range of pore size and porosity, and that combined

with the chemical compatibility requirement results in a high cost for the supports. SEM images confirmed the integrity of the active layer; I,e, free of observable inter-crystalline defects but the authors did not report the thickness of the active layer. Pervaporation testing included tested feeds of 50 and 1400 ppm Na^+ at 25-95 ℃. They obtained a flux of about 20 kg m^{-2} h^{-1} at the highest temperature with the low salinity feed. Further details will be given in the chapter on concentration polarization.

Malekpour et al. tested NaA (LTA) and ZSM-5 (MFI) membranes for pervaporation desalination of feeds of cesium, strontium and iodide salts. [8] The purpose was to develop a means of processing waters containing hazardous wastes. The membranes were synthesized by a hydrothermal method on a α-alumina support. The NaA membranes were about 15 μm and the ZSM-5 membranes about 10 μm by SEM. Dilute salt solutions (0.001 mol L^{-1}) were tested at 25-65 ℃. The highest flux obtained was for Cesium using the NaA membrane of about 2.1 kg m^{-2} h^{-1} at 65℃. Flux increased and rejection increased with increasing feed temperature, rejections were >98% in all cases. Further details will be given in the chapter on concentration polarization.

Non-crystalline (amorphous) inorganic membranes[69]

These are microporous (pore diameter < 2 nm) membranes usually composed of silica or carbon. Silica membranes are synthesized using the sol-gel method. [70] These include the polymeric route, the particulate-sol, and the template methods. The active layer is usually adhered to a mesoporous (pore diameter 2-50 nm) support such as γ-alumina.

Lin et al. tested cobalt oxide doped silica for pervaporation desalination. [7] Cobalt oxide was added to the silica because silica is not stable in water. [7] Cobalt oxide

silica was prepared by the sol-gel method and the membrane was coated onto a α-alumina support by dip-coating. The active layer was 200-350 nm thick. Feed solutions of 1-15 wt% NaCl were tested at 25-75 ℃. Testing was done to ensure stability of the membranes. A flux of 1.8 kg m^{-2} h^{-1} was achieved with a 1 wt% NaCl feed at 75℃ with fluxes increasing with increasing feed temperature and decreasing with increasing feed concentration. Rejection was >98% in all cases, however salt permeate concentration increased substantially between 50℃ and 75℃ with feeds of 7.5-15 wt% NaCl. Further details will be given in the chapter on concentration polarization.

Liang et al. developed a graphene oxide (GO) polyacrylonitrile (PAN) composite membrane for pervaporation desalination. [12] The authors synthesized the composite membrane by a vacuum filtration assisted assembly method. They used XPS to characterize the chemical composition and found the results in agreement with the Lerf-Klinowski model of GO shown in Figure 8. This figure shows GO to consist of 6 member carbon rings with many shared borders. There are numerous double bonds throughout. Oxidation of the graphene results in carboxyl, hydroxyl, and epoxide moieties which account for hydrophilicity.

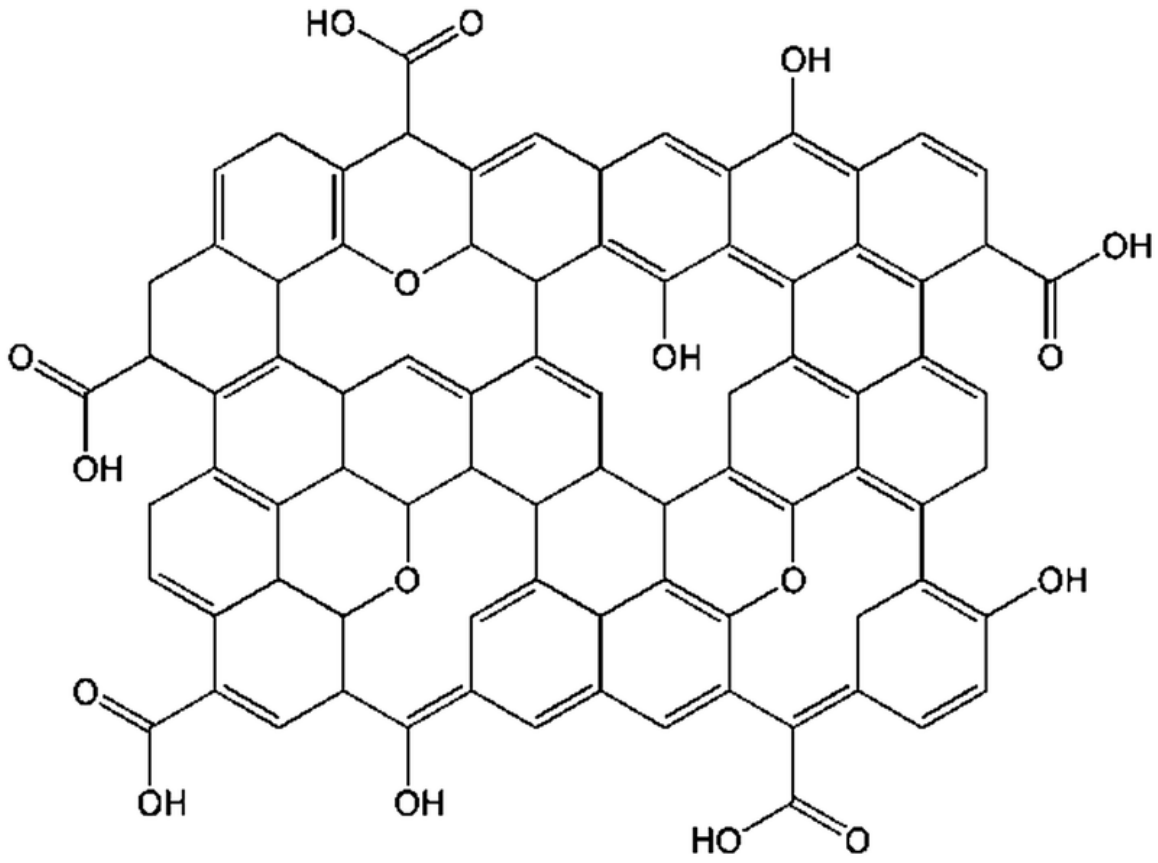

Figure 8: The Lerf–Klinowski model of GO nanosheet structure [12]

The authors describe the GO layer as nanosheets since the synthesized membranes ranged from 30-1400 nm in thickness.

The authors state that salt solutions can be regarded as a pseudo-liquid containing free water molecules and bulkier hydrated ions formed in solution. They state that water molecules easily diffuse through the space between the GO sheets. These spaces apparently function as a molecular sieve excluding the bulkier hydrated ions. The authors describe uniformly high rejection over a range of feed concentrations (2000-100,000 ppm), as shown in Figure 9. [12]

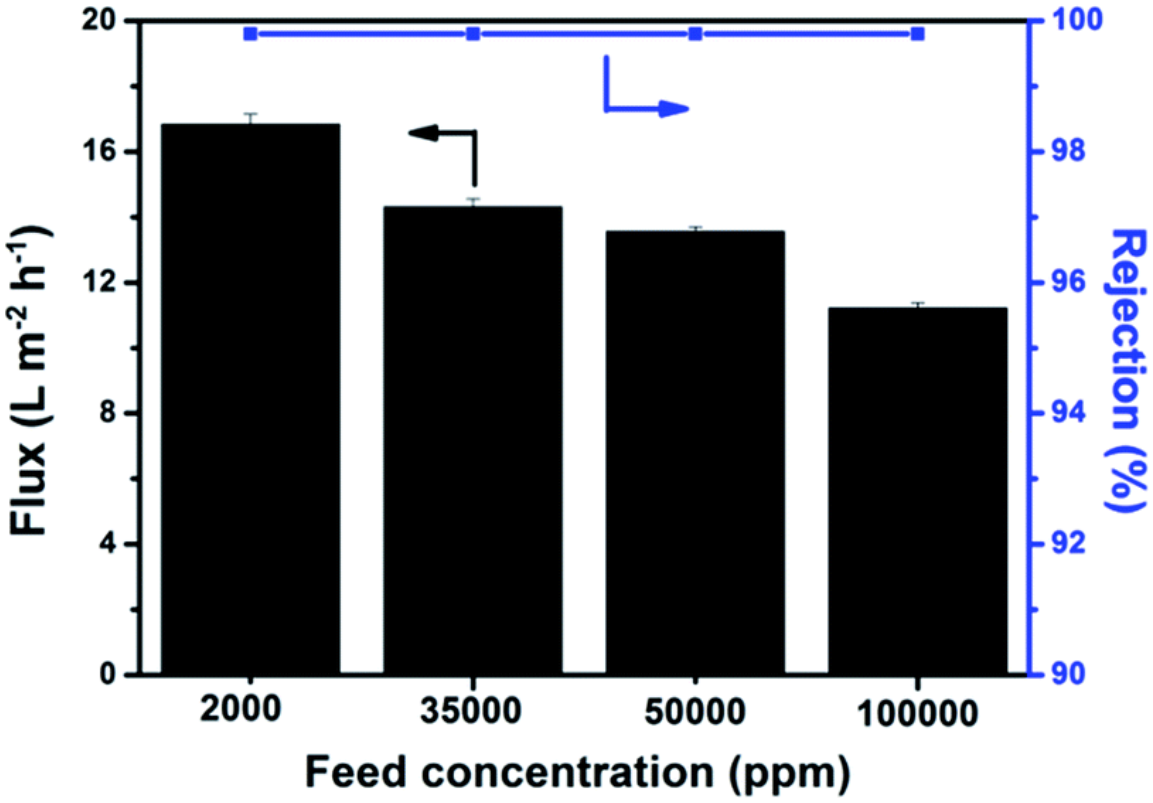

Figure 9: Effects of feed concentration on the pervaporation performance of the GO/PAN membrane at 30℃ [12]

The authors conclude "This makes it possible to use GO based membranes by pervaporation for seawater desalination, brackish water desalination, and reverse osmosis concentrate treatment."[12]

The Table 1 from Liang et al. shows why GO is an exciting material for pervaporation desalination. [12]

Table 1: Pervaporation performance of the membrane skin layer prepared by different materials [12]

material	Feed concentration ppm	T °C	Flux (LMH)	Rejection
polyether amide	35000	68-70	0.2	>99.9
polyether ester	5200	22-29	0.15	>99
NaA zeolite	35000	69	1.9	>99.9
PVA/MA/silica	2000	22	6.93	>99.5
PVA/GA	35000	25	7.36	>99.8
GO	35000	30	14.3	>99.8
GO	35000	90	65.1	>99.8

Polymers used in dense membranes for pervaporation desalination

The polymer materials used for pervaporation desalination are those used for solvent dehydration. [9] The most common of these is polyvinyl alcohol (PVA). [71] The monomer used to make PVA is vinyl acetate ($C_4H_6O_2$). Vinyl acetate is polymerized to polyvinyl acetate using bulk, solution or emulsion polymerization.[72] PVA is then produced by hydrolysis of polyvinyl acetate. Hydrophilicity is proportional to the degree of hydrolysis. PVA has a glass transition temperature of 80℃ and melts above 200 ℃. [71, 72] PVA membranes are cast from aqueous solution and are usually crosslinked to

reduce swelling. [71] PVA membranes are sensitive to impurities including aldehydes, organic acids, amines, mineral acids, and peroxides. [71] According to Vane: "PVA-based membranes were among the first to be commercialized for PV/VP applications and are still commercially available from DeltaMem AG (Switzerland) as part of their PERVAP™ product line of flat sheet membranes. Although the PERVAP™ membranes have been available for many years, DeltaMem AG was only recently formed from a management buy-out of the membrane technology business of Sulzer Chemtech. Sulzer had previously acquired the membrane product line that datesto GFT Ingenieurburo für Industrieanlagenbau. CM Celfa Membrantrenntechnik AG (Switzerland), which is now a special products unit in The Folex Group is mentioned as manufacturing composite membranes with a crosslinked PVA dense layer. Similarly, AzeoSep™-2002 membranes from PetroSep MembraneResearch (Canada) are said to be PVA on a poly(acrylonitrile) (PAN) support. The longevity of PVA in the PV/VP industry reflects the functional stability and performance of this polymer. Although the nature of the polymers used by a company in the manufacture of PV/VP membranes might be openly disclosed or deduced from patent or scientific literature, it is common for the companies to alter the materials over time and/or hold this information as a trade secret. For example, the selective layer in the Azeo Sep™ membranes offered by Petro Sep Corporation (and KmX Membrane Technology) for solvent dehydration is not disclosed and may no longer be based on PVA."[71] PVA membranes from DeltaMem were used in this research. Further details will be given in subsequent chapters.

Xie et al. synthesized a PVA/maleic acid/silica hybrid membrane for pervaporation desalination. [21] The authors state that PVA is not stable in water so that

often inorganic additives are used for the purpose of crosslinking and stabilization.[21] The membranes were prepared by the sol-gel method and cast onto a petri dish. The obtained membranes were 5 μm thick and contained silica nanoparticles (<10nm). The synthetic method maintained the same 80/20 PVA/Maleic acid ratio but the silica content varied between 0-25%. The membranes were tested in a pervaporation cell, presumably with a (unspecified) support. [21] The results of testing are reported in Table **1**[12, 21].

Chaudhri et al. prepared ultrathin PVA/Maleic acid membranes by casting a dilute solution over a polysulfone hollow fiber support. [16] The thinnest membrane active layer was 100 nm. The thinnest coated membrane achieved a flux of 7.4 LMH using a 30,000 ppm NaCl feed at 71 ℃. The permeate was said to be in the conductance range of pure water.[16]

Another polymer used in pervaporation is cellulose acetate. Methyl tertiary butyl ether (MTBE) is an octane enhancer in gasoline. Methanol is used in the production of MTBE. The methanol can be removed, i.e. the MTBE purified by pervaporation using cellulose acetate membranes. [73, 74] This process is similar to dehydration since methanol is a polar molecule as is water.

Naim et al. used a modified cellulose acetate membrane for pervaporation desalination. [9] The membrane was prepared with cellulose acetate powder, acetone, dimethyl phthalate, and dimethyl formamide in "definite proportions" using a smooth uniform glass plate and a doctor's blade. After initial preparation, the membrane was deacetylated. The active layer was found to be 20-25 μm thick by SEM. Feeds consisted of NaCl solutions ranging from 40-140 g L^{-1}. Pervaporation was conducted at feed

temperatures 50-80 ℃. In general, flux increased with increasing feed temperature and decreasing with increasing feed salt concentration. The highest flux reported was 5.97 kg m^{-2} h^{-1} with a 40 g L^{-1} NaCl feed at 70℃. Further details will be given in the chapter on concentration polarization.

This completes a description of the niche pervaporation has in desalination, transport in pervaporation, and the types of membranes used in pervaporation desalination. In the next chapter, concentration polarization in pervaporation desalination will be described.

CHAPTER 2

CONCENTRATION POLARIZATION IN PERVAPORATION DESALINATION

2.1 Introduction to Concentration Polarization

Concentration polarization is a phenomenon that occurs in liquid solvent-solute membrane separations where the solute is depleted or enriched, relative to its presence in the bulk feed, in a thin boundary layer (e.g., 20 μm thick) adjacent to the membrane.[25] In membrane desalination, water is the solvent and sodium and chloride are the major solutes, although other minerals (e.g., calcium, magnesium, potassium, sulfate, bicarbonate) and organic compounds may also be present in the feed. Since the permeate is almost pure water (e.g., typically less than 50 mg L^{-1} total dissolved solids), the concentration polarization layer contains a higher concentration of solute compared with the bulk feed. This is significant because concentration polarization impairs water flux by reducing the mole fraction of water at the feed/membrane interface. Also, precipitation of sparingly soluble salts can occur if concentration polarization is severe, especially in concentrated feeds such as brines and reverse osmosis (RO) retentates. [75-78] Severe concentration polarization, as may be encountered in volatile organic compound (VOC) separation from water, can be prevented by the use of spacers or increased feed velocity which adds to the initial or operating costs of the system. [79] Solute rejection in membrane desalination of seawater and brines (e.g., typically ~99%) can be adversely affected by concentration polarization.

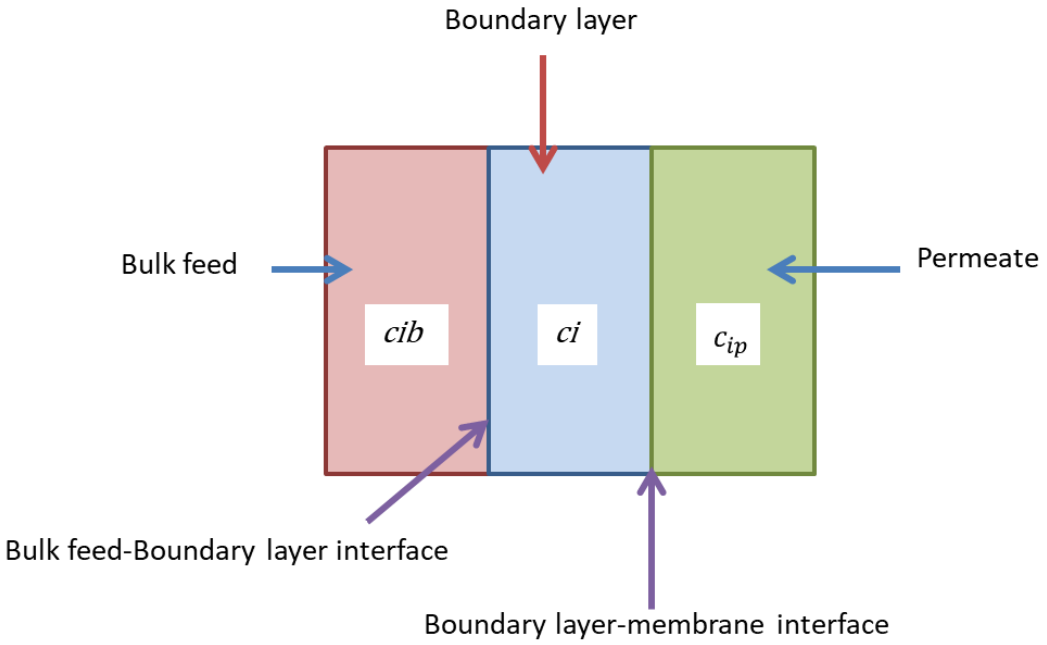

Figure 10: Membrane separation results in the permeate and boundary layer

Figure 10 shows the result of salt rejection by a membrane is three volumes of water, the bulk feed volume, the boundary layer volume and the permeate volume. In desalination, there is salt within each volume such that $c_i > c_{ib} > c_{ip}$. In this discussion, c_i [mol m^{-3}] is the average salt concentration in the boundary layer, c_{ib}[mol m^{-3}] is the salt concentration in the bulk feed, and c_{ip} [mol m^{-3}] is the salt concentration in the permeate condensate.

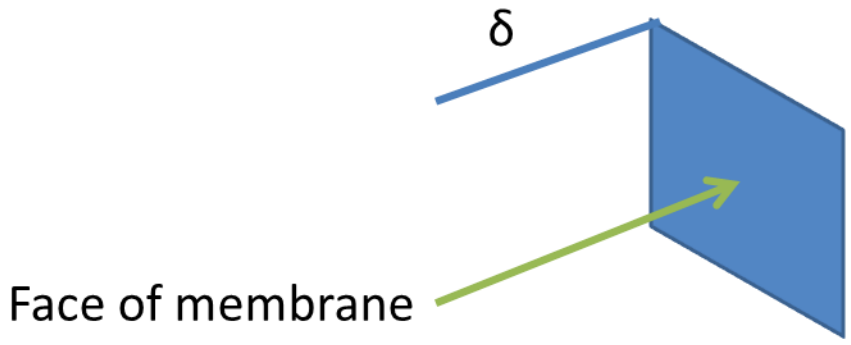

Figure 11: The boundary layer volume is defined by the membrane surface area and the boundary layer thickness δ [m]

Figure 11 shows that the volume of the boundary layer space is determined by the (known) membrane surface area and the boundary layer thickness to be determined, δ. Since the membrane (or overall separation process) creates the three different volumes, and the three different salt concentrations therein:

$$c_i = f(membrane) \quad (32)$$

Assume that δ is constant; this assumption is given in Winograd et al. (states that this is common model for mass transfer).[80] Consider two hypothetical membranes A and B, where A has a higher salt rejection than B. The result of salt separation by each membrane would be:

$$c_i\ (membrane\ A) > c_i(membrane\ B) \quad (33)$$

c_i increases with rejection. c_i is different for membranes having different separation properties.

This relationship is documented in Mattiasson et al. They state that the boundary layer is formed before steady state is reached by the dominance of convective solute flux towards the membrane over diffusive solute flux away from the membrane.[81] Since it

is difficult to directly measure solute concentration in the boundary layer and at the membrane surface, indirect methods have been employed in the literature to quantify concentration polarization.

2.2 Introduction to Methods for Quantifying Concentration Polarization

Mattiasson et al. point out that the evaluation of concentration polarization in lieu of direct measurement requires the solution of a system of non-linear equations of change, which include the rejection performed by the membrane.[81] This approach is mathematically complicated and requires computational assistance.

More commonly, a simpler approach using a steady state approximation is used. The steady state is defined by the equation:

$$\frac{dX}{dt} = 0 \quad (34)$$

I.e. there is no change in process variables with time. For lab-scale pervaporation, these include feed concentration, permeate concentration, feed flow, flux of all species, temperature, vacuum pressure. The state of the membrane, e.g. absence of swelling, absence of change in pore size, etc. is also a process variable. The solute concentration gradient in the boundary layer is also a process variable that does not change with time under steady state conditions.

At steady state, in membrane desalination, the diffusive solute flux away from the membrane is equal to the convective solute flux towards the membrane; with diffusion assumed to be the mechanism for solute transport through a dense membrane. This is shown in Figure 12.

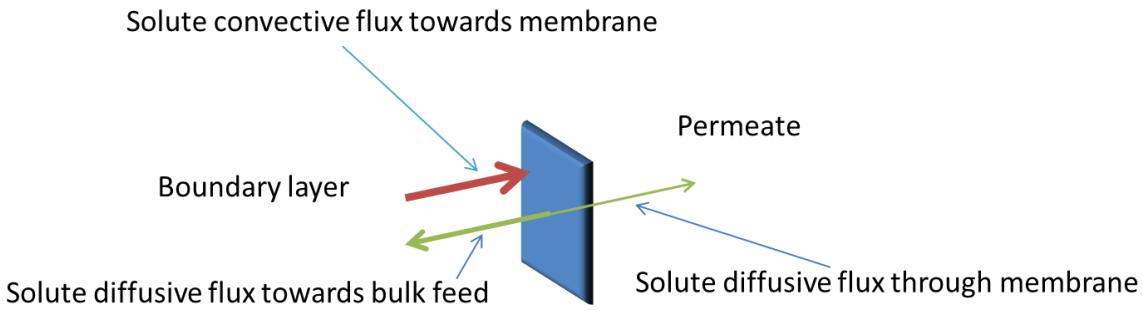

Figure 12: Solute convective flux towards membrane in the boundary layer is equal to the sum of solute diffusive flux in the boundary layer and solute diffusive flux through the membrane at steady state

Since, in membrane desalination, at steady state, the solute convective flux in the boundary layer towards the membrane is equal to the sum of the solute diffusive away from the membrane in the boundary layer and the solute diffusive flux through the membrane, it follows that solute convective flux towards the membrane in the boundary layer is greater than solute diffusive flux away from the membrane in the boundary layer at steady state. The exception to this is when the membrane is completely impermeable to solute and the solute permeate concentration is zero. In that case, the solute convective flux towards the membrane in the boundary layer is equal to the solute diffusive flux towards the bulk feed (away from the membrane).

Many studies of membrane transport in the feed side boundary layer use the steady state dimensionless Peclet number (Pe) help to describe the concentration polarization effect. [2, 25, 28, 29, 40, 79, 82-88] Pe is generally defined by equation (35) and specifically defined by equation (36) for membrane separations.[25, 85] In equation (35), solute convective flux is solute convective flux in the boundary layer, and solute diffusive flux is solute diffusive flux in the boundary layer. In membrane desalination, at

steady state, the Peclet number is greater than one based on the discussion in the previous paragraph. The exception is when the solute permeate concentration is zero: in that case the Peclet number equals one.

Please note all equations in this chapter describe mass transport in the boundary layer. Equation (36) is subject to the assumption that solute convective velocity can be equated with the volumetric water flux, v' [m s^{-1}], water flux is used as a convenient approximation for solute convective flux in membrane desalination and VOC separation.[40, 79, 85-88]

$$Pe = \frac{solute\ convective\ flux}{solute\ diffusive\ flux} \qquad (35)$$

$$Pe = \frac{v'}{D_i/\delta} \qquad (36)$$

In equation (36) the solute convective flux, v', has units of m s^{-1}. In equation (36) Pe is the Peclet number [dimensionless]; v' is the volumetric (solvent) flux, which is the same as the solute convective flux [m^3 m^{-2} s^{-1} or m s^{-1}]; δ is the boundary layer thickness [m]; and D_i is the solute mass diffusion coefficient [m^2 s^{-1}]. Here, equation (35) is used in a semi-quantitative way to estimate if the Pe is greater or less than 1, based on the solute profile in the boundary layer (e.g., whether or not the solute convective flux is larger or smaller than the solute diffusive flux (see supplemental information section 1). Equation (36) allows for quantitative, as opposed to semi-quantitative, evaluation of the Peclet number. If, for example, equation (35) shows a Pe >1, equation (36) should have the same result.

As already stated the steady state Peclet number is widely used to evaluate concentration polarization. That is, the steady state Peclet number is used to quantify the non steady state buildup of a solute concentration gradient in the boundary layer. This is clearly an approximation. Additionally, there is scant evidence, e.g. studies including direct measurement of solute concentration in the boundary layer, to support this usage. The objective of the indirect methods that use the steady state approximation is to obtain the thickness of the boundary layer. The volumetric water flux through the membrane, v', can be obtained directly from experiments. The quantity D_i/δ [m s^{-1}] is the solute boundary layer mass transfer coefficient (SBLMTC). The SBLMTC is calculated using one or more of three methods to be described in detail below: the RIS model, Sherwood correlations, or the Baker method. Since the diffusion coefficient is known, the purpose of all three methods is to find the boundary layer thickness, δ [m]. Once the boundary layer thickness is known, the SBLMTC, Peclet number, and concentration polarization modulus (the ratio of the solute concentration at the membrane surface to the solute concentration in the bulk feed) can be calculated. Baker uses an example of 20 μm and MWH states an expected range of 10-100 μm for δ.[25, 83] These estimates do not include lab scale pervaporation setups with low Reynolds numbers.

The concentration polarization modulus in a membrane process is defined by equation (37). In equation (37) C' is the concentration polarization modulus [-], c_{i0} is the concentration of species i at the feed membrane interface [mol m^{-3}], c_{ib} is the concentration of species i [mol m^{-3}] in the bulk of the feed. For reference, the concentration polarization moduli (equation (37)) found by Sherwood correlations in RO and MD processes are typically 1.0 to 1.2. [2, 25, 29, 83, 89, 90]

$$C' = \frac{c_{i0}}{c_{ib}} \qquad (37)$$

Once the volumetric water flux, v', and the SBLMTC are determined then the concentration polarization modulus, C' [-], can be calculated. The concentration polarization modulus is important because it (1) provides a measure of flux and specific energy impairment because of the solute accumulation in the boundary layer, (2) provides for an assessment of the risk of scaling from sparingly soluble inorganic compounds present in the feed, and (3) is related to the rejection obtained in membrane desalination. Equation (38) derived from the thin film boundary layer theory (TFBLT), requires the assumption that either the solute permeate concentration is close to zero or intrinsic enrichment, the enrichment in the absence of a boundary layer [25] is close to zero. With this assumption, then correspondingly the denominator in equation (35), the solute diffusive flux, is equated to the denominator of equation (36), the SBLMTC, D_i/δ. If equation (36) is substituted into equation (38), equation (39) is obtained.

$$C' = exp\left(\frac{v'\delta}{D_i}\right) \qquad (38)$$

$$C' = exp(Pe) \qquad (39)$$

2.3 TFBLT, 3 Methods for Determining C'

The thin film boundary layer theory (TFBLT) is the underlying theory for the evaluation of concentration polarization using a steady state approximation. [25, 40] The TFBLT postulates turbulent flow in the bulk feed parallel to the membrane. A layer of laminar flow exists between the bulk feed and the membrane, and this layer is regarded as stagnant with mass transport occurring only in a direction perpendicular to the membrane. TFBLT, as described by Brian [91] and as discussed by Baker [25], is based

on the steady state equation (40). Note that since equations (41-48, 38,39,64, and 76) follow from equation (40), they are also steady state equations.

$$v'c_{ip} = v'c_i - D_i\frac{dc_i}{dx} \qquad (40)$$

The left-hand side (LHS) of equation (40) represents the total flux of the solute. The first term on the right-hand side (RHS) of equation (40) represents the solute convective flux in the boundary layer, and the second term is the solute diffusive flux in the boundary layer. c_i [mol m^{-3}] is the concentration of species i in the boundary layer (i.e. a variable concentration based on position within the boundary layer, not the average concentration), c_{ip} [mol m^{-3}] is the permeate concentration of species i, v' [m s^{-1}] is water volumetric flux or water and solute convective velocity, and x [m] is the length dimension normal to membrane at the boundary layer. Equation (40) is represented conceptually as:

$$solute\ permeate\ flux = solute\ boundary\ layer\ flux \quad (41)$$

Where:

$$solute\ boundary\ layer\ flux =$$

$$solute\ convective\ flux + solute\ diffusive\ flux \quad (42)$$

Rearrange equation (40):

$$D_i\frac{dc_i}{dx} = v'\left(c_i - c_{ip}\right) \quad (43)$$

Rearrange equation (43):

$$\frac{v'dx}{D_i} = \frac{dc_i}{\left(c_i - c_{ip}\right)} \qquad (44)$$

Then set up the integration:

$$\frac{v'}{D_i}\int_0^{\delta} dx = \int_{c_{ib}}^{c_{i0}} \frac{dc_i}{(c_i - c_{ip})} \qquad (45)$$

In equation (45), c_{ib}[mol m^{-3}] is the solute concentration at the bulk feed/boundary layer interface (at position 0), i.e. the bulk feed solute concentration, and c_{i0}[mol m^{-3}] is the solute concentration at the boundary layer/membrane interface (at position δ-at the boundary layer/membrane interface).

Note that equation (45) places v' outside the integral, equation (61) assumes v' is a constant, not a function of c_i based on the steady state condition. This illustrates a problem with the steady state assumption: One of the concerns about concentration polarization is that v' is a strong function of c_i or c_{i0}. Also equation (45) does not include any representation of how the membrane separates water from solute, i.e. the boundary condition that the membrane may impose.

Completing the integration:

$$\frac{v'\delta}{D_i} = \ln\left(\frac{c_{i0} - c_{ip}}{c_{ib} - c_{ip}}\right) \qquad (46)$$

Taking the exponent of each side of equation (46):

$$\frac{c_{i0} - c_{ip}}{c_{ib} - c_{ip}} = exp\left(\frac{v'\delta}{D_i}\right) \qquad (47)$$

Equation (47) is also a steady state equation. In equation (47) c_{i0} is the solute concentration at the feed-membrane interface [mol m^{-3}], c_{ip} is the solute permeate concentration [mol m^{-3}], and c_{ib} is the solute concentration in the bulk feed [mol m^{-3}]. The steady state value for c_{ib} is the initial bulk feed concentration. If the volume of the bulk feed is much larger than the volume of the boundary layer then the steady-state condition will persist. In desalination, after significant diffusion of solute from the boundary layer

to the bulk feed has occurred, the bulk feed concentration will change, eventually becoming the retentate. Concentration polarization theory covers the time over which steady-state persists, i.e. that c_{ib} retains its initial value.

If c_{ip} is assumed to be close to zero:

$$\frac{c_{i0}}{c_{ib}} = exp\left(\frac{v'\delta}{D_i}\right) \quad (48)$$

Substituting from equation (37) results in:

$$C' = exp\left(\frac{v'\delta}{D_i}\right) \quad (38)$$

Equation (38) or equation (48) appear in numerous publications discussing concentration polarization. [2, 25, 29, 40, 79, 83, 90-92]

A brief introduction to the three methods:

One indirect method for determining the Peclet number is the resistance in series (RIS) model. This method has been employed to evaluate concentration polarization in the pervaporation separation of VOCs from water. [40, 82, 85-88]

Sherwood correlations have also been used to evaluate concentration polarization in pervaporation separation of VOCs from water, and have also been used extensively to evaluate concentration polarization in reverse osmosis and membrane distillation (MD). [2, 29, 92-96] Sherwood and P.L.T. Brian described this in 1967 for reverse osmosis. [92] However in his 1975 book on mass transfer, Sherwood describes the correlation as used for mass transfer to and from a smooth walled pipe carrying fluid having turbulent flow with a laminar boundary layer adjacent to the wall of the pipe.[97] Sherwood correlations are empirical in nature and are modified to account for the change of the boundary wall

from a smooth pipe to a porous membrane that experiences flux. Essentially, Sherwood correlations use the Reynolds number and Schmidt number to calculate the boundary layer thickness from the hydraulic diameter of the feed channel. While the use of Sherwood correlations is generally accepted in the membrane desalination literature their validity has also been questioned. [98]

The RIS model and Sherwood correlations rely on thin film boundary layer theory (equation (33)) for obtaining the concentration polarization modulus. A third method, also based on thin film boundary layer theory was developed by Wijmans and Baker, and applied to VOC separations. [79, 99] This method, to be described in detail below, was discussed in Baker's Membrane Technology and Applications, and will be referred to, for the sake of brevity, as "Baker's method". [25]

In the RIS model, D_i/δ is solute boundary layer permeance obtained by dividing solute molar flux, J [mol m^{-2} s^{-1}] by the boundary layer concentration differential [mol m^{-3}] (see supplemental information section 2b). [40, 85-88] In the cases of Sherwood correlations and the Baker method, D_i/δ [m s^{-1}] is defined by dividing the solute diffusion coefficient, D_i [m^2 s^{-1}], by the boundary layer thickness, δ [m]. [25, 93, 98] Sherwood correlations obtain the boundary layer thickness δ [m] from the feed channel hydraulic diameter using the Reynolds and Schmidt numbers. Since D_i [m^2 s^{-1}] is known the SBLMTC can be calculated. With Baker's method, the SBLMTC is obtained by graphical analysis as shown below.

This section discusses three different methods of determining the solute boundary layer mass transfer coefficient (SBLMTC), D_i/δ [m s^{-1}], (the RIS model, Sherwood correlations, and the Baker method) where D_i is the solute diffusion coefficient [m^2 s^{-1}]

and δ is the boundary layer thickness [m]. The Baker method is used to evaluate the concentration polarization effect in pervaporation desalination by applying it to data from published pervaporation desalination studies (which report flux and separation at different feed temperatures).[25] These results will be compared with previously reported results of Sherwood correlation analysis of the concentration polarization effect in MD in a following section.

This section has three objectives:

1. To show that the equation relating the concentration polarization modulus to the exponent of the Peclet number is derived from thin film boundary layer theory.
2. To explain three methodologies for obtaining the solute boundary layer mass transfer coefficient and the Peclet number: Sherwood correlations, the Resistance in Series model, and the method of Baker (based on thin film boundary layer theory).
3. To show how Baker's method can be applied to pervaporation desalination and to explain the limitations of the method..

RIS model

The resistance – in – series (RIS) model has been used extensively to describe concentration polarization in VOC separations. Figure 13 illustrates the steady state solute concentration profile in the boundary layer in the case of volatile organic compound (VOC) separation from water.

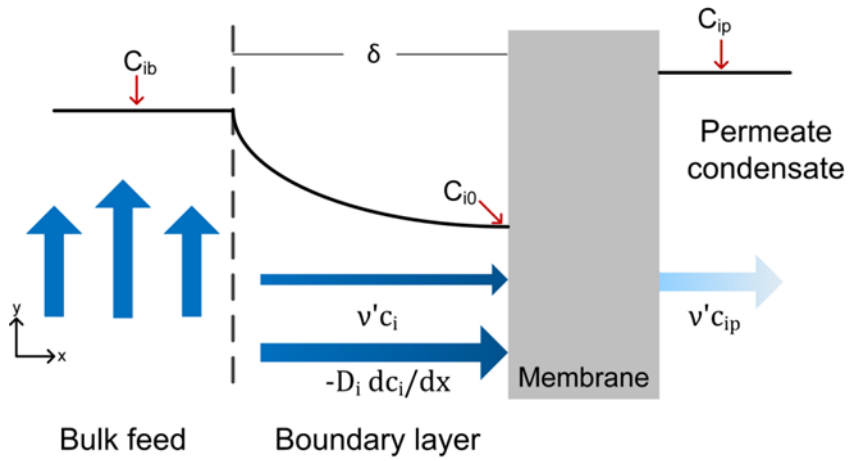

Figure 13: Pervaporation VOC separation from water. Solute concentrations in bulk feed, boundary layer and permeate condensate; relative contributions of convective and diffusive solute flux in the boundary layer to permeate flux.

Note that because the solute permeate concentration in the permeate vapor is governed by a vacuum in lab scale pervaporation, c_{ip}(permeate vapor) $< c_{i0}$. This separation increases the VOC concentration in the liquid permeate relative to the bulk feed. As a consequence, at steady state, VOC concentration in the boundary layer is depleted. Convective solute (VOC) flux and diffusive solute flux in the boundary layer are towards the membrane resulting in positive permeate flux. VOC transport in the boundary layer is dominated by diffusion. [79] When equation (35) is used to assess the Peclet number semi-quantitatively, it can be seen that the Peclet number should be less than one for this separation.

Table 2 is a summary of the semi-quantitative analysis using equation (35). As discussed the Peclet number is greater than one for pervaporation desalination and less than one for VOC separations by semi-quantitative analysis. In the membrane

desalination literature it is sometimes stated that the solute permeate concentration is zero or that the solute permeate concentration is stable over the range of operating conditions. Semi-quantitative analysis of those scenarios is represented by rows three and four in Table 2.

Table 2: Summary of semi-quantitative analysis using Peclet number

Semi-quantitative analysis	Where seen	Result
$D_i \frac{dc_i}{dx} > v' c_i$	Pervaporation VOC separation from water	$Pe < 1$
$v' c_i > D_i \frac{dc_i}{dx}$	Pervaporation desalination	$Pe > 1$
$v' c_i = D_i \frac{dc_i}{dx}$	Membrane desalination literature	$Pe = 1$
c_{ip} stable over range of operating conditions	Membrane desalination literature	$\delta = 0$, $\frac{v'\delta}{D_i} = 0$, SBLMTC undefined

If the convective term in equation (40) is assumed to be zero (i.e. diffusive VOC flux is much greater than convective VOC flux in the boundary layer), equation (49) is obtained.

$$\frac{D_i}{\delta} = \frac{J}{c_{ib} - c_{i0}} \qquad (49)$$

In equation (49), J is VOC flux [mol m^{-2} s^{-1}]. $\frac{D_i}{\delta}$ [m s^{-1}], the SBLMTC defined by equation (49) is equivalently defined by the resistance-in-series (RIS) model described below. There are two parts to the resistance in series model. First Ohm's law is used:

$$V = IR \qquad (50)$$

In Ohm's law, equation (50), R is the resistance [ohms], V is the driving force [volts], and I is the current [amperes]. In membrane applications, the driving force, "V" can be defined in terms of the partial pressure difference between two layers, $\Delta P_{i,layer}$, [kPa], or the chemical potential difference between two layers for species i $\Delta \mu_{i,layer}$, [J mol^{-1}], or the difference in concentration of species i between two layers, $\Delta c_{i,layer}$, [mol m^{-3}]:

$$\mathrm{V} = -\Delta P_{i,layer} \qquad (51)$$

$$\mathrm{V} = -\Delta \mu_{i,layer} \qquad (52)$$

$$\mathrm{V} = -\Delta c_{i,layer} \qquad (53)$$

Figure 14 shows the concentration profile that has to exist for the RIS model to be applied, for equation (55) to be valid.

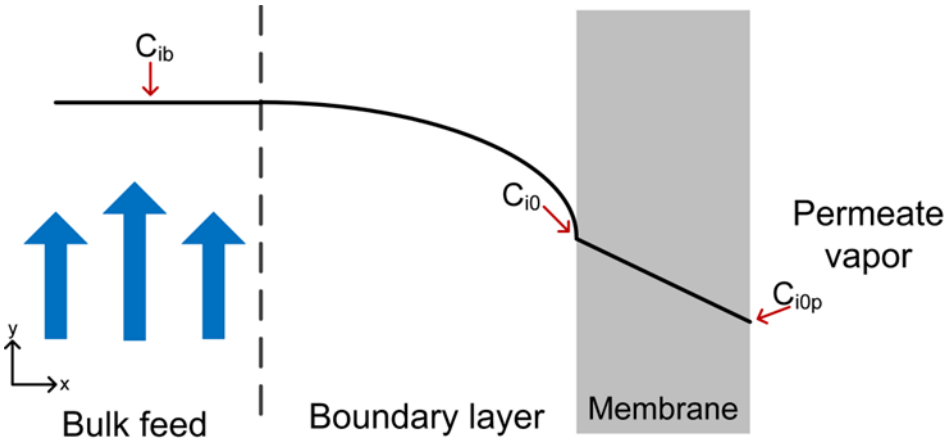

Figure 14: Pervaporation separation of VOC from water, VOC concentration profile in bulk feed, boundary layer, and permeate vapor.

The "current" can be defined as J_i the molar flux of species *i* [mol m^{-2} s^{-1}] (equation (60)).Therefore the resistance can be obtained as the reciprocal of the permeance of the species *i* of a layer, $F_{i,layer}$, in [mol m^{-2} s^{-1} kPa^{-1}], or [mol^2 m^{-2} s^{-1} J^{-1}], or [m s^{-1}]:

$$\mathrm{R} = \frac{1}{F_{i,layer}} \qquad (54)$$

Secondly, the RIS model states that the total resistance is the sum of the individual resistances. The result is equation (55).

$$\frac{1}{F_{i,total}} = \frac{1}{F_{i,boudary\ layer}} + \frac{1}{F_{i,membrane}} \qquad (55)$$

The solute permeance of the boundary layer, $F_{i,boudary\ layer}$, is the SBLMTC, $\frac{D_i}{\delta}$ [m s^{-1}].

In the RIS model the SBLMTC, $\frac{D_i}{\delta}$, is designated as k_0, [m s^{-1}] and is defined as:

$$k_0 = \frac{J_i}{(c_{ib} - c_{i0})} \qquad (56)$$

The RHS of equation (56) is identical to the RHS of equation (49). It is, therefore, logical to conclude that k_0 $\left(\frac{D_i}{\delta}\right)$ is equivalent to the solute diffusive velocity, the denominator of the RHS of equation (36).

This formulation of the RIS SBLMTC allows for comparison with the Sherwood SBLMTC, k_{SH}. k_0 can be obtained experimentally by evaluation of equation (57). [82, 100]

$$\frac{1}{F_{i,total}} = \frac{1}{k_0} + \frac{l}{Q_{i,int}} \qquad (57)$$

In equation (57) $F_{i,total}$ is the total permeance of species *i* [m s^{-1}],

$= total\ permeance, i$ $(\frac{m}{s})l$ is the membrane thickness [m], $Q_{i,int}$ is the intrinsic

membrane permeability of species i [m^2 s^{-1}]$= intrinsic\ membrane\ permeability, i.$ The total permeance is determined as a function of membrane thickness. Then a plot of equation (57) gives $\frac{1}{k_0}$ as the intercept and $\frac{1}{Q_{i,int}}$ as the slope. Once k_0 ($\frac{D_i}{\delta}$) is known then the concentration polarization modulus can be determined using the equation (4) from the main paper. This approach has been extensively used for the evaluation of concentration polarization in the pervaporation separation of VOCs from water. [40, 79, 82, 85-88, 99] The resulting $\frac{v'\delta}{D_i}$ values that have been obtained, as reported in the literature, either with k_0, the SBLMTC obtained by the RIS model approach, or with k_{SH}, the SBLMTC obtained by a Sherwood correlation, are less than one. This is the same result as predicted by the semi-quantitative approach described above. Figure 15 shows the concentration profile that exists in pervaporation desalination. NaCl concentration in the permeate vapor is close to zero.

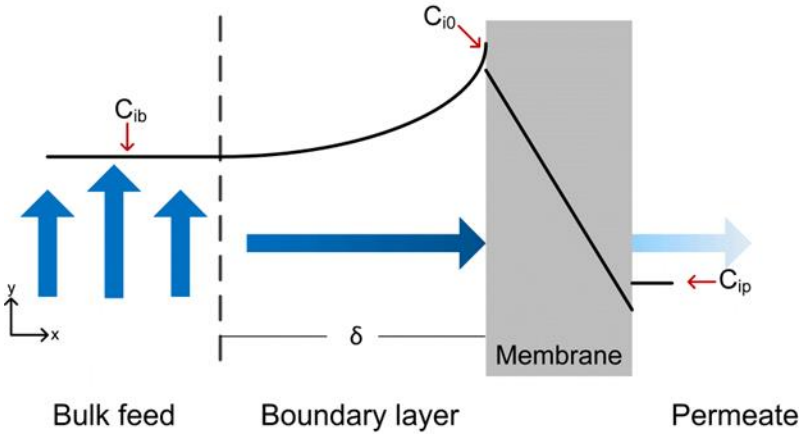

Figure 15: Pervaporation desalination, the salt concentration in the bulk feed, boundary layer, and permeate vapor.

In order to use the RIS model to determine the SBLMTC, the concentration profile $c_{ib} > c_{i0} > c_{ip}$, as seen in VOC separations, must exist. Solute flux in the positive x-

direction is generated by the convective component in pervaporation desalination. Convective solute flux in the boundary layer, not diffusive solute flux in the boundary layer, causes solute permeate flux in pervaporation desalination; because $c_{i0} > c_{ib}$, solute diffusion is away from the membrane. Although the solute (e.g. NaCl) does not fit the concentration profile necessary for the use of the RIS model, the solvent (water) does. Recently Wu et al. used the RIS model to show that concentration polarization was not significant in pervaporation desalination of high salinity water. [78] However their analysis did not include quantification of the SBLMTC. As Table 3 shows, concentration polarization moduli up to 6 could easily fall within experimental error. For example a reported flux of 1.2 kg m^{-2} h^{-1} results in a total permeance, F_T of about 0.86 kg m^{-2} h^{-1} kPa^{-1}.

Table 3: Membrane water permeance $\mathbf{F_M}$ as function of assumed concentration polarization modulus $\mathbf{C'}$ x_{wb} is the bulk feed water mole fraction, p^{sat} is the water saturation pressure, p_p is the permeate pressure, F_T is the total water permeance (membrane + boundary layer), C´ is the concentration polarization modulus, x_{w0} is the water mole fraction at the feed/membrane interface, F_B is the water permeance of the boundary layer, F_M is the water permeance of the membrane.

p^{sat}	p_p	Flux	F_T	$1/F_T$	Assumed C´	x_{w0}	F_B	$1/F_B$	F_M	$1/F_M$	$100F_M/F_T$
kPa	kPa	kg m^{-2} h^{-1}	kg m^{-2} h^{-1} kPa^{-1}				kg m^{-2} h^{-1} kPa^{-1}		kg m^{-2} h^{-1} kPa^{-1}		
3.17	1.7	1	0.707	1.41	2	0.97	18.4	0.05	0.74	1.36	103.98
3.17	1.7	1	0.707	1.41	3	0.95	9.39	0.11	0.76	1.31	108.14
3.17	1.7	1	0.707	1.41	4	0.93	6.37	0.16	0.80	1.26	112.49
3.17	1.7	1	0.707	1.41	5	0.92	4.86	0.21	0.83	1.21	117.04
3.17	1.7	1	0.707	1.41	6	0.90	3.95	0.25	0.86	1.16	121.81

A common method used to determine the SBLMTC in membrane desalination is with a Sherwood correlation. [2, 29, 83, 91, 92] In VOC separations from water, Sherwood correlations are used to obtain the SBLMTC and the results can be verified with a second method, the RIS model.

When Brian discussed the TFBLT to evaluate concentration polarization in reverse osmosis, he used the Chilton-Colburn analogy to obtain the SBLMTC.[91] The Chilton-Colburn analogy is similar to a Sherwood correlation. The Sherwood SBLMTC, k_{SH}, [m s^{-1}] is defined by the following equation:

$$k_{SH} = \frac{D_i}{\delta} \quad (58)$$

According to a review by Gegas and Hallstrom [98] the Sherwood correlation has the general form:

$$Sh = (constant) Re^{\alpha} Sc^{\beta} \quad (59)$$

The Sherwood number in equation (59) is also defined by the following equation:

$$Sh = \frac{k_{SH} d_h}{D_i} \quad (60)$$

Combining equations (59) and (60) results in equation (61).

$$\frac{k_{SH} d_h}{D_i} = (constant) Re^{\alpha} Sc^{\beta} \quad (61)$$

In equation (59), Sh is the Sherwood number [-], Re is the Reynolds number [-], Sc is the Schmidt number [-], α, β are empirical exponents [-], and, d_h is the hydraulic diameter [m].

Substituting equation (58) into equation (61) results in:

$$\frac{d_h}{\delta} = (constant) Re^{\alpha} Sc^{\beta} \quad (62)$$

Equation (62) allows for the determination of the boundary layer thickness, δ, if the diffusion coefficient and the bulk feed properties necessary for the determination of the Reynolds and Schmidt numbers are known. k_{SH} is equivalent to the SBLMTC, $\frac{D_i}{\delta}$ [m s^{-1}], and can be used in equation (38) to obtain the concentration polarization modulus.

There are a number of caveats to using Sherwood correlations; the reader is referred to the Gegas and Hallstrom review [98] for a complete discussion of these. Included in their discussion is the observation that the density and viscosity of the fluid changes in the boundary layer making predictions based on bulk fluid properties less accurate. Also, Sherwood correlations do not commonly take the roughness of the membrane surface, membrane pores, and the separation property of the membrane into account.

A Sherwood correlation can be represented as: [84]

$$\frac{d_h}{\delta} = \lambda Sc^{\frac{1}{3}} Re^{\beta} \quad (63)$$

The ratio of the hydraulic diameter to the boundary layer thickness is related to a product of exponents of the Reynolds number and Schmidt number. When the hydraulic diameter, Reynolds number, and Schmidt numbers are known, the Sherwood correlation determines the boundary layer thickness, δ. **When calculated with a Sherwood correlation, δ is independent of the membrane used for separation. Since C' and c_{i0} are related to $\exp(\delta)$, these quantities are also independent of the membrane used for separation when δ is calculated with a Sherwood correlation. In fact, a membrane is not necessary for the use of Sherwood correlations as they were originally intended to describe mass transfer to and from a smooth walled pipe. [97]**

This conclusion is supported by Marinas et al. They state that the solute boundary layer mass transfer coefficient (SBLMTC), $\frac{D_h}{\delta}$ or K_{cp} is related to feed channel geometry and feed water velocity: In their equation for the Sherwood number, λ and β are related to feed channel geometry. [84] Neither the SBLMTC or the Sherwood number is related to the separation performed by the membrane or the flux through the membrane. Sherwood correlations used to obtain the concentration polarization modulus are therefore approximations since the boundary layer solute concentration profile is defined by the separation ability of the membrane, as discussed.

The governing equation for the third methodology, the Baker method, is obtained from the TFBLT, equation (47). [25] The numerator and denominator on the LHS of equation (47) are divided by c_{ip} to obtain the following equation for membrane desalination (note that to derive a similar equation for VOC separations, the 1st and 2nd terms in the logarithmic arguments have to be switched to avoid taking the logarithm of a negative number):

$$ln\left(\frac{1}{E}-1\right)=ln\left(\frac{1}{E_0}-1\right)-\left(\frac{v'\delta}{D_i}\right) \qquad (64)$$

Where E is the enrichment and E_0 is the intrinsic enrichment, in equation (64) are defined by equations (65) and (66).

$$E=\frac{c_{ip}}{c_{ib}} \qquad (65)$$

$$E_0=\frac{c_{ip}}{c_{i0}} \qquad (66)$$

Equation (64) has not been previously described or used in the membrane desalination literature to date. The data required for the use of this method are flux and rejection

values at different temperatures, with other operating conditions (e.g., feed composition) remaining constant. Examination of equation (64) shows that:

$$\lim_{\delta \to 0} E = E_0 \qquad (67)$$

Intrinsic enrichment is the enrichment found in the absence of a boundary layer, according to Baker, and is a constant for a given membrane and feed concentration. [25] A plot of equation (64) results in a line. The 1st term on the RHS of equation (64) is the intercept, the 2nd term on the RHS is the volumetric water flux, v', the independent variable, and, δ/D_i, the reciprocal of the SBLMTC is the slope. The LHS of equation (64) is the dependent variable.

The 2nd term on the LHS of equation (64) is the product of the volumetric water flux, v', and the reciprocal of the SBLMTC, D_i/δ. This product is the Peclet number if equation (36) is used. When equation (64) is solved graphically, the slope has to be negative; if the slope is zero then $\delta = 0$. If the slope is positive, a negative value for Pe results, which is not possible.

Equation (64), a variant of the TFBLT equations, predicts that c_{ip} varies directly with v' in desalination (and inversely with v' in VOC separation). That is, rejection is inversely related to water flux in membrane desalination. Equation (64) is not applicable when c_{ip} or δ is equal to zero. The TFBLT equation (64) can be applied to separations such as pervaporation desalination where the solute is enriched at the feed side membrane surface and also to separations such as the VOC separation from water where the solute is depleted at the feed-membrane interface. For example, equation (64) was used to evaluate concentration polarization in VOC separation by varying membrane thickness or permeate vacuum pressure while keeping other operating conditions constant. [79, 99] As

shown in Figure 16 solute (toluene) enrichment (permeate concentration) decreased with increasing water flux.

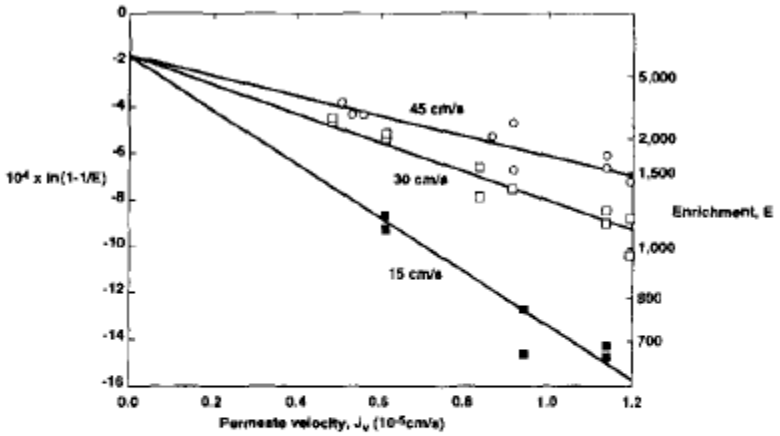

Fig. 12. TCE enrichment $\ln(1 - 1/E)$ as a function of permeate velocity (J_v). Feed temperature – 50°C; permeate pressures – 40, 60, 80 torr; and TCE concentration 0.1–100 ppm. The intrinsic enrichment of TCE obtained from this figure is ≈5700. The feed channel velocity for each set of data is shown in the figure.

Figure 16: Figure 12 from Baker et al. [99]. Enrichment (i = toluene, (c_{ip})) decreases with increasing flux (permeate velocity, J_v in the figure). J_v is obtained at different vacuum pressures in this case, instead of at different feed temperatures.

Equation (64) can be rearranged as:

$$c_{ip} = c_{ib}\left(\frac{\exp(Pe) - C'}{\exp(Pe) - 1}\right) \quad (68)$$

Equation (68) is not informative. When equation (39) is applied, the numerator on the RHS becomes zero. If equation (39) is not applied then it is not possible to obtain a solution for c_{ip}.

It is important to realize that equation (38) contains a simplification: water flux (v') is not represented as a function of c_i. In VOC separations, the bulk feed is dilute. Often the bulk feed has a water mole fraction greater than 0.99. [86] Concentration polarization in VOC separation results in a higher water mole fraction in the boundary layer. Therefore, v' does not change significantly with c_i due to concentration polarization in VOC separation by pervaporation. In desalination, the bulk feed water mole fraction varies depending on the salinity of the feed. A simulated sea water feed (3.2 wt% NaCl) has a water mole fraction of 0.99. Concentration polarization results in a higher salt concentration in the boundary layer, and often lower mole fraction of water, and water flux (v').

v' is held constant as part of the steady state assumption, but equation (40) and its progeny are used to calculate the concentration polarization modulus which is then used to show that v' is impacted by concentration polarization. Additionally at steady state convective solute flux in the boundary layer is equal to or greater than diffusive solute flux in the boundary layer so that at steady state the Peclet number is always equal to or greater than 1. Therefore, equation (38), equation (47), and equation (64) should be regarded as approximations.

Water flux in pervaporation desalination can be calculated based on the solution-diffusion model: [25]

$$v' = \frac{\text{Þ}_i}{l}\left(x_i \gamma_i p_i^{sat} - y_i p_p\right) \quad (27)$$

In equation 27, v' is water flux [kg m^{-2} s^{-1} or m^3 m^{-2} s^{-1} or m s^{-1}], Þ$_i$ is the permeability coefficient of water [kg m m^{-2} s^{-1} bar^{-1}], l is the membrane thickness [m], x_i is the liquid

phase feed side mole fraction of water [-], γ_i is the liquid phase activity coefficient of water [-], p_i^{sat} is the vapor pressure of water at the operating temperature , y_i is the gas phase mole fraction of water on the permeate side [-], and p_p is the permeate pressure. It can be seen from equation (27) that if the water mole fraction in the feed side boundary layer is reduced due to concentration polarization then water flux will also be reduced. In desalination, water flux (v') has a significant dependence on c_i.

TFBLT, equation (40) has another simplification: it does not consider membrane properties that affect salt permeate concentration or salt concentration in the boundary layer. Examination of equation (64) shows that salt permeate concentration increases with increased water flux (v') Peclet number, and concentration polarization modulus (C'). However, many dense membranes used in RO and pervaporation limit salt permeation so that salt permeate concentration decreases with increasing water flux (v'). [83] Equation (64) (rearranged for VOC separation as discussed above) was successfully used in a study (Baker et al.) showing a decrease in permeate VOC concentration with increasing water flux and Peclet number. [99]

Summary of the limitations of the indirect methods used to determine the concentration polarization modulus

The first limitation is the applicability of the steady state equations (38-48, 64, 76), which can collectively be referred to as the thin film boundary layer equations, to defining the concentration polarization modulus, a representation of the concentration gradient that builds up in the boundary layer prior to steady state.

The second limitation is that there is no functionality imparted by c_i to v' in equation (40). This is appropriate to equation (40) because v' is a constant at steady state. In

membrane desalination ν' is a significant function of c_i. Once the concentration polarization modulus is obtained, equation (27) is used to show the degree of flux impairment due the decreased water mole fraction in the boundary layer.

The third limitation is that equation (40) does not include a boundary condition imposed by the membrane. Equation (64), a reformulation of equation (40) requires that the solute permeate concentration increase with increasing water flux. As will be shown this is true in some, but not most cases. Since all three indirect methods rely on equation (38) to calculate the concentration polarization modulus, all three are subject to the three limitations described.

The third limitation is compounded by using Sherwood correlations since Sherwood correlations do not include the ability of the membrane to separate the feed components.

Three sections will follow:

1) A section on an analysis of the application of Baker's method to five previously published studies of pervaporation desalination
2) A section describing experimental work on pervaporation desalination with commercial membranes to demonstrate whether or not Baker's method can be applied
3) A section on RO/Pervaporation hybrid modelling with a focus on concentration polarization

2.4 Baker's Method Applied to Data from Previous Studies

The following section will briefly describe the five pervaporation desalination studies and three MD studies used for analysis. MD is compared to pervaporation

desalination because they are both thermally driven. This will then allow for a comparison of the concentration polarization moduli from the MD studies, obtained by Sherwood correlations, to the concentration polarization moduli in pervaporation desalination, obtained by Baker's method. For the pervaporation desalination studies, the method of data extraction for use in equation (64) will be given. The information provided in the MD studies was not sufficient for data extraction; in those studies, the SBLMTC was obtained by using Sherwood correlations.

Summary of the analyzed literature studies:

Pervaporation desalination studies:

The general method employed for data analysis was to extract flux and rejection data from each of the pervaporation studies. Table 4 presents the data extracted from the published studies. As can be seen in the experimental studies analyzed in this paper, flux, in general, is an increasing function of temperature while salt rejection is a decreasing function of temperature. Note that *E=1-R* so that *(1/E)-1* is also a decreasing function of temperature; c_{ip} is an increasing function of temperature.

Table 4: Input values for equation (64) pervaporation desalination studies.

Lead author	Membrane material	Feed	T [°C]	v' x10^7 [m s^{-1}]	ln((1/E)-1) [-]
An [5]	Clinoptilolite phosphate	1.4 g L^{-1} NaCl	25	19.4	3.32
			50	27.8	3.28
			75	33.3	2.84
			95	41.7	1.89
Drobek [6]	Silicate-1	75 g L^{-1} NaCl	20	4.86	5.29
			50	5.56	4.6
			75	8.33	3.89
Drobek [6]	Silicate-1	150 g L^{-1} NaCl	20	4.17	4.6
			50	4.86	4.18
			75	6.25	3.66
Lin [7]	Cobalt	40 g L^{-1} NaCl	20	0.88	6.9
			50	1.81	5.8
			75	3.33	4.7
Malekpour	NaA	0.15 g L^{-1} NaI	25	0.32	6.1
			40	0.33	6
			50	0.33	6
			65	0.36	5.8
Malekpour	NaA	0.21 g L^{-1}	25	0.6	5.08
			40	0.63	5.05
			50	0.65	5.01
			65	0.7	4.95
Malekpour	NaA	0.19 g L^{-1} $CsNO_3$	25	0.64	4.98
			40	0.66	4.95
			50	0.76	4.93
			65	0.9	4.95
Naim [9]	Cellulose	140 g L^{-1} NaCl	50	5.28	5.76
			60	6.94	4.3
			70	10.4	2.44
			80	8.33	5.34

plot $ln((1/E)-1)$ as a function of flux using equation (80) as discussed above. From these plots the intercept and the slope are obtained, with intercept $ln((1/E_0)-1)$ and slope δ/D_i. R values varied as shown in All the studies analyzed showed a significant difference in solute permeate concentration at the high and low temperatures tested The exception to this trend was the Naim et al. study [9] where the solute permeate concentration at 50 ℃ was similar to the solute concentration at 80 ℃. Below there are brief descriptions of each published pervaporation summarizing feed velocities and system geometries (if known), as well as details of the data extraction. In general, the analysis below is of the highest concentration feed solutions, which are most prone to concentration polarization.

In the An et al. study, natural zeolite, clinoptilolite, powder was combined with monopotassium phosphate and magnesium hydroxide; this was synthesized into a 2-inch diameter 1.3-1.5 mm thick membrane by dry powder pressing and high temperature steaming. [5] The discs were mounted on ceramic supports by autoclaving. The final shape of the membrane was 3.1 x 2.3 cm. The feed solution consisted of either 50 ppm Na or 1400 ppm Na. The feed was pumped across the membrane surface at a flow rate of 1 L min^{-1} in a cross-flow system. Feed temperatures were 25°C, 50°C, 75°C, and 95°C. The permeate was collected by means of a vacuum pump (unspecified level) and alcohol (unspecified alcohol type)-dry ice cold trap. [5] Flux and permeate conductivity were measured for each feed at each feed temperature and the data were presented in An et al. (Figure 7 and Table 3 in [5]) The results for the high conductivity feed were chosen for evaluation. To determine intrinsic enrichment, E_0, and concentration modulus through the use of equation (64), the flux measurements at the various temperatures were read from the bar graph (Figure 7 in [5]); and the enrichment values were determined from the table

(Table 3 in [5]), calculated as the ratio of the permeate conductivity to the feed conductivity at various temperatures. The lowest rejection in the An et al. study was 90.6 %. The flux and enrichment data, *ln((1/E)-1)*, are presented in Figure 17 and summarized in Table 4.

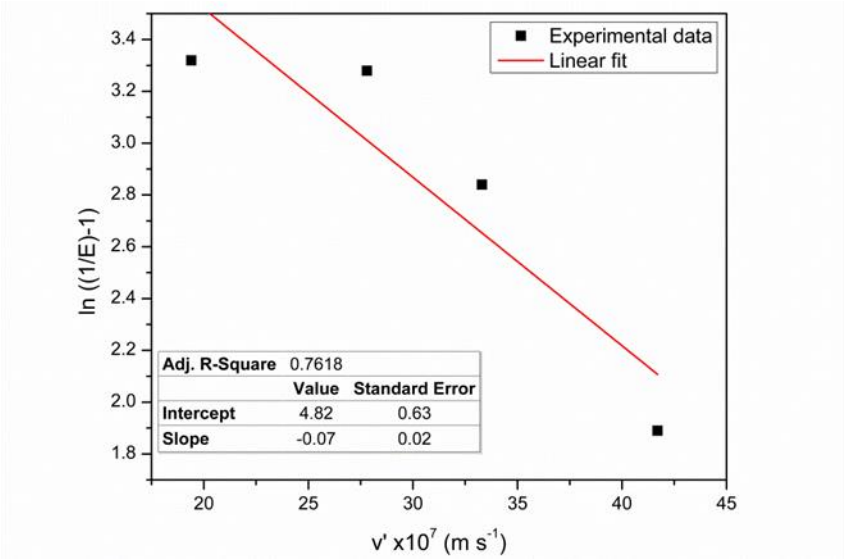

Figure 17: Experimental data extracted from [5] An et al. TFBLT data representation (points) and linear best fit, using equation (64), Baker's method. The intercept determines the intrinsic enrichment (E_0) and the slope determines the solute boundary layer mass transfer coefficient (SBLMTC).

In the Drobek et al. study, Silicalite-1 and ZSM-5 membranes were synthesized by secondary growth on ceramic tubular supports having dimensions 10/7 mm OD/ID and 50 mm length. [6] The feed solutions consisted of NaCl in concentrations of 0.3, 1, 3.5, 7.5, and 15 wt.%. Feed temperatures were varied for each feed concentrations; the operating temperatures were 21°C, 50°C, and 75°C. The feed was circulated through the stirred-batch pervaporation cell at 40 ml min^{-1}. The permeate was collected using a

vacuum pump and cold trap. Flux and rejection data were collected for each membrane, feed concentration, and temperature. The results were presented in Figure 3 in [6] Data for the Silicalite-1 membrane at 7.5 and 15 wt.% were selected for evaluation. The lowest rejection was 97.5%. The rejections were converted to enrichments, *E=1-R*. The flux and enrichment data (as *ln((1/E)-1)*) are presented in Figure 18 and Figure 19 and summarized in Table 4.

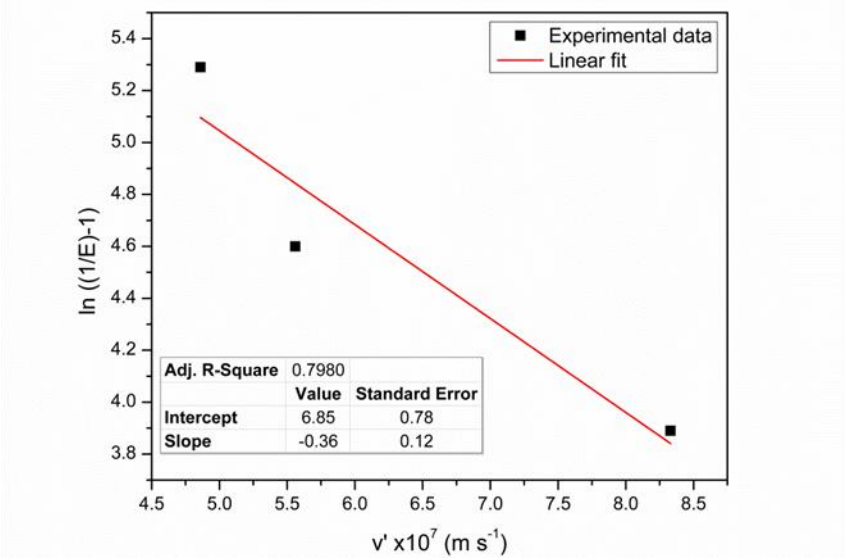

Figure 18: Experimental data extracted from [6] Drobek et al. 7.5 wt. % NaCl feed. TFBLT data representation (points) and linear best fit, using equation (64), Baker's method. The intercept determines the intrinsic enrichment (E_0) and the slope determines the solute boundary layer mass transfer coefficient (SBLMTC).

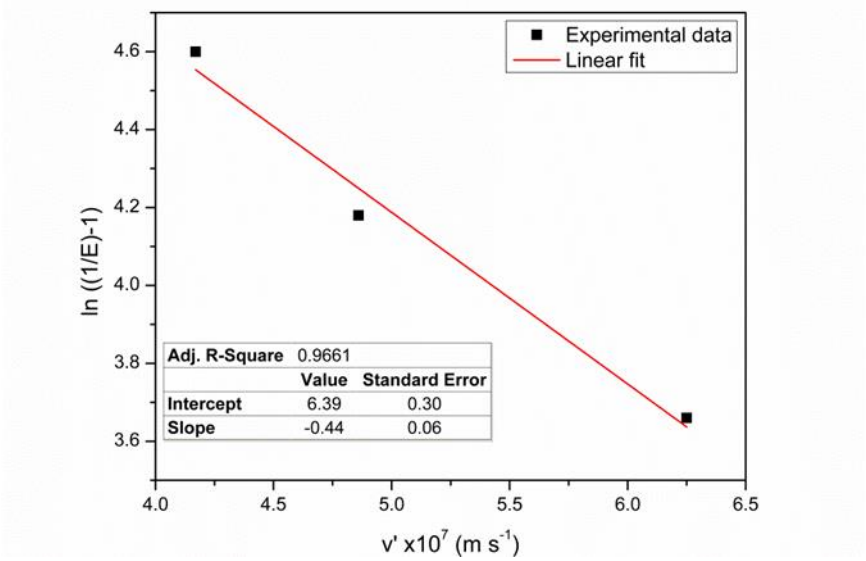

Figure 19: Experimental data extracted from [6] Drobek et al. 15 wt. % NaCl feed. TFBLT data representation (points) and linear best fit, using equation (64), Baker's method. The intercept determines the intrinsic enrichment (E_0) and the slope determines the solute boundary layer mass transfer coefficient (SBLMTC).

In the Lin et al. study Cobalt oxide silica was synthesized by a sol-gel method and membrane layers were coated on α-alumina tubes 15 cm in length and 1 cm outer diameter. [7] For pervaporation, the membrane tube was sealed at one end and at the other end a vacuum pump and cold trap were connected. The membrane tube was inserted into a 1.5 liter feed tank. The retentate was recycled at a flow rate of 8 ml min^{-1} and the feed was constantly stirred in this batch system. Feed concentrations were from 1 to 15 wt.% and the temperature of the feed tank was varied from 20 °C to 75 °C.
The data points selected for evaluation were for a feed of 3.5 wt.%. The flux data, at 3.5 wt.% feed, was read from Figure 7a in [7] and the rejection data was read from Figure 7b in [7]. The lowest rejection was 99%. The rejections were converted to enrichments

(*E=1-R*). The flux and enrichment data (as *ln((1/E)-1)*) are presented in Figure 20 and Table 4.

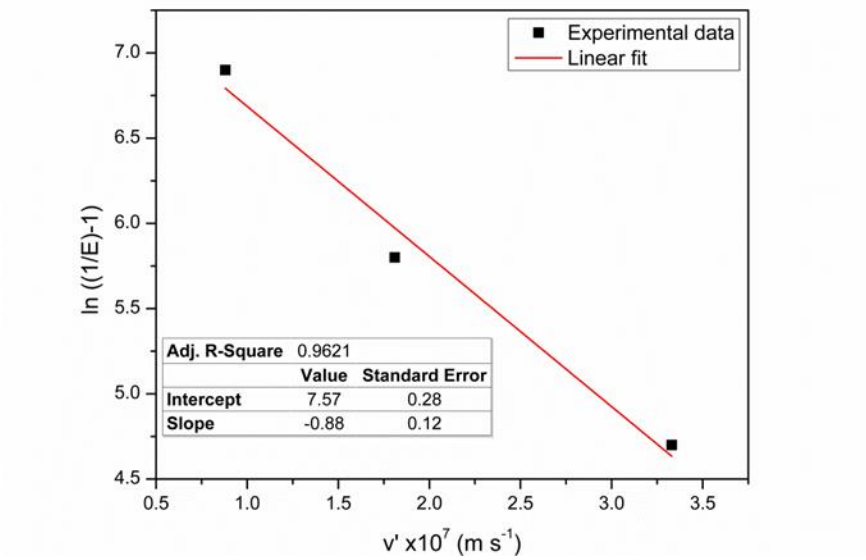

Figure 20: Experimental data extracted from [7] Lin et al. TFBLT data representation (points) and linear best fit, using equation (64), Baker's method. The intercept determines the intrinsic enrichment (E_0) and the slope determines the solute boundary layer mass transfer coefficient (SBLMTC).

In the Malekpour et al. study, ZSM-5 and NaA zeolite membranes were synthesized hydrothermally on the surface of α-alumina supports. [8] The membrane surface area in contact with the feed was 3.14 x 10^{-4} m^2. Pervaporation was conducted where the feed was pumped into the membrane module and the retentate was recirculated. Information as to the feed flow rate and whether the feed was stirred was not provided. The feed consisted of 0.001 mol l^{-1} analytical grade cesium nitrate ($CsNO_3$), strontium nitrate ($Sr(NO_3)_2$), or sodium iodide (NaI). Feed temperatures were 298 K, 313

K, 323 K, and 338 K. The permeate was collected using a vacuum pump and a liquid nitrogen trap.[8]

Flux and rejection data were presented in Figure 7 in [8]. The data for the NaA membrane were selected for evaluation in this paper. The flux data for I, Sr, and Cs were read from Figure 7a in [8] at the various temperatures. The rejection data was read from Figure 7b in [8]. The lowest rejection was 99.2%. The rejections were converted to enrichments (*E=1-R*). The flux and enrichment data (as *ln((1/E)-1)*) are presented in, Figure 21, Figure 22,and, Figure 23 and summarized in Table 4.

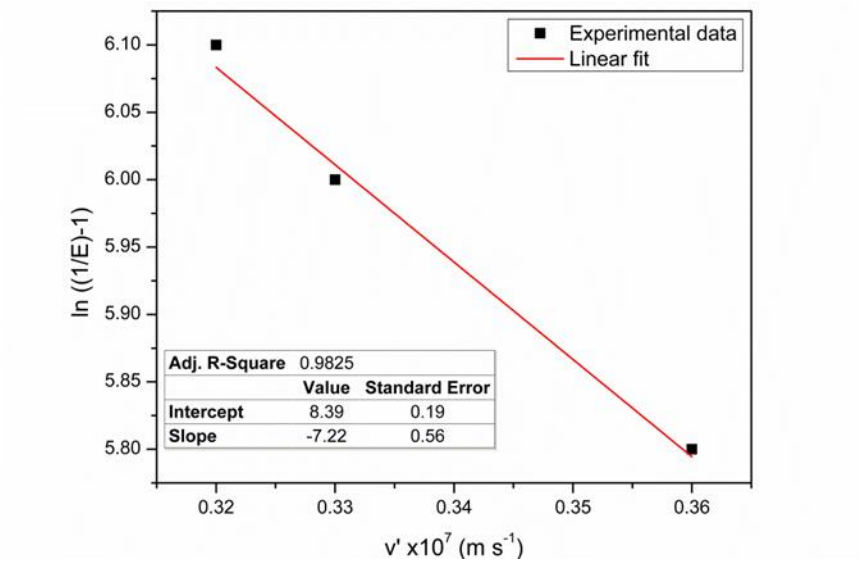

Figure 21: Experimental data extracted from [8] Malekpour et al. NaI feed. TFBLT data representation (points) and linear best fit, using equation (64), Baker's method. The intercept determines the intrinsic enrichment (E_0) and the slope determines the solute boundary layer mass transfer coefficient (SBLMTC).

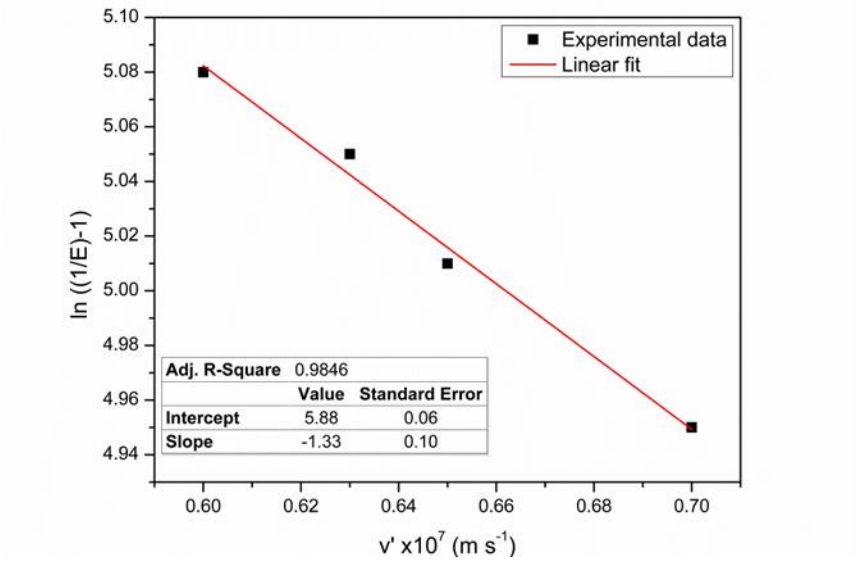

Figure 22: Experimental data extracted from [8] Malekpour et al. $Sr(NO_3)_2$ feed. TFBLT data representation (points) and linear best fit, using equation (64), Baker's method. The intercept determines the intrinsic enrichment (E_0) and the slope determines the solute boundary layer mass transfer coefficient (SBLMTC).

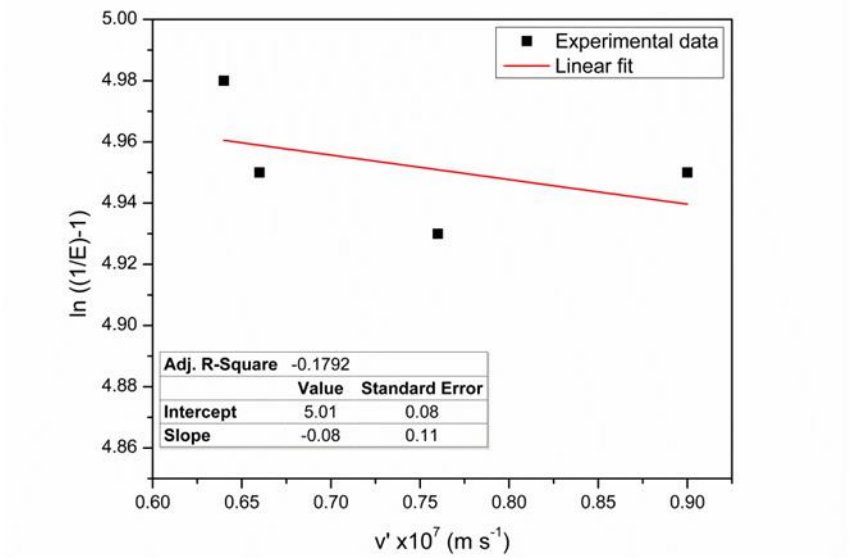

Figure 23: Experimental data extracted from [8] Malekpour et al. $Cs(NO_3)$ feed. TFBLT data representation (points) and linear best fit, using equation (64), Baker's method.

In the Naim et al. study, the membranes were asymmetric polymeric membranes consisting of "definite proportions" of cellulose acetate, dimethyl phthalate, dimethyl formamide, glycerol, and acetone. [9] The pervaporation cell consisted of two plexiglass rectangular parts, 2.5 cm thick, 15 cm long and 10 cm wide. 5 mm deep grooves were cut to induce feed turbulence. The feed was pumped into the cell and the retentate was recirculated; the flow rate was not specified. The feed consisted of NaCl solution ranging from 40-140 g L^{-1}. The feed temperatures were 50 °C, 60 °C, 70 °C, and 80 °C. The permeate was collected by means of a Liebig condenser through which cooling water was circulated. [9]

Flux and separation factors were determined for each feed composition at each temperature and the data was presented in Figure 4 and Figure 6 in [9]. The data for the 140 g L^{-1} NaCl was selected for evaluation. The flux data were read at various temperatures from Figure 4 in [9]. The separation factors were read from Figure 6 in [9] and converted to enrichments by means of equation (3) from Naim et al. [9] (the feed composition was known). The lowest rejection was 90%. The flux and enrichment data (as $ln((1/E)-1)$) are presented in Figure 24 and summarized in Table 4.

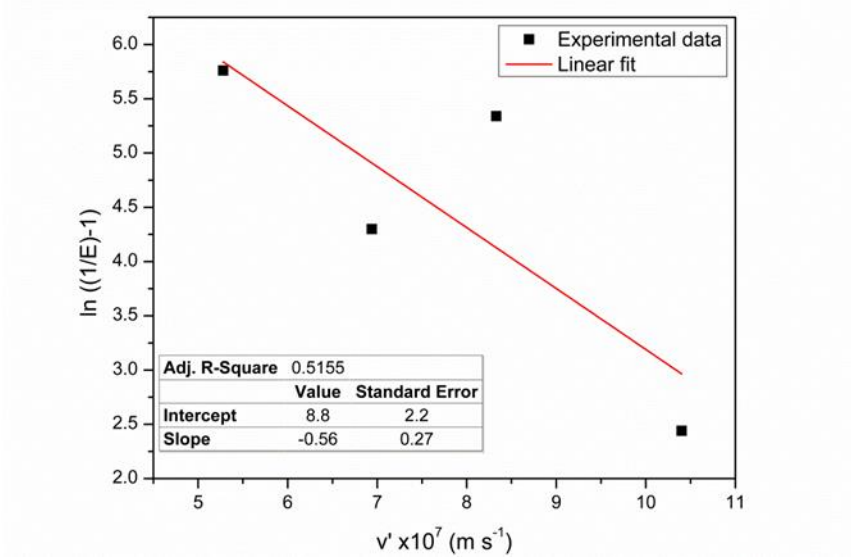

Figure 24: Experimental data extracted from [9] Naim et al. TFBLT data representation (points) and linear best fit, using equation (64), Baker's method. The intercept determines the intrinsic enrichment (E_0) and the slope determines the solute boundary layer mass transfer coefficient (SBLMTC).

2.5 Concentration Polarization in Membrane Distillation

In the Martinez-Diez et al. study, the membrane consisted of a flat sheet of porous polytetrafluoroethylene (PTFE) with an effective surface area of 33.7 x 10^{-4} m^2. [29] The feed solutions were 0, 0.55, 1.15, and 1.67 molar NaCl. The feed flow rate was 7, 11, or 15 mL s^{-1}. This was a direct contact membrane distillation setup where the permeate flow was countercurrent to the feed. The feed temperature was varied between 20 °C and 50 °C at 7 °C intervals. The temperature difference between the feed and permeate was maintained at 10°C. Flux measurements were made at various conditions, but salt rejection was not reported. Sherwood correlations were performed and concentration

polarization values were calculated according to equation (54). The main focus of this study was temperature polarization.

In the Jang et al. study, the setup up was a modified vacuum membrane distillation module using a porous PTFE membrane. The feed was 1 molar NaCl, with an initial volume of approximately 10 L. [90] The feed flow rate was varied between 20 and 40 L h^{-1} and the vacuum pressure varied between 70 and 90 mbar. The feed temperature was 60°C in all cases. Flux and rejection data were reported for the experiments, with all rejections >99.8%. Sherwood correlations were done, and concentration polarization values were calculated according to equation (54) and shown in The main focus of this study was temperature polarization.

In the Ali et al. study, the setup was a direct contact membrane distillation module using a polyvinylidene fluoride (PVDF) membrane with an effective surface area of 24.9 cm x 9.85 cm. [89] Three different types of experiments were done. In the first set of experiments, distilled water was the feed. Feed flow rates were varied between 30 L h^{-1} and 150 L h^{-1} while keeping the permeate flow rate at 50 L h^{-1}. The feed inlet temperature was kept constant at 55 °C while the permeate temperature was 10 °C. Secondly, the effect of feed temperature was evaluated by fixing the feed (distilled water) flow rate at 70 L h^{-1} and varying the feed temperature between 45 °C and 75 °C at 10 °C intervals. Third, the effect of solute was evaluated by changing the feed to 1 molar NaCl. Flux data was reported, but rejection data was not. Concentration polarization was calculated according to equation (54). The source of the boundary layer mass transfer coefficients was not specified, however, the Martinez-Diez et al. paper was cited. Presumably, the boundary layer mass transfer coefficients were calculated by means of Sherwood

correlations, as they were in Martinez-Diez et al. The main focus of this study was temperature polarization. Quantification of concentration polarization provided in the membrane distillation studies is summarized in Table 5.

Table 5: $v'\delta/D_i$ and concentration polarization in MD, C' is the concentration polarization modulus, the SBLMTC used to obtain $v'\delta/D_i$ were obtained by using Sherwood correlations.

Lead author	NaCl feed concentration	MD type	Membrane material	$v'\delta/D_i$, [-]	C'
Martinez-Diez [29]	0.155–1.67 M	DCMD	PTFE	0.04	1.04
Jang [90]	1 M	Modified VMD	PTFE	0.3	1.35
Ali [89]	1–2 M	DCMD	PVDF	0	1

2.6 Results and Discussion: Baker's Method applied to Previous Studies

Intrinsic enrichment values, E_0, are obtained from the intercepts from Figure 17-Figure 24 and are shown in Table 6. The values for the Peclet numbers ($v'\delta/D_i$) found in Table 6 are obtained by multiplying the volumetric water flux values v' [m s^{-1} x10^{7}] from Table 4 by the δ/D_i [s m^{-1} x10^{-6}] values found in Table 6. C' values in Table 6 are obtained by using equation (54).

Table 6 shows the results of the evaluation of the data from Table 4 with equation (64).Table 6 presents a summary of the SBLMTC, the Peclet numbers, C' (concentration polarization modulus), and E_0 (the intrinsic enrichment) for the data presented in Table 4 and Figure 17-Figure 24.

Table 6: v'δ/D_i and Concentration polarization in pervaporation desalination, δ/D is the reciprocal of the SBLMTC, C' is the concentration polarization modulus, E_0 is the intrinsic enrichment.

Lead author	Feed	δ/D x10^{-6} [s m^{-1}]	$v'\delta/D_i$ [-]	C' [-]	E_0 x10^3 [-]
An [5]	1.4 g L^{-1} NaCl	0.65	1.26–2.71	3.53–15.1	0.8
Drobek [6]	75 g L^{-1} NaCl	3.61	1.76–3.19	5.79–24.3	1
Drobek [6]	150 g L^{-1} NaCl	4.33	1.82–2.73	6.19–15.4	2
Lin [7]	40 g L^{-1} NaCl	8.81	0.78–2.93	2.170–18.8	0.5
Malekpour [8]	0.15 g L^{-1} NaI	68.39	2.19–2.46	8.92–11.7	0.3
Malekpour [8]	0.2 g L^{-1} $Sr(NO_3)_2$	13.94	0.78–0.91	2.19–2.49	3
Malekpour [8]	0.19 g L^{-1} $CsNO_3$	0.8	0.05–0.07	1.05–1.07	7
Naim [9]	140 g L^{-1} NaCl	5.61	2.96–4.68	19.4–107	0.3

The values for the concentration polarization moduli for the membrane distillation studies found in Table 5 are significantly lower than the concentration polarization moduli for the pervaporation desalination studies found in Table 6. This is likely due to differences in process design. However as will be seen in the next section, Sherwood correlations appear to produce lower values for the concentration polarization modulus then the method of Baker.

2.7 Comparison of Baker's Method with Sherwood Correlations:

MWH uses the following Sherwood correlation to obtain the SBLMTC (K_{cp}):[83]

$$K_{cp} = \frac{(0.023)(1.35 * 10^{-9}\left(\frac{m^2}{s}\right))Re^{0.83}Sc^{0.33}}{D_h(m)} \quad (69)$$

This equation for $K_{cp}$is the one used in the process design example (p1390) and is for a spiral wound membrane module. It differs from the three other Sherwood correlations given for the same process on (p1371-1372). MHW states "numerous" correlations exist (p1372).[83]

It can be seen that smaller values of K_{cp}will result from larger values of hydraulic diameter (D_h) and smaller Reynolds numbers or smaller Reynolds number exponents. Smaller values of K_{cp}will result in larger values for the Peclet number and concentration polarization modulus.

In the example given in 17-7, [83]

$$K_{cp} = 5.36 * 10^{-5}\left(\frac{m}{s}\right) \quad (70)$$

Then:

$$\delta = \frac{D_i}{K_{cp}} \quad (71)$$

$$\delta = 30\ \mu m$$

In the MWH example, D_h=0.25 mm, Re= 192, and Sc= 742 [83]

Where:

$$Sc = \frac{\eta}{\rho D_i} \quad (72)$$

I.e. water viscosity divided by the product of water density and the salt diffusion coefficient.

Note: p418 in MHW states [83]

$$\delta \cong 10 - 100\ \mu m$$

A Reynolds number obtained from the corresponding author of the Naim et al. study was 2190.

Their pervaporation cell had dimensions of 15cm x 10cm x 2.5cm [9]

Using the following equation from MWH,[83]

$$D_h = \frac{4 * cell\ volume}{wetted\ surface} \quad (73)$$

$$D_h = \frac{4 * 15 * 10 * 2.5}{15 * 10}\ cm$$

$$D_h = 0.1\ m$$

Using 0.1 m for $D_{h,}$ 2190 for the Reynolds number and 742 for the Schmidt number (same number as in the MWH example) results in:

$$K_{cp} = 1.63 * 10^{-6}\left(\frac{m}{s}\right)$$

$$\delta = 830\ \mu m$$

$$Pe = 0.63$$

Using Baker's method:

$$K_{cp} = 1.78 * 10^{-7}\left(\frac{m}{s}\right)$$

$$\delta = 7584\ \mu m$$

$$Pe = 5.84 \quad \left(v' = 10.4 * 10^{-7}\ \left(\frac{m}{s}\right)\right)$$

MWH gives this Sherwood correlation for laminar flow past a flat plate (p419):[83]

$$K_{cp} = \frac{(0.664)(1.35 * 10^{-9}\left(\frac{m^2}{s}\right))Re^{0.5}Sc^{0.33}}{D_h(m)} \quad (74)$$

Using the Reynolds number and D_h from the Naim study results in

$$K_{cp} = 3.8 * 10^{-6} \left(\frac{m}{s}\right)$$

$$\delta = 355\ \mu m$$

$$Pe = 0.27$$

Both Sherwood correlations result in Peclet numbers less than one. The Baker method results in a Peclet number of 5.84

It is not stated in MWH where the Sherwood correlation for flow past a flat plate came from or whether there are also numerous correlations for this. Naim et al. put grooves in the feed channel-the presence of these may require a different Sherwood correlation. Gomez et al. give the following Sherwood correlation for a plate and frame module:[101]

$$K_{cp}\left(\frac{m}{s}\right) = \frac{1.85\ [ReSc\left(\frac{D_h}{L}\right)]^{.33} *}{D_h(m)} 1.35 * 10^{-9} \frac{m^2}{s} \qquad (75)$$

Where D_h is two times the height or 5 cm, and L is the length or 15 cm.

The result is:

$$K_{cp} = 4.07 * 10^{-6} \left(\frac{m}{s}\right)$$

$$\delta = 331\ \mu m$$

$$Pe = 0.26$$

$$C' = 1.30$$

If the Reynolds number exponent in equation (91) is changed to 0.27, the following values are obtained:

$$K_{cp} = 2.05 * 10^{-6} \left(\frac{m}{s}\right)$$

$$\delta = 540\ \mu m$$

$$Pe = 0.42$$

$$C' = 1.52$$

Discussion of comparison between Baker's method and Sherwood correlations. Although only one example was given, the results show that the values for the Peclet number determined by Baker's method are significantly higher than the values obtained by Sherwood correlations. This is significant since the concentration polarization modulus is computed by taking the exponent of the Peclet number (equation (54)). The difference in Peclet numbers between the two methods is caused by the difference in the boundary layer thickness, δ, obtained by the two methods. The boundary layer thickness calculated by Baker's method was an order of magnitude higher than those obtained by Sherwood correlations. The boundary layer thickness, calculated in the example given, as obtained by a Sherwood correlation was significantly higher (almost an order of magnitude) than the range stated in MWH. Varying the Reynolds number from 0.33 to 0.27 caused a small change in the calculated concentration polarization modulus. The effect of varying the Reynolds number exponent will be explored again in the section on pervaporation modelling.

2.8 Factors Affecting C' using Baker Method

To discuss the factors influencing *C'* equation (92), obtained from equations (53) and (63), will be used.

$$C' = \frac{exp\left(\frac{v'\delta}{D_i}\right)}{1 + E_0\left(\left(exp\left(\frac{v'\delta}{D_i}\right) - 1\right)\right.} \qquad (76)$$

Equation (76) shows C' is a function of intrinsic enrichment, E_0. As discussed, intrinsic enrichment is an enrichment in the absence of a boundary layer (see equation (67)). However, examination of equation (64) and Figure 17-Figure 24 suggest an alternate definition of intrinsic enrichment:

$$\lim_{v' \to 0} E = E_0 \qquad (77)$$

According to equation (77), intrinsic enrichment is enrichment as volumetric flux approaches zero. It follows from equations (65) and (66) that as enrichment approaches intrinsic enrichment, the bulk feed concentration approaches the feed concentration at the feed-membrane interface. It can also be seen from an examination of Figure 17-Figure 24 and equation (64) that as enrichment approaches intrinsic enrichment, the solute permeate concentration approaches a minimum value. Considering equations (64) and (77), this reflects an often seen trade-off between permeability and selectivity.

Intrinsic enrichment is similar to the separation factor used frequently in pervaporation in that it depends on operating conditions (e.g., feed concentration). Intrinsic enrichment can be thought of as an "ideal" separation factor. In membrane desalination, the objective is to have the solute separation factor as small as possible. With the feed salinities typically investigated in membrane desalination (e.g., simulated seawater), solute enrichment and separation factor agree within 1%. In general, for desalination, the intrinsic enrichment can take on a maximum value of 1 and is usually much less than 1. For example, the intrinsic enrichments obtained in this study are in the range of 10^{-4} to 10^{-3}. The ability of the membranes used in the studies, from which the data were extracted, to separate water from the feed solutions has little effect on the concentration polarization observed. This is seen by comparing the result of calculating C' using

equation (38) as presented in Table 6 with those obtained using equation (76) as seen in Figure 25.

The conclusion that the membranes have little to no effect on the level of concentration polarization is based on TFBLT equation (76) and illustrates one of the limitations of the theory. The membranes effect the separation and determine the concentration gradient in the boundary layer, and the thickness of the boundary layer, prior to steady state being reached. [81]

Figure 25 is a theoretical plot of the concentration polarization modulus as a function of exp(Pe) using equation (76). The X axis scale and intrinsic enrichments shown in Figure 25 are based on the values in Table 6.

The largest difference in the concentration polarization modulus was found with the Naim et al. data, obtained by equation (38) and equation (76); a concentration polarization modulus of 107 was obtained using equation (38). Using equation (76) the calculated value for the concentration polarization modulus is 103.7, about a 3% difference. The low values of E_0 also show why it is appropriate to simplify equation (76) to equation (38) to calculate the concentration polarization modulus in pervaporation desalination. The Malekpour et al. study is not represented in Figure 25 since the low levels of polarization observed suggest that separation has virtually no effect on polarization.

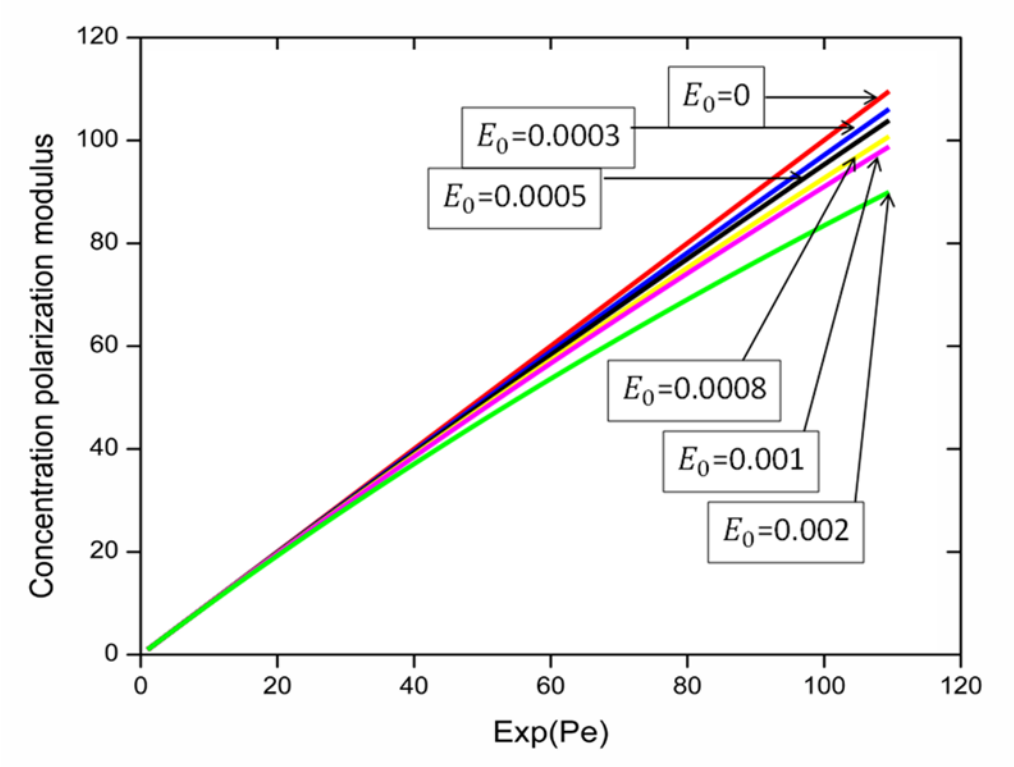

Figure 25: Concentration polarization modulus, C', as a function of exp(Pe) using equation (38), (E_0 = 0), and for values of intrinsic enrichment found for the Naim et al., An et al., Lin et al., and Drobek et al. studies using equation (76).

The diffusion coefficient, D_i also can influence the value of the concentration polarization modulus, *C'*. A value for the NaCl diffusion coefficient in membrane desalination of 10^{-9} m^2 s^{-1} can be assumed (Baker). [25] The differences in concentration polarization in the studies using NaCl solution feeds, therefore, cannot be attributed to differences in the NaCl diffusion coefficient.

The concentration polarization modulus, *C'*, is also a function of boundary layer thickness, δ. Strategies to reduce boundary layer thickness, δ, are often used to reduce concentration polarization, consisting of different ways to increase fluid turbulence in the feed channel. Conventionally, a first estimate of the degree of turbulence is based on the

Reynolds number. However, none of the studies from which the data for calculation of concentration polarization moduli were obtained included enough information to calculate the Reynolds number.

In the Naim et al. study the feed channel consisted of "hexagonal grooves, 5 mm deep, with numerous lateral corrugations to induce partial turbulence of the flowing liquid on the feed side of the membrane". [9] The Malekpour et al., Lin et al., and Drobek et al. studies used a dead end configuration. [6-8] The Drobek et al. and Lin et al. studies included a stirrer on the feed side to "reduce concentration polarization". [6, 7] The An et al. study used a cross-flow configuration. [5]The Martinez-Diez et al. and Ali et al. studies used a cross-flow configuration and the Jang et al. study used a cross-flow configuration and was pilot scale. [29, 89, 90]

Using the literature value for the NaCl diffusion coefficient of 10^{-9} m^2 s^{-1} together with the values for the reciprocal of the SBLMTC given in Table 6 results in values for δ of 4-9 mm for the Naim et al., Lin et al., and Drobek et al. studies and 650 μm for the An et al. study. The values for δ in the Malekpour et al. study ranged from 800 μm to 68 mm. Using the values for the concentration polarization moduli provided by the MD studies, it was possible to calculate the values for the SBLMTC and then calculate the value for the boundary layer thickness, δ. The value for δ in the Martinez-Diez et al. study was 47 μm and the value for δ in the Jang et al. study was 107 μm. The values for the boundary layer thickness for the MD studies are based on Sherwood correlations. The values for δ for the pervaporation desalination studies obtained here are very high and make a significant contribution to the observed severity of concentration polarization. The cross-flow setup

used by An et al., and the MD studies, was the most effective in reducing boundary layer thickness.

The value for δ in the Ali et al. study was negligible, since the Peclet number was nearly zero. At steady state, the bulk feed concentration was identical to the solute concentration in the boundary layer (see Table 10 in the Ali et al. study [89]). The values for the solute concentration in the boundary layer were calculated by Ali et al. by using an equation similar to equation (54). Presumably, the SBLMTC was calculated by using a Sherwood correlation, although this was not specifically stated. Ali et al. claim that starting with a bulk feed of initial volume and concentration, at steady-state part of the bulk feed initial volume has become permeate with a solute concentration that approaches zero. They suggest this occurs while the remainder of the initial volume of the bulk feed (now as bulk volume and boundary layer volume) has retained the initial concentration of the bulk feed. That is, a simple mass balance suggests that what Ali et al. described is not possible, unless one or more of the underlying assumptions of TFBLT, for example, the steady-state assumption, are not valid. It is also possible that the Sherwood correlation is not accurately representing the SBLMTC, i.e., that the value for the boundary layer thickness, δ, is not accurate.

The last variable that can influence the concentration polarization modulus, C', is the volumetric water flux, v'. One effect of increasing the volumetric water flux is to increase the Peclet number thereby increasing the concentration polarization modulus. For example, the volumetric water fluxes in the Naim et al. study were higher than those obtained in the Lin et al. and Drobek et al. studies, as seen in Table 4. Since the boundary layer thickness was similar in those studies, the result of the higher volumetric fluxes in

the Naim et al. study was higher values for the concentration polarization moduli. Another effect of increasing volumetric water flux in the studies examined is seen from an examination of equation (64). Increasing volumetric water flux by increasing the feed temperature for a given solute feed concentration results in a higher solute permeate concentration.

The values for the Peclet number for the pervaporation desalination studies, in general, conform to the expectation according to the semi-quantitative analysis because they are almost all greater than 1. On the other hand, the values for the Peclet number for the MD studies do not conform to the semi-quantitative analysis. This suggests, as described above for the Ali et al. study, that one or more of the assumptions of the TFBLT may not be valid or that the Sherwood correlations are not accurately producing the SBLMTC.

The Drobek et al. study used two different NaCl feed concentrations. As seen in equation (76), the concentration polarization modulus is not a direct function of feed concentration. Concentration polarization was less severe at the higher feed concentration, consistent with the findings in the Jang study. On the other hand, it appears that there is a threshold feed concentration below which concentration polarization is not easily detectable. The higher feed concentration resulted in a higher solute concentration in the boundary layer. At 150 g L^{-1} the concentration of NaCl at the membrane surface, based on the concentration polarization modulus, was 40 M. At 75 g L^{-1} the NaCl concentration at the membrane surface was 31 M. These concentrations resulted in water mole fractions at the membrane surface of 0.64 for the 150 g L^{-1} NaCl feed and 0.58 for the 75 g L^{-1} feed. In addition, at the NaCl concentrations at the

membrane surface, the water activity coefficient will be significantly less than one. The result of the low water mole fraction and activity coefficient yielded significantly lower water flux at the higher, 150 g L^{-1}, feed concentration as seen in Table 4. An additional result was that the intrinsic enrichment was higher at the higher feed concentration as seen in Table 6. Water flux through a pervaporation membrane is a direct function of water mole fraction at the feed-membrane interface. The Lin et al. study of a 40 g L^{-1} NaCl feed is representative of a seawater feed. The bulk feed water mole fraction is 0.987. At 75°C, the concentration polarization modulus was 18.8 which results in a water mole fraction at the feed-membrane interface of 0.811. Thus, the observed flux is about 80% of what would have been realized in the absence of concentration polarization, according to the Baker method analysis. Since the solubility limit of sodium chloride is exceeded at the calculated level of polarization this result is, again, an approximation.

Summary:

In this section, the results (the levels of concentration polarization) of analysis of five previously reported studies using Baker's method (equation (64)) were presented. Comparisons were made to results of previously published membrane distillation studies and results of Sherwood correlations. A theoretical analysis of the factors affecting concentration polarization was presented (equation (76) and Figure 25). Examination of Figure 17 -Figure 24 and Table 6 shows negative values for the slopes of the lines and positive values for the Peclet numbers.

2.9 Evaluation of Experimental Data using Baker Method

The pervaporation setup, shown in Figure 26 and Figure 27, consists of a pervaporation cell accommodating a 20.25 cm^2 membrane. The membrane is supported

within the cell by a porous 316 stainless steel support. The cell holds approximately 45 cc of fluid on the feed side. The feed is fed into the cell from a feed reservoir holding approximately 80 cc by a peristaltic pump at a rate of 1 cc/second. The 316 stainless steel feed reservoir can be heated with a heating jacket. The feed channel is equipped with thermocouples. The driving force on the permeate side is created by an Edwards vacuum at 20 millitorr. The permeate vapor is collected in a cold trap cooled by liquid nitrogen.

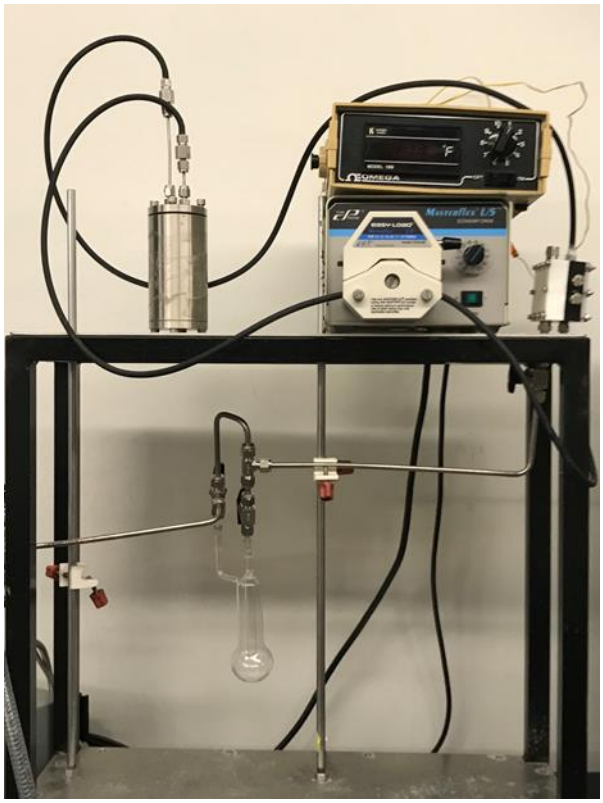

Figure 26: Lind lab pervaporation setup

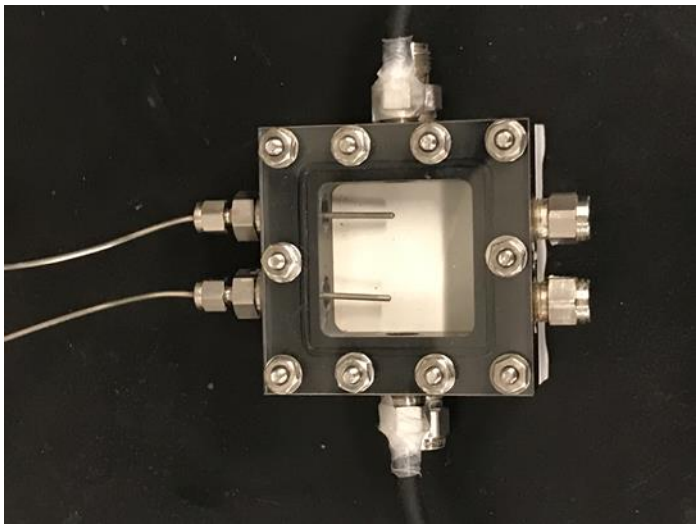

Figure 27: Top view of pervaporation cell

The membranes used for the experimental work were supplied by DeltaMem. These membranes are designed for organic dehydration. Membrane type 4155-80 was selected for the experimental work after preliminary studies showed it to have the highest flux compared with the other membrane types obtained from DeltaMem. Stability testing showed 4155-80 to have stable fluxes and rejections. Membrane 4155-80 CB is type 4155-80 membrane coated with carbon black for the purpose of nanophotonic flux enhancement (these results will be shown in the next chapter). Experimental runs using a 3.2 wt % NaCl feed were for 30 minute collection time. Prior to starting collection, the system was allowed to run under vacuum until the thermocouples registered a stable temperature for 30 minutes. The heating jacket was set at temperatures ranging from 30℃ to 90℃. However, as can be seen from the tables, there was significant heat loss so that, for example, the maximum achieved temperature within the cell, with the heating jacket

set for 90℃ was about 42℃. Table 7-Table 13 are for a membrane sample 4155-80 CB designated as DC1.

Table 7: DC1 Room Temperature

Feed T	flux	permeate conc	rejection	Permeance
°C	kg m^{-2} h^{-1}	g/L	%	kg m^{-2} h^{-1} bar^{-1}
21.7	1.29	0.011	99.97	49.4
21.7	1.32	0.006	99.98	50.7
21.3	1.46	0.006	99.98	57.5
average	1.36		99.98	52.53
SD	0.09		0.01	4.35

Table 8: DC1 30℃

Feed T	flux	permeate conc	rejection	Permeance
°C	kg m^{-2} h^{-1}	g/L	%	kg m^{-2} h^{-1} bar^{-1}
25	1.77	0.008	99.98	56.4
25	1.75	0.094	99.71	55.3
24.8	1.83	0.025	99.92	58.6
average	1.78		99.87	56.77
SD	0.04		0.14	1.68

Table 9: DC1 40℃

Feed T	flux	permeate conc	rejection	Permeance
°C	kg m^{-2} h^{-1}	g/L	%	kg m^{-2} h^{-1} bar^{-1}
28.7	2.15	0.007	99.98	54.5
27.7	2.01	0.01	99.97	54.1
28.2	2.12	0.012	99.96	55.5
average	2.09		99.97	54.70
SD	0.07		0.01	0.72

Table 10: DC1 60℃

Feed T	flux	permeate conc	rejection	Permeance
°C	kg m^{-2} h^{-1}	g/L	%	kg m^{-2} h^{-1} bar^{-1}
33.8	3.36	0.007	99.98	63.9
34.4	3.39	0.006	99.98	62.1
33.9	3.32	0.007	99.98	62.7
average	3.36		99.98	62.90
SD	0.04		0.00	0.92

Table 11: DC1 70℃

Feed T	flux	permeate conc	rejection	Permeance
°C	kg m^{-2} h^{-1}	g/L	%	kg m^{-2} h^{-1} bar^{-1}
37.4	4.19	0.008	99.98	65.3
37.6	4.29	0.006	99.98	66
36.3	4.02	0.004	99.99	66.5
average	4.17		99.98	65.93
SD	0.14		0.01	0.60

Table 12: DC1 80℃

Feed T	flux	permeate conc	rejection	Permeance
°C	kg m^{-2} h^{-1}	g/L	%	kg m^{-2} h^{-1} bar^{-1}
40.1	5.11	0.006	99.98	68.8
38.8	4.89	0.007	99.98	70.6
39.4	5.16	0.006	99.98	71.5
average	5.05		99.98	70.30
SD	0.14		0.00	1.37

Table 13: DC1 90℃

Feed T	flux	permeate conc	rejection	Permeance
°C	kg m^{-2} h^{-1}	g/L	%	kg m^{-2} h^{-1} bar^{-1}
41.7	5.88	0.006	99.98	72.7
41.8	6.15	0.007	99.98	75.8
42.8	5.94	0.006	99.98	69.4
average	5.99		99.98	72.63
SD	0.14		0.00	3.20

The average fluxes and rejections from Table 7 - Table 13 were used to create Figure 28.

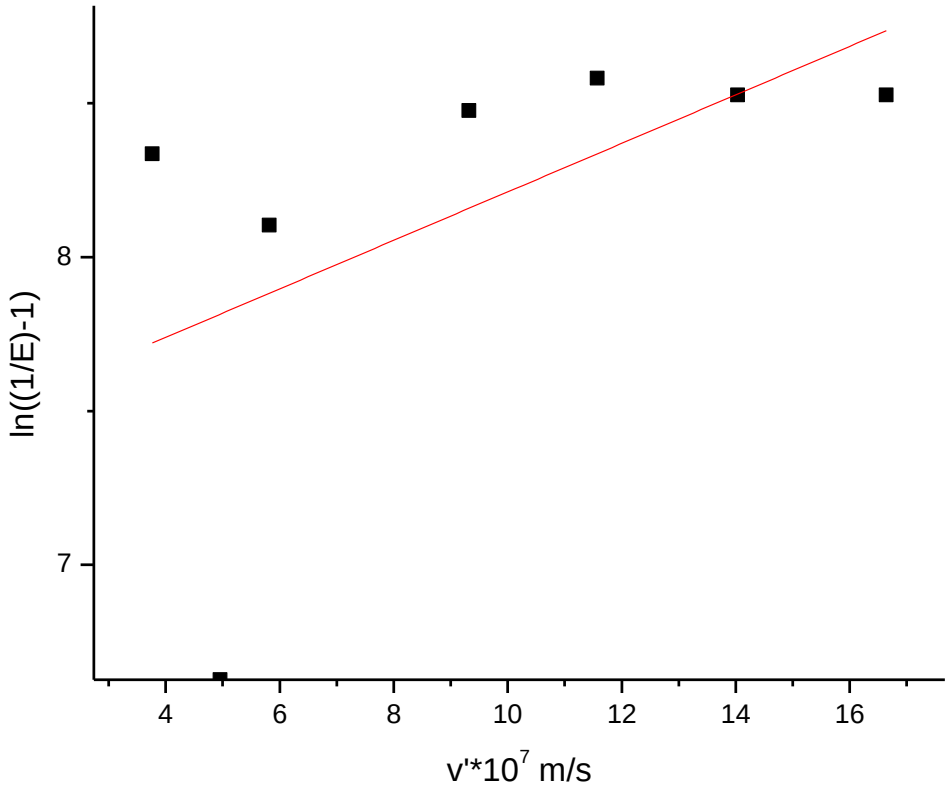

Figure 28: Experimental data fitted to equation (64) for membrane DC1

The R square value for the best fit is 0.16, i.e. a poor correlation. The slope of the line is about 0.08, a positive slope.

Table 14-Table 18 are for 4155-80 membrane “6/22/17”:

Table 14: “6/22/17” 40 ℃

Feed T	flux	permeate conc	rejection	Permeance
°C	kg m^{-2} h^{-1}	g/L	%	kg m^{-2} h^{-1} bar^{-1}
25.5	2.24	0.005	99.98	68.5
27.2	2.3	0.01	99.97	65.7
26.6	2.44	0.008	99.98	69.9
average	2.33		99.98	68.03
SD	0.10		0.01	2.14

Table 15: "6/22/17" 60 ℃

Feed T	flux	permeate conc	rejection	Permeance
°C	kg m^{-2} h^{-1}	g/L	%	kg m^{-2} h^{-1} bar^{-1}
30	2.88	0.003	99.99	67.7
32.2	3.32	0.015	99.95	69
33.3	3.14	0.006	99.98	70.7
average	3.11		99.98	69.13
SD	0.22		0.02	1.50

Table 16: "6/22/17" 70 ℃

Feed T	flux	permeate conc	rejection	Permeance
°C	kg m^{-2} h^{-1}	g/L	%	kg m^{-2} h^{-1} bar^{-1}
36.1	4.48	0.007	99.98	74.9
36.1	4.41	0.007	99.98	73.7
35	4.1	0.007	99.98	72.8
average	4.33		99.98	73.8
SD	0.20		0.00	1.05

Table 17: "6/22/17" 80 ℃

Feed T	flux	permeate conc	rejection	Permeance
°C	kg m^{-2} h^{-1}	g/L	%	kg m^{-2} h^{-1} bar^{-1}
38.8	5.09	0.007	99.98	73.4
37.7	4.97	0.006	99.98	76.1
38.3	5.62	0.006	99.98	83.4
average	5.23		99.98	77.63
SD	0.35		0.00	5.17

Table 18: "6/22/17" 90 ℃

Feed T	flux	permeate conc	rejection	Permeance
°C	kg m^{-2} h^{-1}	g/L	%	kg m^{-2} h^{-1} bar^{-1}
42.2	6.15	0.007	99.98	74.1
39.4	5.22	0.007	99.98	73
41.1	5.99	0.007	99.98	76.5
average	5.79		99.98	74.53
SD	0.50		0.00	1.79

The average fluxes and rejections obtained from Table 14- Table 18 are represented in Figure 29.

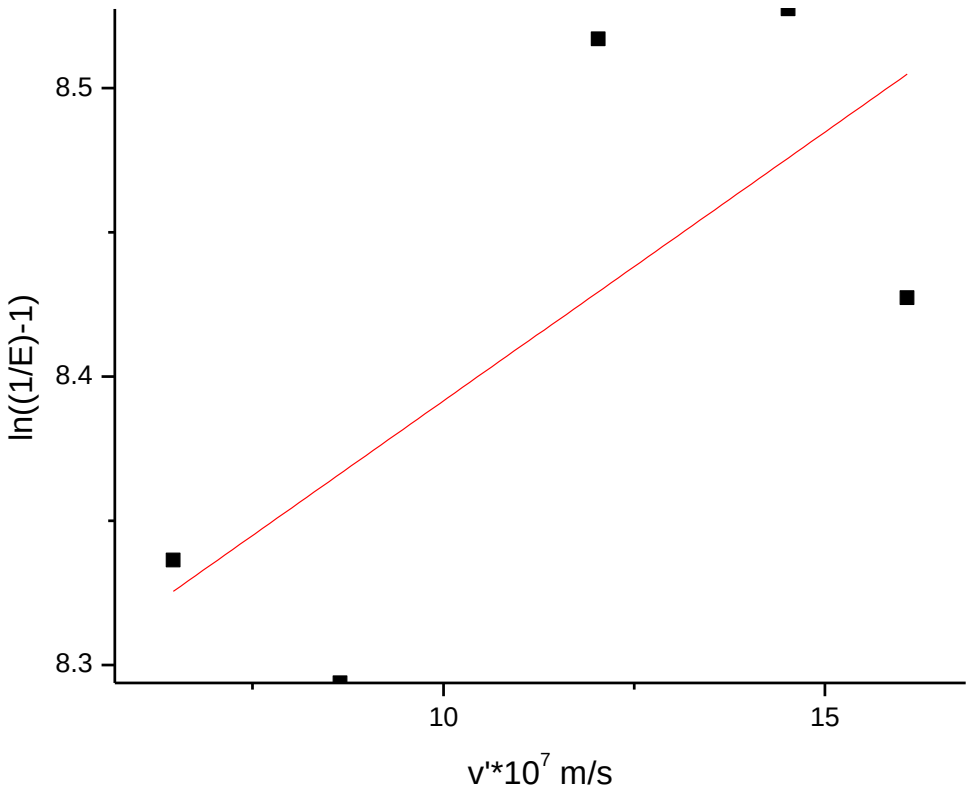

Figure 29: Experimental data fitted to equation (64) for membrane "6/22/17"

The R square value is 0.34, a poor correlation. The slope of the line is about 0.02, a positive number.

Discussion of results of experimental work:

Examination of Figure 28 and Figure 29 shows that the lines have positive slopes. The positive slopes result in a negative value for the Peclet number. This is not possible. In general dimentionless numbers cannot take on a negative value. Specifically, the

variables comprising the Peclet number, volumetric flux, the solute diffusion coefficient, and the boundary layer thickness are all positive numbers.

2.10 Excel Modeling of Concentration Polarization

Calculations and experiments were performed at Arizona State University and the University of Texas at El Paso, using Excel for modeling. The modeling methodology for the Excel program was obtained from Crittenden et al. [83] The Excel modeling was done in collaboration with Fred Rivers and Mitch Durbin. [102]

The model used for concentration polarization in RO and pervaporation is taken from Crittenden et al. [83] and built into an Excel program (Crittenden et al.'s RO model was modified for pervaporation). [102] This model uses a Sherwood correlation to calculate the SBLMTC and a reformulation of the steady state TFBLT equation (63) to calculate the concentration polarization modulus, C'.

Figure 30, Figure 31, Figure 32, and Figure 33 represent the physical aspects of the RO portion of the model. The pervaporation portion of the model is similar to the RO portion, the exception is the calculation of solute permeate concentration. In RO solute permeate concentration decreases with increasing water flux. In pervaporation solute permeate concentration increases with increasing water flux. The first set of equations are for the RO portion of the model. The modification for the pervaporation solute permeate concentration calculation is described below.

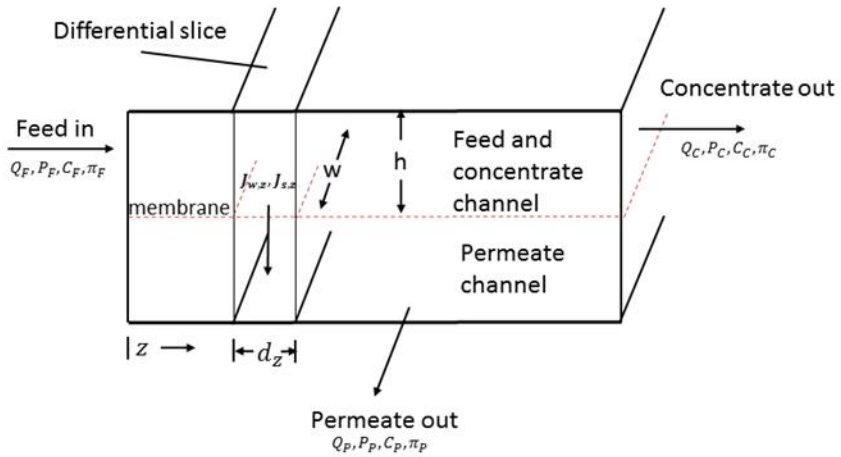

Figure 30: MWH model increment [83]

The Excel model performs iterative calculations per increment to obtain recovery and rejection per increment, per element, per stage, and per process. In Figure 30, showing the process variable of one increment in the model, dz represents one increment (0.1 meter [m]). Figure 31, Figure 32, and Figure 33 show a top-down illustration of the model. In Figure 33 increment 1, etc. is the same as dz in Figure 30.

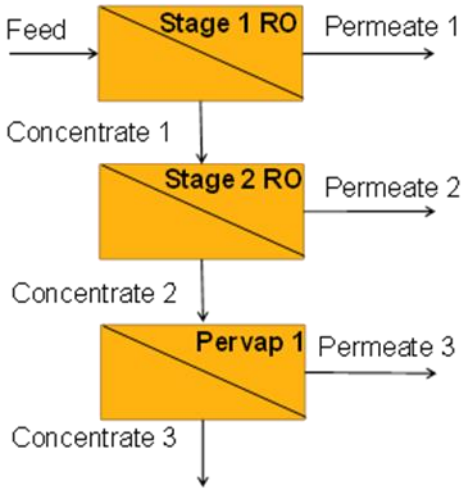

Figure 31: Stages of RO/pervap hybrid model

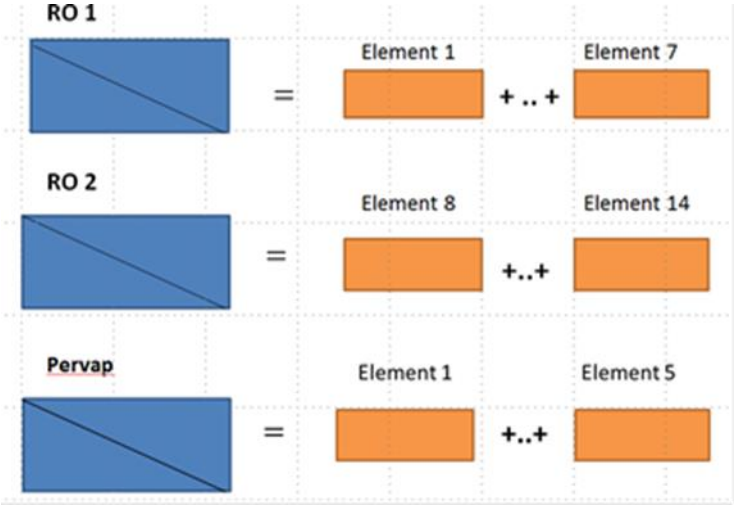

Figure 32: Number of elements in each stage of RO/pervap hybrid model

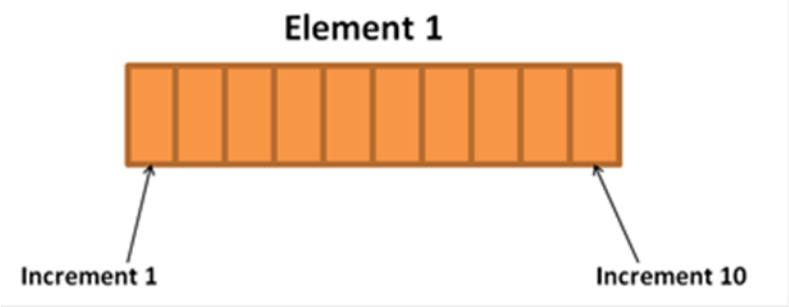

Figure 33: Each element contains 10 increments

The calculations make use of the values in Table 19 and Table 20.

Table 19: Process variables (initial) for first RO stage RO/pervap hybrid model

Parameter	Units	Value
Feed flow	$m^3 s^{-1}$	$3.125*10^{-3}$
Feed Pressure (P_F)	bar	14.2
Feed Concentration	mg L^{-1} NaCl	2000
Permeate Pressure	bar	0.3
Head loss coefficient	bar s^2 m^{-3}	0.8

Table 20: RO membrane properties for RO/pervap hybrid model

Membrane properties	Units	Value
Water mass transfer coefficient (k_w)	L m^{-2} h^{-1} bar^{-1}	2.87
Solute (NaCl) mass transfer coefficient	m h^{-1}	$6.14*10^{-4}$
Diffusion coefficient NaCl (D_{NaCl}) – boundary layer	m^2 s^{-1}	$1.35*10^{-9}$

The process variables presented in Table 21 can be adjusted. For example, for the pervaporation model the feed temperature, water mass transfer coefficient, and Reynolds number exponent were varied to assess the effect of the variations on the outputs.

Table 21: Adjustable process variables for RO and Pervaporation stages in hybrid model

Input	Semi-fixed	Output
Feed volumetric flow rate	# elements per stage	Permeate flow rate
Feed concentration	Element length	Permeate solute concentrate
Feed hydraulic pressure (RO only)	# of increments per element	
Feed temperature	Feed channel width	
	Feed channel height	
	Feed channel head loss (RO)	
	Water mass transfer coefficient	
	Solute mass transfer coefficient	
	Diffusion coefficient NaCl	
	Reynolds number exponent	

The equations for the excel method, equation (78) – (98) were adapted from Crittenden. [83]

Step 1: Calculate the SBLMTC

Calculating the solute boundary layer mass transfer coefficient, k_{cp} [m s^{-1}], is done by using a Sherwood correlation, Sh, (equation (69)). First calculate the feed velocity using equation (78):

$$v_z = \frac{Q_F}{hw} \quad (78)$$

In equation (78),v_z is the feed channel velocity [m s^{-1}], Q_F is the feed volumetric flow [m^3 s^{-1}], h [m] is the feed channel height, and w [m] is the feed channel width.

Then obtain the hydraulic diameter using equation (79):

$$d_H = 2h \quad (79)$$

In equation (79) d_H [m]is the hydraulic diameter and h [m] is the feed channel height.

Obtain the Reynolds and Schmidt numbers:

$$Re = \frac{\rho v_z d_H}{\mu} \quad (80)$$

In equation (80) Re is the Reynolds number [ ], ρ is the water density [kg m^{-3}], μ is the water viscosity [kg m^{-1} s^{-1}], v (v_z) is the feed channel velocity [m s^{-1}], and d_H [m] is the hydraulic diameter.

$$Sc = \frac{\mu}{\rho D_{NaCl}} \quad (81)$$

In equation (81) Sc is the Schmidt number [ ], ρ is the water density [kg m^{-3}], μ is the water viscosity [kg m^{-1} s^{-1}], and D_{NaCl} is the solute diffusion coefficient [m^2 s^{-1}].

Calculate the SBLMTC (k_{cp}):

$$k_{cp} = 0.023\left(\frac{D_{NaCl}}{d_H}\right) Re^{0.83} Sc^{0.33} \quad (69)$$

In equation (69) D_{NaCl} is the solute diffusion coefficient [m^2 s^{-1}], d_H [m]is the hydraulic diameter, Re is the Reynolds number [ ], Sc is the Schmidt number [ ], and k_{cp} is the solute boundary layer mass transfer coefficient [m s^{-1}].

Equation (69) shows a Reynolds number of 0.83 for RO as obtained from Crittenden. [83] For pervaporation desalination, a Reynolds number of 0.3 was found to correlate with the experimental data obtained from literature analysis.

Step 2 Calculate the feed osmotic pressure:

Calculate the feed osmotic pressure using equation (82):

$$\pi = CRT \quad (82)$$

In equation (82) π is the osmotic pressure [bar], C is the ion concentration [mol L^{-1}], R is the gas constant [L bar mol^{-1} K^{-1}], and T is the temperature [K].

Step 3. Calculate Water Flux and Concentration Polarization Modulus for the First Increment

Equation (83) and equation (84) are solved simultaneously to obtain the concentration polarization modulus C_z' and the incremental water flux $J_{w,z}$.

Assume rejection = 1 for first increment.

$$C_z' = exp\left(\frac{J_{w,z}}{k_{cp}}\right) * Rej + (1 - Rej) \quad (83)$$

In equation (83) C_z' is the concentration polarization modulus [ ] in increment z, k_{cp} is the solute boundary layer mass transfer coefficient [m s^{-1}], $J_{w,z}$ is the incremental water flux [L m^{-2} h^{-1}], and Rej is rejection [ ]. Note that equation (83) is equation (47) rearranged, a steady state equation.

$$J_{w,z} = k_w[(P_F - P_P) - (C_z'\pi_F - \pi_P) \quad (84)$$

In equation (84) $J_{w,z}$ is the incremental water flux [L m^{-2} h^{-1}], k_w is the membrane water mass transfer coefficient (an assumed constant) [L m^{-2} h^{-1} bar^{-1}], P_F is the hydraulic feed pressure [bar], P_P is the hydraulic permeate pressure [bar], C_z' is the concentration polarization modulus [ ], π_F is the feed osmotic pressure [bar], and π_P is the permeate osmotic pressure [bar].

Step 4. Calculate the Solute Flux and Solute Transport Across the Membrane

Equations (85) and (86) are used to calculate the solute flux and solute transport across the membrane:

$$J_{s,z} = k_s C_z'(C_F - C_P) \quad (85)$$

In equation (85) $J_{s,z}$ is the solute flux [mg m^{-2} h^{-1}], k_s is the solute membrane mass transfer coefficient [m h^{-1}], C_z' is the concentration polarization modulus [ ], C_F is the solute feed concentration [mg m^{-3}], and C_F is the solute feed concentration[mg m^{-3}].

$$M_{s,z} = J_{s,z}(w)(dz) \quad (86)$$

In equation (86) $M_{s,z}$ is the solute transmembrane mass transfer rate [mg s^{-1}], $J_{s,z}$ is the solute flux [mg m^{-2} h^{-1}], w is the feed channel width [m], and dz is the feed channel incremental length [0.1 m].

Step 5. Calculate the Permeate Flow Rate

Use equation (87) to calculate the permeate flow rate:

$$Q_P = J_{w,z}(w)(dz) \quad (87)$$

In equation (87) Q_P is the permeate flow rate [$m^3\ s^{-1}$], $J_{w,z}$ is the incremental water flux [$L\ m^{-2}\ h^{-1}$],

w is the feed channel width [m], and dz is the feed channel increment length [0.1 m].

Step 6. Calculate the Inputs for the Second and Subsequent Increments

The second and subsequent increments are calculated using the output from the previous increment. In increments following the first increment the permeate concentration is not zero. Calculate the feed volumetric flow and velocity using equations (88) and (89).

$$Q_{F2} = Q_F - Q_P \quad (88)$$

In equation (88) Q_{F2} is the feed volumetric flow in the second increment [$m^3\ s^{-1}$], Q_F is the feed volumetric flow rate for the first increment [$m^3\ s^{-1}$], and Q_P is the permeate flow rate for the first increment [$m^3\ s^{-1}$].

$$v_{z2} = \frac{Q_{F2}}{hw} \quad (89)$$

In equation (89) v_{z2} is the feed velocity in the second increment [$m\ s^{-1}$], Q_{F2} is the feed volumetric flow in the second increment [$m^3\ s^{-1}$], h is the feed channel height [m], and w is the feed channel width [m].

Use equation (90) to calculate the feed concentration for the second increment:

$$C_{F2} = \frac{Q_F C_F - M_{s,z}}{Q_{F2}} \quad (90)$$

In equation (90) C_{F2} is the feed concentration in the second increment [$mg\ L^{-1}$], Q_F is the feed volumetric flow rate in the first increment [$m^3\ s^{-1}$], C_F is the feed concentration in the first increment, [$mg\ L^{-1}$], $M_{s,z}$ is the solute transmembrane mass transfer rate [$mg\ s^{-1}$], and Q_{F2} is the feed volumetric flow in the second increment [$m^3\ s^{-1}$].

Use equation (91) to calculate the permeate concentration for the second increment.

$$C_{P2} = \frac{J_{s,z}}{J_{w,z}} \quad (91)$$

In equation (91) C_{P2} is the solute concentration in the second increment permeate [mg L^{-1}]

$J_{w,z}$ is the incremental water flux [L m^{-2} h^{-1}], and $J_{s,z}$ is the solute flux [mg m^{-2} h^{-1}].

Use equation (92) to calculate the head loss for the second increment.

$$h_{L2} = \delta_{HL}(v_z)^2 dz \quad (92)$$

In equation (92) h_{L2} is the head loss in the second increment [bar], δ_{HL} is the head loss coefficient [bar s^2 m^{-3}], v_z is the feed velocity in the first increment, and dz is the feed channel incremental length [0.1 m]

Use equation (93) to calculate the feed pressure in the second increment.

$$P_{F2} = P_{F1} - h_{L2} \quad (93)$$

In equation (93) P_{F2} is the feed pressure in the second increment [bar], P_{F1} is the feed pressure in the first increment [bar], and h_{L2} is the head loss in the second increment [bar].

Use Equation (94) to calculate the osmotic pressure of the permeate in the second increment.

$$\pi = C_{P2}RT \quad (94)$$

In equation (94) π is the osmotic pressure of second increment permeate [bar], R is the gas constant [L bar mol^{-1} K^{-1}], T is the temperature [K], and C_{P2} is the solute ion concentration in the second increment permeate [mol L^{-1}].

Use equation (95) to calculate the osmotic pressure of the feed in the second increment.

$$\pi = C_{F2}RT \quad (95)$$

In equation (95) π is the osmotic pressure of the second increment feed, R is the gas constant [L bar mol^{-1} K^{-1}], T is the temperature [K], and C_{F2} is the ion concentration of the second increment feed [mol ion L^{-1}].

Repeat steps 1-6 for each RO increment.

When there is a stage change, the permeate concentration of the first increment of the new stage is zero.

Calculate Flux and Rejection

The pervaporation portion of the model was modified to include the inverse relationship between flux (recovery) and rejection found by applying the thin film boundary layer theory to published pervaporation desalination data as shown in equation (96)

$$c_{ip,z} = \frac{c_{ib}}{\frac{\frac{1}{E_0} - 1}{exp\left(\frac{v'\delta}{D_i}\right)} + 1} \quad (96)$$

In equation (96) $c_{ip,z}$ is the incremental solute permeate concentration [mg L^{-1}], E_0 is the intrinsic enrichment [],c_{ib} is the bulk solute feed concentration [mg L^{-1}], v' is the incremental volumetric water flux [m s^{-1}], D_i/δ is the solute boundary layer mass transfer coefficient, obtained by a Sherwood correlation [m s^{-1}], D_i is the solute (e.g. sodium chloride) diffusion coefficient [m^2 s^{-1}], and δ is the thickness of the boundary layer at the feed/membrane interface [m].

Equation (96) is equation (64) rearranged. A value of 0.0008 for E_0 was chosen from Table **6** for the purpose of model calculations.

The pervaporation portion of the model uses equation (27) for water flux. In equation (27), P_w^{sat} is obtained from the inputted temperature from the Antoine equation. Two simplifying assumptions are made:

1) Use zero as the permeate pressure because a vacuum exists on the permeate side in pervaporation.
2) Use a water activity coefficient (γ_w) of 1. This assumption is valid up to about 3M NaCl and covers most of the feed concentrations obtained or used in the model.[103]

Additionally, hydraulic and osmotic pressures were not used for the pervaporation portion of the model.

The differences between the RO and pervaporation portion are:

1) Hydraulic and osmotic pressure differences do not drive flux in pervaporation (not an input to the pervaporation model) – pervaporation operates without a hydraulic pressure head
2) The solute permeate concentration decreases with increasing water flux in RO and increases with increasing water flux in pervaporation
3) Use zero as the permeate pressure because a vacuum exists on the permeate side in pervaporation.
4) Use a water activity coefficient (γ_w) of 1. This assumption is valid up to about 3M NaCl and covers most of the feed concentrations obtained or used in the model.[103]

Additionally, hydraulic and osmotic pressures were not used for the pervaporation portion of the model.

The differences between the RO and pervaporation portion are:

1. Hydraulic and osmotic pressure differences do not drive flux in pervaporation (not an input to the pervaporation model) – pervaporation operates without a hydraulic pressure head
2. The solute permeate concentration decreases with increasing water flux in RO and increases with increasing water flux in pervaporation

The RO solute permeate concentration is a simple function using a constant solute mass transfer coefficient whereas in pervaporation desalination, the solute permeate concentration is a more complicated function of the solute bulk feed concentration, intrinsic enrichment and the Peclet number ($\frac{v'\delta}{D_i}$). To obtain the total solute permeate concentration in RO, equation (97) is used.

$$c_{ip} = \frac{\sum J_{i,z}}{\sum J_{w,z}} \quad (97)$$

In equation (97) c_{ip} is the total solute permeate concentration [mg L^{-1}].

To obtain the total solute permeate concentration in pervaporation, equation (98) is used.

$$\mathrm{c_{ip}} = \frac{\sum \mathrm{c_{ip,z}Q_{p,z}}}{\sum \mathrm{Q_{p,z}}} \quad (98)$$

In equation (98) $Q_{p,z}$ is the incremental permeate volumetric flow rate [L s^{-1}] and $c_{ip,z}$ is obtained from equation (96)

There is a major difference in the results obtained from Equation 97 and Equation 98 In RO, total solute permeate concentration decreases with increased water flux. In pervaporation, total solute permeate concentration increases with increased water flux. Equations (78)-(98) were used to simulate RO and Pervaporation processing of a variety of feed waters in an Excel program. Hundreds of simulations were run. The results of these simulations as they apply to concentration polarization are presented in Table 22.

Table 22: Recovery, Rejection, and Permeate concentration as function of initial feed pressure RO model, feed concentration 2000 mg L^{-1}

Feed Pressure (bar)	Recovery	Rejection	Permeate Conc (mg/L)	Concentration Polarization
8.5	0.253	0.951	98.1	1.04-1.06
10	0.324	0.959	82.6	1.06-1.07
14.2	0.514	0.968	64.9	1.12-1.15
16	0.591	0.968	63	1.14-1.20
16.7	0.62	0.968	62.9	1.14-1.22
17	0.632	0.968	63	1.15-1.23
17.5	0.652	0.968	63.3	1.15-1.24
18	0.671	0.968	63.7	1.16-1.26
18.3	0.682	0.968	64.1	1.16-1.27
20	0.744	0.966	67.5	1.18-1.33
25	0.876	0.953	93.4	1.23-1.40

The values in Table 22 were used to obtain the plot of recovery and rejection as a function of feed pressure shown in Figure 34, and the plot of rejection as a function of feed pressure shown in Figure 35.

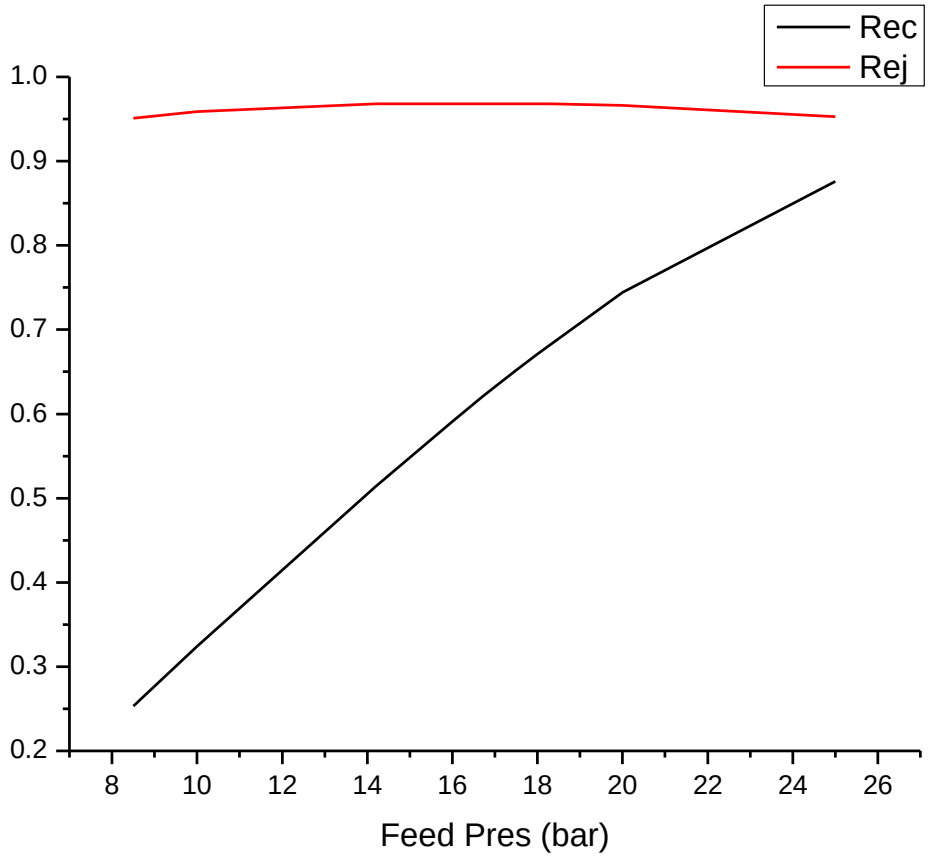

Figure 34: Recovery and Rejection from Table 22 as function of initial feed pressure in RO model

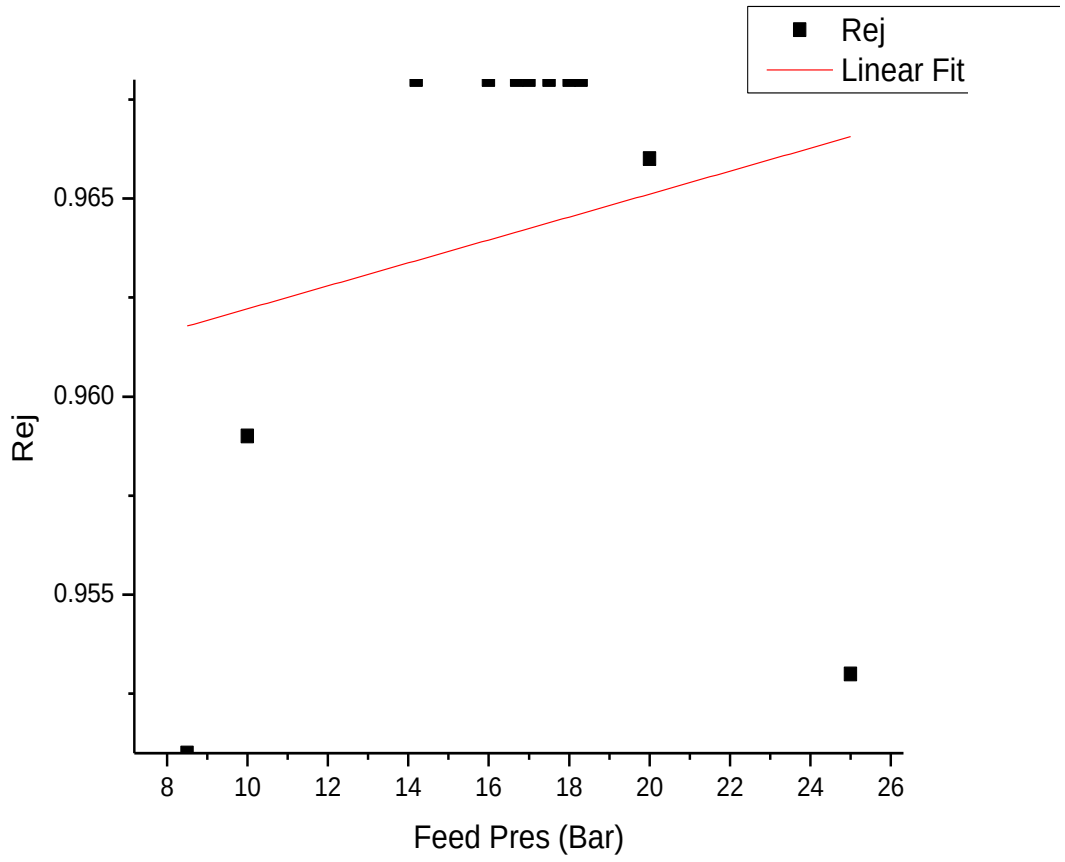

Figure 35: Rejection as function of feed pressure. R square -.06.

Figure 35 shows that rejection increases with increasing feed pressure in RO. Although there is a poor correlation, the correlation would improve significantly if the value for 25 bar (higher than typically used in RO) were dropped.

Table 23 shows the results obtained for the pervaporation model for recovery, rejection, and the concentration polarization modulus when the Reynolds number exponent and feed temperatures are varied.

Table 23: Pervaporation C′ values with varying Tf and Re exponent at feed 2000 mg L^{-1}

Re Exponent	Feed Temperature	Recovery	Rejection	Concentration Polarization
0.3	74	0.811	0.942	20.8-66.2
0.3	75	0.836	0.929	23.5-73.4
0.3	76	0.861	0.914	26.8-89
0.3	77	0.883	0.897	30.5-100.7
0.31	74	0.815	0.948	17.9-60.5
0.31	75	0.841	0.936	20.2-71.2
0.31	76	0.866	0.922	22.3-82.5
0.31	77	0.889	0.905	25.8-93.7
0.29	74	0.806	0.935	24.3-72.5
0.29	75	0.831	0.922	27.7-84.2
0.29	76	0.855	0.906	31.6-96.3
0.29	77	0.877	0.888	36.2-108.5
0.33	74	0.821	0.958	13.5-50.6
0.33	75	0.849	0.947	15-60.6
0.33	76	0.875	0.934	16.8-71.3
0.33	77	0.899	0.919	18.9-81.2
0.27	74	0.796	0.92	33.9-87.4
0.27	75	0.819	0.905	39-100
0.27	76	0.842	0.887	45-113.7
0.27	77	0.863	0.867	51.9-127.6

Figure 36 shows a plot of the maximum concentration polarization modulus at various temperatures as a function of Reynolds number exponent using the values obtained from Table 23.

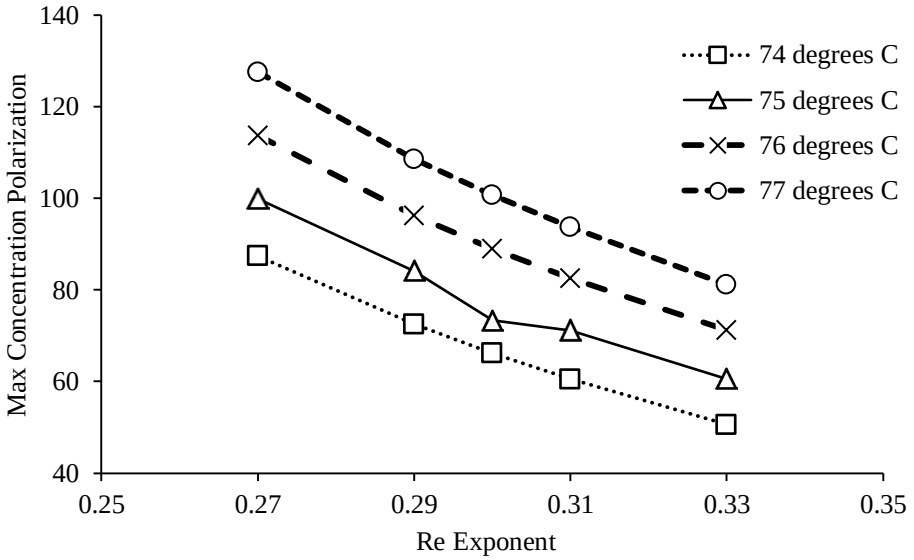

Figure 36: Maximum concentration polarization, C', Pervaporation model, as function of Reynolds number exponent at various temperatures

Figure 36 shows a significant decrease in the maximum concentration polarization modulus when the Reynolds number is increased. For example, when the Reynolds number is increased from 0.27 to 0.29 (about a 6% increase), the concentration polarization modulus, at 77℃, decreases from 130 to 90 (about a 30% decrease). Figure 37, Figure 38, Figure 39, Figure 40, and Figure 41 show for the pervaporation model, plots of recovery and rejection as a function of feed temperature for Reynolds numbers 0.27-0.33, for values obtained from Table 23. In pervaporation, flux increases with increasing feed temperature according to equation (27).

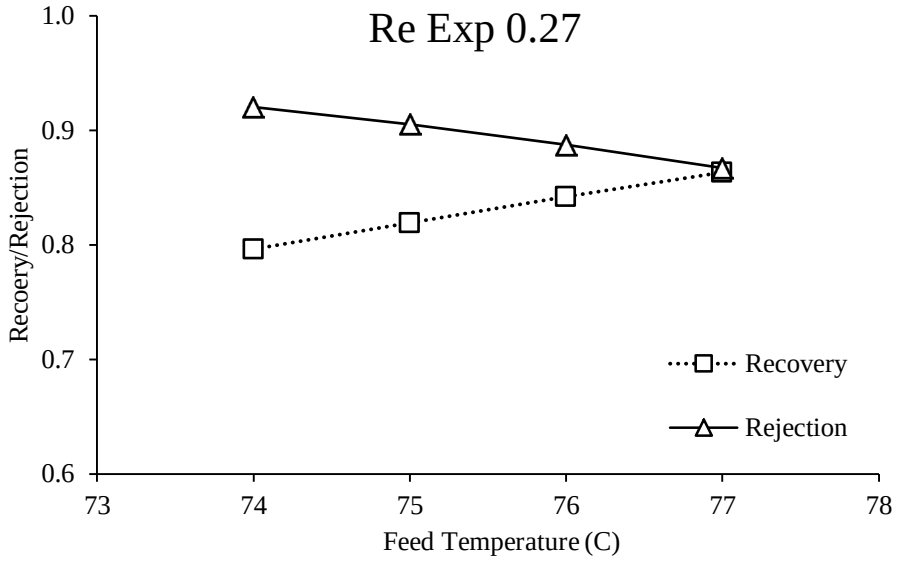

Figure 37: Recovery and rejection, Pervaporation model, as function of Temperature, Reynolds exponent 0.27

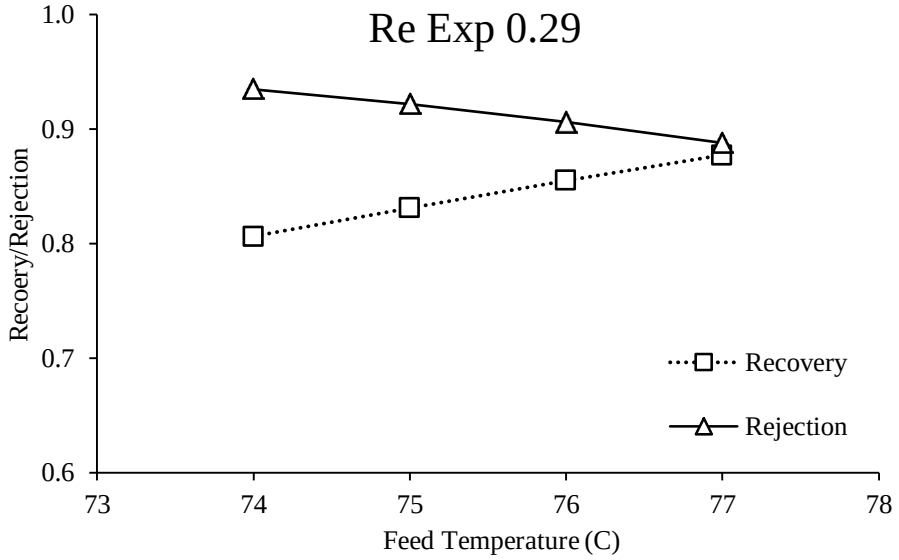

Figure 38: Recovery and rejection, Pervaporation model, as function of Temperature, Reynolds exponent 0.29

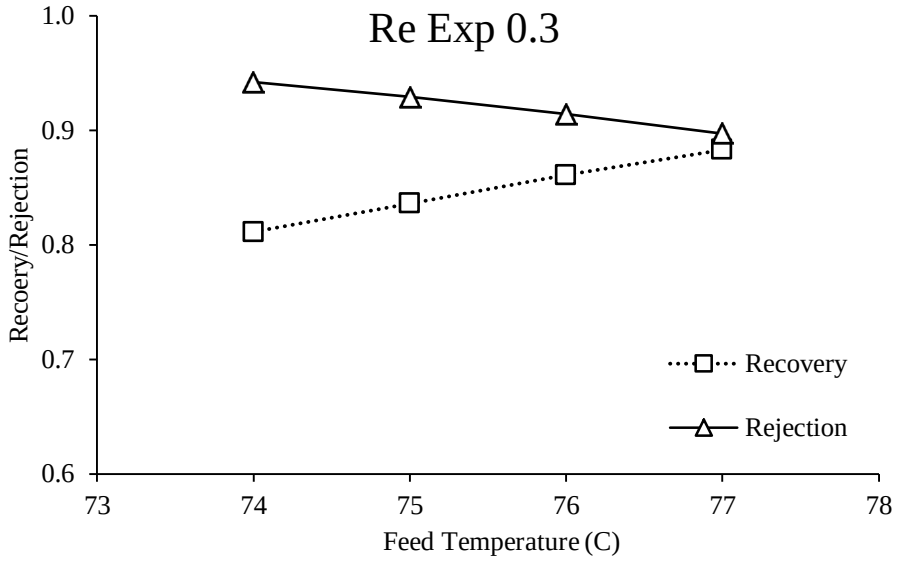

Figure 39: Recovery and rejection, Pervaporation model, as function of Temperature, Reynolds exponent 0.3

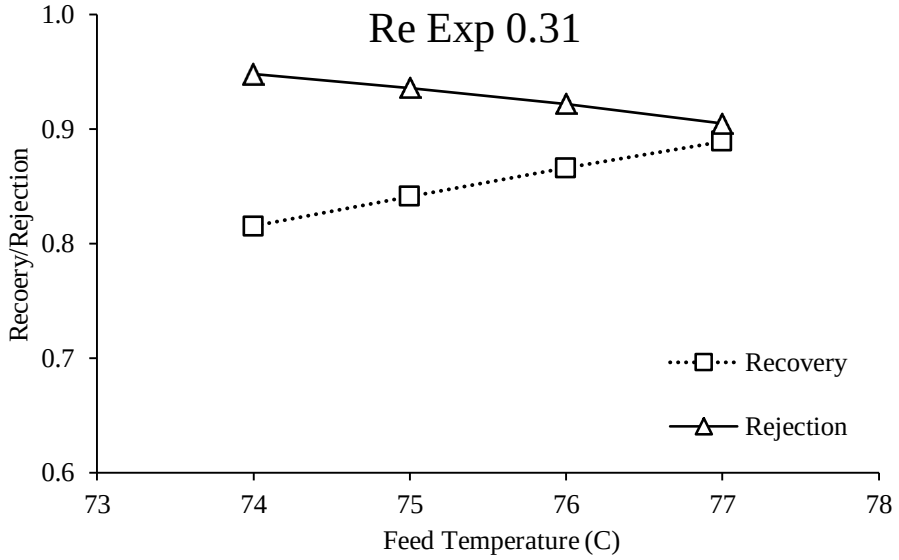

Figure 40: Recovery and rejection, Pervaporation model, as function of Temperature, Reynolds exponent 0.31

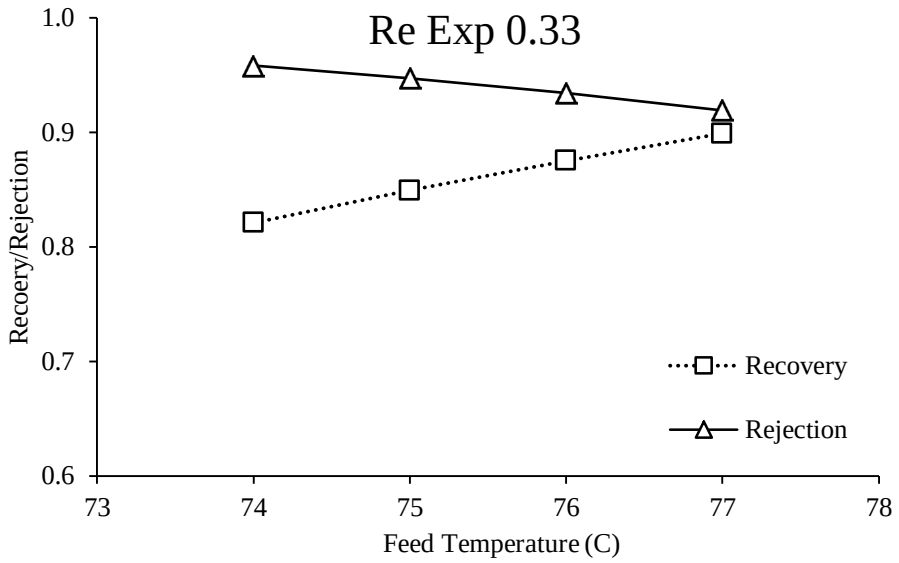

Figure 41: Recovery and rejection, Pervaporation model, as function of Temperature, Reynolds exponent 0.33

Figure 37, Figure 38, Figure 39, Figure 40, and Figure 41 show that, regardless of the Reynolds number exponent used in the pervaporation model, recovery increases with feed temperature and rejection decreases. In pervaporation flux increases with increasing feed temperature according to equation (27).

2.11 Conclusions for Chapter 2

Analysis of concentration polarization in the pervaporation desalination studies examined showed that the feed channel configuration and feed flow velocity, and, water flux through the membrane are the main factors affecting concentration polarization. A cross-flow configuration both in pervaporation desalination and MD results in lower boundary layer thickness and less concentration polarization. High water flux is desirable in general; however, there is a price to be paid in terms of increased concentration polarization. In membranes producing high water flux, it is especially important to take

measures to reduce boundary layer thickness. In cases where the feed contains sparingly soluble salts, it may be necessary to reduce water flux to avoid scaling, as previously noted by Baker The applicability of TFBLT in the form of equation (80) requires that solute permeate concentration increases with increasing water flux. Four out of five of the pervaporation desalination studies examined here, where that relationship was observed, used zeolite membranes. It is possible that intercrystalline defects in the zeolite layer contributed to the observed relationship between water flux and solute permeate concentration

The studies analyzed characterized membranes for which the salt removals were over 90%. Within that range, the separation ability of the membranes in the pervaporation desalination studies had virtually no effect on concentration polarization. This conclusion illustrates one of the limitations of TFBLT since the concentration gradient in the boundary layer is determined by the membrane prior to steady state being reached. The results of the semi-quantitative analysis for membrane desalination using TFBLT show that the Peclet number should be greater than or equal to one since for salt to be transported through the membrane, convective solute flux through the boundary layer must be greater than solute diffusive flux away from the membrane. In most of the pervaporation desalination studies, the Peclet number was greater than one whereas in the MD studies the Peclet numbers were all less than one. It is possible that the Sherwood correlations used in the MD studies resulted in inaccurately low values for boundary layer thickness. Further studies of concentration polarization in pervaporation desalination and MD where concentration polarization is evaluated using both the method of Baker used here and Sherwood correlations are recommended.

Using Baker's method (equation (80)) it was found that, in pervaporation desalination, the concentration polarization moduli may range up to 100. The difference in the severity of concentration polarization between pervaporation desalination, and, for example, vacuum membrane distillation (vacuum membrane distillation and pervaporation desalination are similar processes, differing only in the porosity and hydrophobicity of the membrane) may be explained by differences in process design which resulted in higher boundary layer thicknesses in pervaporation desalination than MD for the studies examined here. The resistance in series model used to determine the Peclet number in pervaporation VOC separation from water serves as a cross-check on the use of Sherwood correlations for that separation. Similarly, the Baker method can potentially serve as a cross-check on the use of Sherwood correlations in membrane desalination. There was a large difference in the calculated boundary layer thickness and Peclet number obtained in the analysis of the Naim et al. study by using Sherwood correlations and Baker's method. Although the comparison between Sherwood correlations and Baker's method consists of only one example, it raises the concern that neither method accurately predicts the concentration polarization modulus since both methods involve a number of approximations, including the steady state approximation. Baker's method yielded values for the concentration polarization modulus that in general conformed to the results of the semi-quantitative analysis presented. Semi-quantitative analysis suggests a minimum value of 2.78 (exp(1)) as a minimum value for the concentration polarization modulus in desalination. Further comparisons between Baker's method and Sherwood correlations are suggested as an objective of future research.

The results of the experimental work suggest that Baker's method (equation (80)) may not have wide applicability in membrane desalination. Solute permeate concentration did not increase with increasing water flux. Equation (80) could not be applied because a negative value for the Peclet number resulted. This discrepancy likely is due to the limitations of the steady state TFBLT. The steady state assumption that TFBLT is based on may not accurately reflect the boundary layer solute concentration gradient that develops prior to the steady state condition. The commercial PVA membranes used for the experimental work may impose a boundary condition not represented in TFBLT. The commercial PVA membranes are similar to membranes used industrially in RO and impose a limit to the amount of solute that can permeate the membrane. Consequently solute rejection will increase, not decrease, with increasing water flux.

The difference in RO membranes and pervaporation membranes, i.e. zeolite membranes, that conform to Baker's method is illustrated in the RO/pervaporation hybrid modelling. In the RO portion of the model rejection increased or remained the same with increasing water flux. In the pervaporation portion of the model, rejection decreased with increasing water flux.

The use of feed spacers, and high feed flows industrially does not mean that those usages are based on TFBLT, in particular equation (54). The use of feed spacers and high feed flows are intended to reduce the thickness of the boundary layer. The assumption is that reducing the boundary layer thickness will reduce the mass of solute in the boundary layer and the size of the solute concentration gradient present in the boundary layer. The analysis presented here, based on steady state TFBLT, suggest that significant differences

in concentration polarization may exist at the lab scale depending on the feed channel properties represented in the Reynolds number. For example the Reynolds number in the Naim et al. study was 2190, placing it in the laminar flow regime. It is likely that lower values for the concentration polarization modulus and higher water fluxes would have been observed under conditions of turbulent flow. It is suggested that the Reynolds number of the feed channel be taken into account when comparing the results of lab scale studies of membrane desalination.

CHAPTER 3

NANOPHOTONIC FLUX ENHANCEMENT IN PERVAPORATION DESALINATION

The objective of nanophotonic photothermal heating of the feed is to raise the feed temperature, in particular the temperature of the feed at the feed/membrane interface. This will result in a higher water vapor pressure at the feed/membrane interface and a larger driving force and increased water flux.

3.1 Temperature Polarization

A discussion of temperature polarization that normally occurs in pervaporation is important to develop an understanding of the nanophotonic heating effect that occurs when nanophotonic particles are incorporated into desalination membranes and solar irradiation is applied to the membrane during the pervaporation process. This section will discuss the modelling of temperature polarization in pervaporation and MD. The purpose of this discussion is to illustrate that the modelling of temperature polarization in pervaporation does not include heat loss through the membrane by conduction. Heat is transferred through the membrane in pervaporation and VMD because of the latent heat of vaporization, ΔH_v [J kg^{-1}], which is unavoidable. A consequence of heat loss across the membrane from the feed to the permeate side is that the temperature of the liquid feed adjacent to the membrane on the feed side will drop. This phenomenon is called temperature polarization. As Favre points out, the mechanism for temperature polarization in pervaporation is similar to that of vacuum membrane distillation. [104] When the temperature drops at the feed/membrane interface the water saturation pressure

drops according to the Antoine equation resulting in a drop of the feed side driving force as can be seen from examination of equation (27).

$$v' = \frac{Þ_i}{l}\left(x_i \gamma_i p_i^{sat} - y_i p_p\right) \quad (27)$$

In equation 27, v' is water flux [kg m^{-2} s^{-1} or m^3 m^{-2} s^{-1} or m s^{-1}], $Þ_i$ is the permeability coefficient of water [kg m m^{-2} s^{-1} bar^{-1}], l is the membrane thickness [m], x_i is the liquid phase feed side mole fraction of water [-], γ_i is the liquid phase activity coefficient of water [-], p_i^{sat} is the vapor pressure of water at the operating temperature , y_i is the gas phase mole fraction of water on the permeate side [-], and p_p is the permeate pressure. The effect is similar the effect of concentration polarization of reducing the water mole fraction in the boundary layer; in the case of temperature polarization the water saturation pressure is reduced. The result in either case is reduction of water flux.

In contrast, in DCMD transmembrane conductive heat loss from the feed to the liquid water on the permeate side can occur. Temperature polarization in DCMD occurs both on the feed and permeate sides of the membrane. As will be shown, temperature polarization in DCMD is more severe than occurs in pervaporation or VMD. .

According to Favre, there are only a few studies on temperature polarization in pervaporation. [104]

In Karlsson and Trägårdh, temperature polarization was evaluated by using the Arrhenius expression for flux as shown in equation (99): [105]

$$J_w = J_0 \exp\left(\frac{-E_a}{RT}\right) \quad (99)$$

In equation (99), J_w is water flux [kg m^{-2} s^{-1}], E_a is the activation energy of permeation [J mol^{-1}], R is the gas constant [J mol^{-1} K^{-1}], T is the "wall" (feed/membrane interface)

temperature [K] and J_0 is the pre-exponential factor [kg m^{-2} s^{-1}].

Karlsson and Trägårdh used a feed of pure water and set up their experiment so that the feed inlet and outlet temperatures were 75℃. Karlsson and Trägårdh found that the observed flux varied inversely with feed flow velocity. Then equation (99) was used by Karlsson and Trägårdh to determine the "wall" temperature, i.e. the temperature at the feed side membrane surface. A temperature drop of 1.1 K was found for the lowest feed flow velocity. [105]

Kuhn et al. modeled pure water pervaporation through a Linde Type A zeolite membrane using Maxwell-Stefan type equations. The reader is referred to the original study to view how the model was constructed. The result of the modeling was that, using a water feed temperature of 348 K and a flux of 0.15 mol m^{-2} s^{-1}, they found a transmembrane temperature change of 1.3 K. [106]

Favre uses a similar approach to Karlsson and Trägårdh to model temperature polarization for pure liquid feeds (water, ethanol, butanol, pentanol, ethyl propionate). In this case, the governing equation is: [104, 105]

$$J = J_0 \, exp\left(\frac{-E_A}{R\left(T_b - \frac{\varphi}{h_0 + a\omega^{\gamma}}\right)}\right) \quad (100)$$

In equation (100), J is flux of the pure liquid feed [kg m^{-2} s^{-1}], E_A is activation energy of permeation [J mol^{-1}], T_b is bulk feed temperature [K], R is the gas constant [J mol^{-1} K^{-1}], h_0 is the boundary layer heat transfer coefficient [W m^{-2} K^{-1}], ω is the feed impeller rotational speed [s^{-1}], φ is the transmembrane heat flux [W m^{-2}], a and γ are fitting parameters [-],and J_0 is the pre-exponential factor [kg m^{-2} s^{-1}].

h_0 is obtained by using a Nusselt correlation.

The Nusselt number is defined as:

$$Nu = \frac{h_0 d_h}{k} \quad (101)$$

In equation (101) Nu is the Nusselt number [-], h_0 is the boundary layer heat transfer coefficient [W m^{-2} K^{-1}], d_h is the hydraulic diameter of the feed channel [m], and k is the thermal conductivity of the feed fluid [W m^{-1} K^{-1}].

Nusselt correlations are similar to Sherwood correlations and take the form of the Graetz-Leveque equation:

$$Nu = 1.86(RePr\frac{d_h}{L})^{0.33} \quad (102)$$

In equation (102), Nu is the Nusselt number [-],Re is the Reynolds number [-],Pr is the Prandtl number [-],d_h is the feed channel hydraulic diameter [m], and L is the feed channel length [m].

The Prandtl number is defined as:

$$Pr = \frac{c_p \mu}{k} \quad (103)$$

In equation (103), Pr is the Prandtl number [-],c_p is the specific heat of the feed fluid [J kg^{-1} K^{-1}], μ is the feed fluid viscosity [Pa s], and k is the thermal conductivity of the feed fluid [W m^{-1} K^{-1}].

In equation (100) φ is obtained by equation (104):

$$\varphi = J\Delta H_v \quad (104)$$

In equation (104) ΔH_v is the enthalpy of vaporization for the permeating species [J kg^{-1}], φ is the transmembrane heat flux [W m^{-2}], and J is flux of the pure liquid feed [kg m^{-2} s^{-1}].

In the expression in parenthesis in the denominator on the RHS of equation (100) is the temperature at the feed/membrane interface, T_m [K] as shown in equation (121):

$$T_m = T_b - \frac{\varphi}{h_0 + a\omega^{\gamma}} \quad (105)$$

Although Favre did not specify what values he obtained by his modeling for T_m he did show, for example, a significant effect on the calculated activation energy due to changes in the impeller rate. [104]

Alsaadi et al., used pure water feeds. Alsaadi et al.s modeling objective was to calculate the temperature polarization coefficient, TPC [-]: [107]

$$TPC = \frac{T_m - T_p}{T_b - T_p} \quad (106)$$

In equation (106) T_m is the temperature at the feed/membrane interface [K], T_p is the permeate side temperature [K], and T_b is bulk feed temperature [K].

According to Alsaadi et al. temperature polarization in VMD occurs only on the feed side of the membrane. [107]

Equation (107) was used by Alsaadi et al. to obtain T_m: [107]

$$(T_b - T_m) = J\Delta H_v = \mathcal{P}_m(p_m - p_p)\Delta H_v \quad (107)$$

In equation (107) $\mathcal{P}_m$ is the water permeance of the membrane [kg m^{-2} s^{-1} kPa^{-1}], p_m is the water vapor pressure at the feed/membrane interface [kPa], p_p is the permeate water vapor pressure [kPa], ΔH_v is the enthalpy of vaporization for the permeating species [J

kg^{-1}], T_b is bulk feed temperature [K], T_m is the temperature at the feed/membrane interface [K], and J is water flux [kg m^{-2} s^{-1}].

As in Favre, h_0 was obtained by Alsaadi et al. (2014) using a Nusselt correlation. [104, 107]

An iterative process was used by Alsaadi et al. to solve for T_m and the TPC. A linear relationship was found between TPC and T_b, with a TPC of about 0.9 at 20 ℃ and a TPC of about 0.7 at 95℃. [107]

All of the studies discussed so far in this section found that the temperature at the feed/membrane interface was less than the bulk feed temperature. The difference between the bulk feed temperature and the temperature at the feed/membrane interface varied between the studies. In Karlsson and Trägårdh and Kuhn et al., the temperature difference was small (about 1 ℃). [105, 106]

In pervaporation and VMD, the vacuum on the permeate side has negligible thermal conductivity so that there is negligible transmembrane conductive heat loss from the feed to the permeate side of the membrane. In DCMD heat can be transferred across the membrane by conduction because the water on the permeate side has significant thermal conductivity. The evaluation of temperature polarization in DCMD will not be discussed in depth. However the following equation for the TPC from Martinez-Diez is representative of the difference between temperature polarization in pervaporation and DCMD: [29]

$$TPC = \frac{T_{m1} - T_{m2}}{T_{b1} - T_{b2}} \qquad (108)$$

In equation (108), TPC is the temperature polarization coefficient [-], T_{m1} is the temperature at the feed/membrane interface [K], T_{m2} is the temperature at the permeate/membrane interface [K], $T_{b1}$is the temperature of the bulk feed [K], and T_{b2} is the temperature of bulk permeate [K]. Martenez-Diez report TPC between 0.4 and 0.6, i.e. significantly less than found by Alsaadi et al. [29, 107] Unfortunately, Martenez-Diez does not report values for T_{m1} and T_{m2}, however they state that the transmembrane driving force is reduced as much as 65% from (bulk feed vapor pressure – permeate vapor pressure). [29] The large amount of temperature polarization that can occur in DCMD can be reversed by incorporating nanoparticles into the membrane and applying a suitable solar light source. As shown in Figure 42, in Dongare et al. the temperature at the feed/membrane interface was higher, not lower, than the bulk feed temperature (20°C). Flux improvement was achieved by the photothermal heating of the feed, as discussed below. [30]

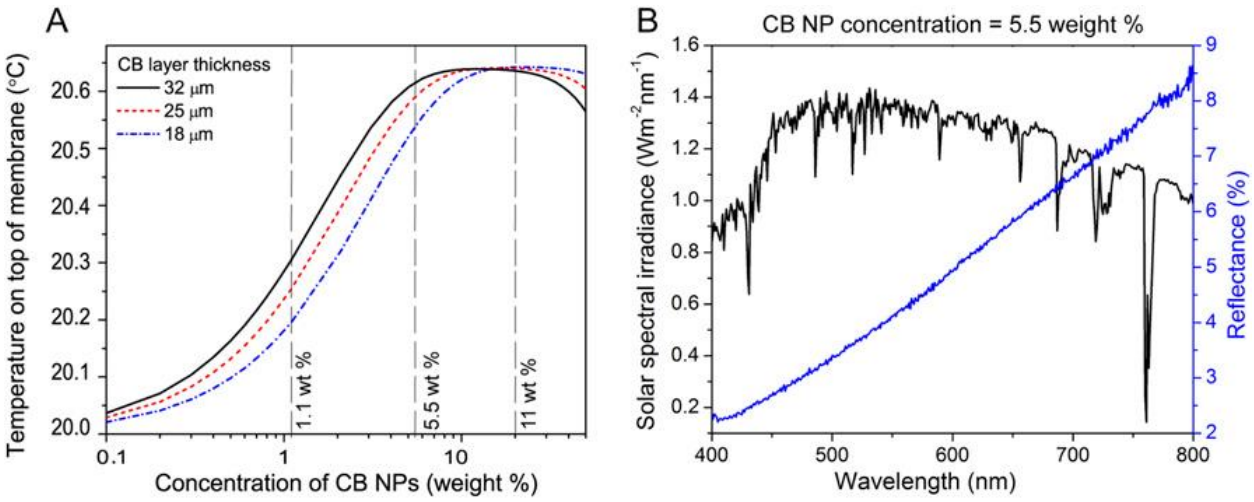

Figure 42: Reversal of Temperature Polarization (A), Solar spectral irradiance and Relflectance vs Wavelength (B)[30]

3.2 The Nanophotonic Photothermal Effect in MD and Pervaporation

Carbon black and noble metal nanoparticles can produce a photothermal effect. Gold nanoparticles exhibit plasmonic resonance. Jiang et al. document absorption peaks between 500 and 900 nm, depending on the size and configuration of the gold nanoparticle. [108] Jiang et al. and Dongare et al. describe the light absorbance of carbon black as broadband (i.e., no peaks) between about 400 and 900 nm. [30, 108] Jiang et al. and Chen et al. also discuss the photothermal conversion efficiency, which is based on an energy balance conducted on noble nanoparticles while under illumination. [108, 109] However, it is not necessary to apply to membrane nanophotonics to quantify photothermal conversion efficiency. For example, Dongare et al. used a Monte Carlo photon transport method, taking into consideration light scattering and absorption, to help arrive at the optimal CB concentration for photothermal DCMD. [30]

Li et al. published a study in 2013 on incorporating silver nanoparticles in polydimethylsiloxane (PDMS) membranes to improve pervaporative ethanol (a VOC) separation from water using a 5 percent weight (wt%) ethanol feed. Silver nanoparticles were included into a thin PDMS membrane by an *in situ* method which was then layered onto a poly vinylidene fluoride (PVDF) support. The silver nanoparticles were found to have an absorption peak at about 400 nm, and a 400 nm light-emitting diode (LED) light at an intensity up to 920 Watts per square meter (Wm^{-2}) was used for their experiments. Details of the pervaporation setup did not include the pervaporation cell dimensions or feed flow rate—except to indicate that the membrane had a surface area of 120 square centimeters (cm^2). Results included improved flux and selectivity for the membranes, incorporating silver nanoparticles under irradiation compared to the same membranes

with the light off. Li et al. did not include any measurement or modeling of the temperature profile within the membrane and boundary layer, although a diagram with a proposed mechanism showed the reversal of temperature polarization when the nanophotonic photothermal effect was in place. [110]

Dongare et al. used a membrane comprised of a thin (25 micron) carbon black coated porous polyvinyl alcohol (PVA) layer, coated onto a PVDF support. A 1% NaCl feed was used with a feed flow rate of 0.54 cubic centimeters per second (cm s^{-1}). This study of DCMD also had a permeate flow rate of 4.34 cm s^{-1}. The cell dimensions were 3.46x8.10x0.15 centimeters (cm). A 1 millimeter (mm)-thick quart plate was used to cover the feed channel. Tests were conducted in Houston, Texas, where the ambient solar intensity was 700 Wm^{-2}. Experiments were conducted with unfocused light and at 25x magnification. The fluxes were separated into the contributions from localized photothermal heating, the flux due to the experimental temperature difference between the bulk feed and distillate streams, and the flux due to residual heating of the system upon illumination. According to Figure S4 in Dongare et al., the flux of the illuminated membrane was about 0.6 kg m^{-2} h^{-1} after 10 minutes, about twice that of the unilluminated membrane under the same conditions. (These fluxes are low compared with those usually reported for conventional DCMD due to the small temperature difference between the feed and permeate, about 3-5 ℃). [30]

Dongare et al. included an estimate of the energy efficiency of nanophotonic-enabled solar membrane distillation (NESMD). The measurement was based on the amount of distillate produced, and the enthalpy of vaporization, compared with the incident solar power. Dongare et al. (2017) reported an efficiency of 21.45 % for the

unfocused condition and 21% for the focused condition. A simulation showed that for the unfocused condition, the temperature at the feed/membrane interface was about 1 ℃ higher than the bulk feed. [30]

However, additional simulations, unpublished, reported at the recent Industrial Practitioners Advisory Board (IPAB) meeting by the Dongare et al. 2017 showed about a 75 ℃ local difference when 10x magnifying lenses were used. Significant findings included: [111]

1) NESMD was more efficient at lower feed velocities (opposite to conventional DCMD)

2) The average distillate flux increased with the length and width of the module (opposite to conventional DCMD)

3) The solar energy efficiency of NESMD improved with increased ambient temperature [111]

Politano et al. conducted a study of photothermal VMD for seawater desalination. They used silver nanoparticles (NPs) incorporated into a microporous poly vinylidene fluoride (PFDF) membrane. The maximum absorbance for silver nanoparticles (NP) is at about 420 nm. For this study, an ultraviolet (UV) lamp with an emission wavelength of 365 nm and an intensity (at the distance from the VMD cell) of 23,000 Watts per square meter (Wm^{-2}) was used. The feed was either pure water or 0.5 M NaCl. The feed volumetric flow was 5.5 $cm^3 s^{-1}$. The membrane surface area was 21.21 cm^2. The initial

feed temperature was 303 K. For the purpose of calculating the temperature at the feed/membrane interface, T_m, two equations were used. is the energy balance: [112]

$$q_r + q_p = q_v + \left(q_{f,out} - q_{f,in}\right) \quad (109)$$

In equation (109) q_r is the heat flux due to irradiation from the UV lamp [W m^{-2}], q_p is the plasmonic heat flux [W m^{-2}], q_v is the heat flux required to vaporize water [W m^{-2}], and $\left(q_{f,out} - q_{f,in}\right)$ is the heat flux through the liquid feed stream [W m^{-2}].

Equation (109) is similar to that used by Favre, except a plasmonic heating term is used as shown in equation (110): [104, 112]

$$h_0(T_b - T_m) + q_p = J_w \Delta H_v \quad (110)$$

In equation (110), h_0 is the boundary layer heat transfer coefficient [W m^{-2} K^{-1}], T_b is the bulk feed temperature [K], T_m is the temperature at the feed/membrane interface [K], J_w is water flux [kg m^{-2} s^{-1}], and ΔH_v is the enthalpy of vaporization for the permeating species [J kg^{-1}].

The results include an increase in flux from 2.2 kg m^{-2} h^{-1} using an irradiated uncoated membrane to 25.7 kg m^{-2} h^{-1} using a 25% silver NP membrane. In the latter case, T_m rose to 327.3 K, about a 23 K increase above the baseline feed temperature, producing a TPC greater than 1. For unloaded PFVD membranes, the bulk feed temperature was raised about 2.5 K while for the 25% silver NP membranes the bulk feed temperature was raised about 4 K. [112]

The boundary layer temperature polarization profiles for uncoated membranes (the baseline case) and for nanophotonic particle coated membranes having a photothermal effect are shown in Figure 43. Figure 43 (a) shows the typical temperature profile for temperature polarization that occurs in MD and pervaporation on the feed side

of the membrane. Figure 43 (b) shows the temperature profile on the feed side of the membrane that results from the nanophotonic photothermal effect: the reversal of temperature polarization.

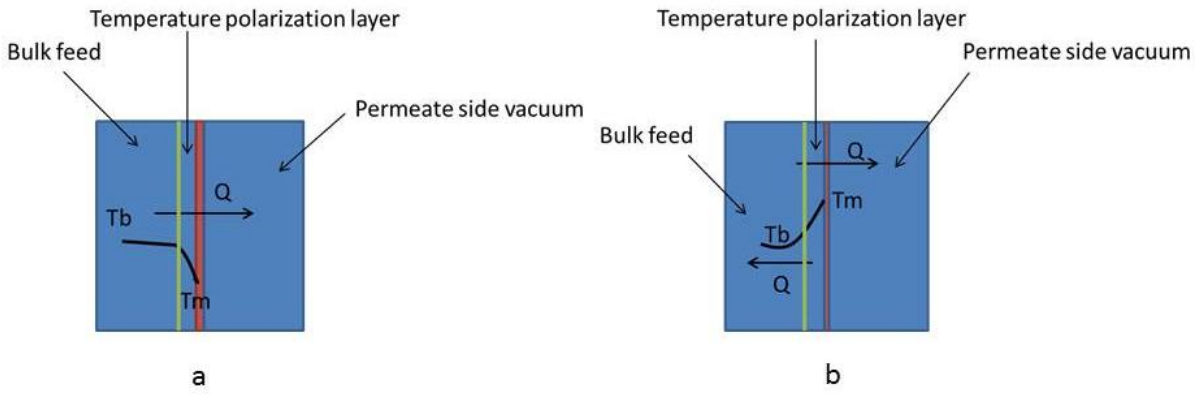

Figure 43: The boundary layer temperature profile in (a) a non-illuminated coated or uncoated membrane, and (b) an illuminated coated membrane.

3.3 Synthesizing and Testing Nanophotonic Pervaporation Membranes

The nanophotonic material we used to make nanophotonic pervaporation membranes was 350 nm carbon black, (Emperor). The synthesis technique is simple. A paste made of carbon black (1.4 g), water (0.2 g), and tetrahydrofuran (THF) (1.3 g) is painted onto the 4155-40 or 4155-80 membranes. The painted membrane is allowed to dry overnight under a vacuum hood and then is suitable for pervaporation testing. compares scanning electron microscope (SEM) for the coated and uncoated membranes. The painted and unpainted DeltaMem membranes are shown in Figure 44.

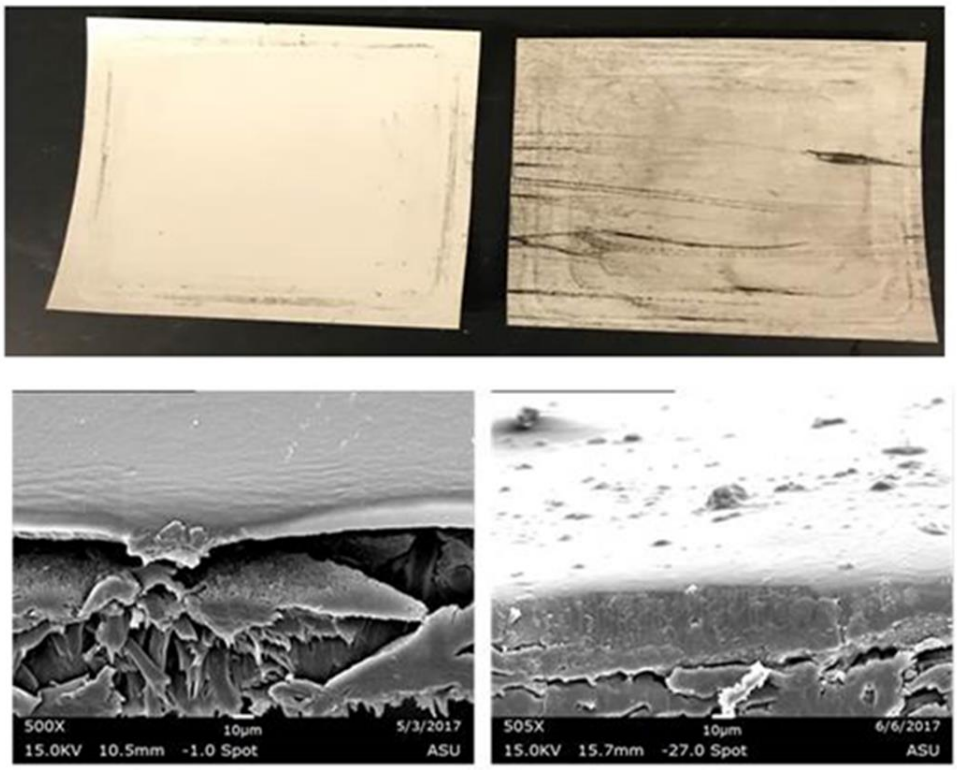

Figure 44: Uncoated (left) and CB coated (right) DeltaMem membranes as shown with SEM.

In the pervaporation experiments to test the efficacy of the nanophotonic coating, we used a solar simulator lamp (Di Star 300 W Xenon lamp). The solar light source supplied light at an intensity of approximately 3,000 Wm^{-2} (3 suns), as determined by a Thor labs PM100D - Compact Power and Energy Meter Console.

The pervaporation cell used for the experiments is shown in Figure 45.

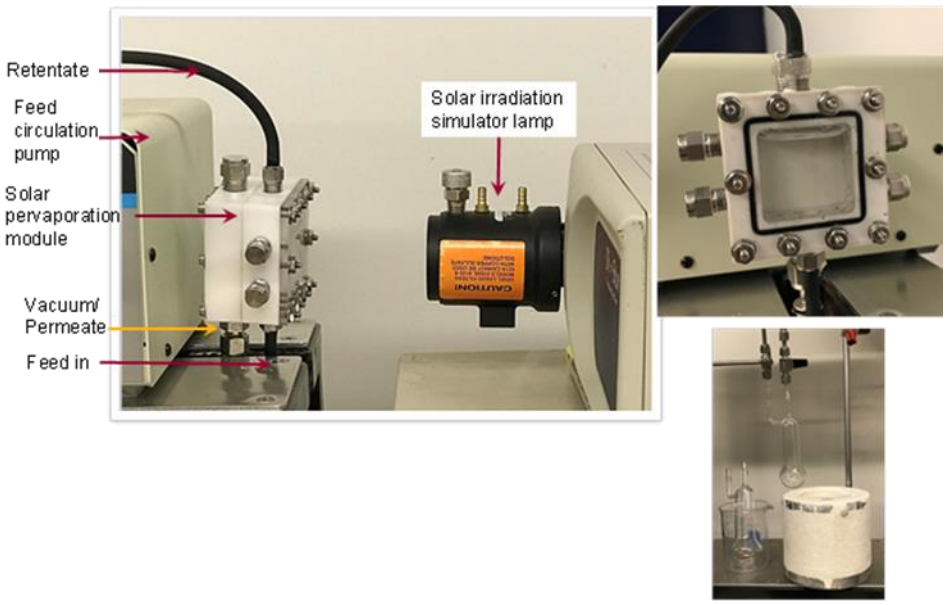

Figure 45: Pervaporation setup for solar irradiation

Four pervaporation tests were done with a 32 g L^{-1} feed at room temperature to show the flux improvement imparted by the nanophotonic (CB) layer:

1) Pervaporation with uncoated membrane, no solar light
2) Pervaporation with uncoated membrane with solar light
3) Pervaporation with coated membrane, no solar light
4) Pervaporation with coated membrane with solar light

3.4 Results of Testing Nanophotonic Enhanced Pervaporation Desalination

The results of pervaporation experiments demonstrating the efficacy of the nanophotonic (carbon black) layer applied to the commercial DeltaMem membranes are shown in Figure 46.

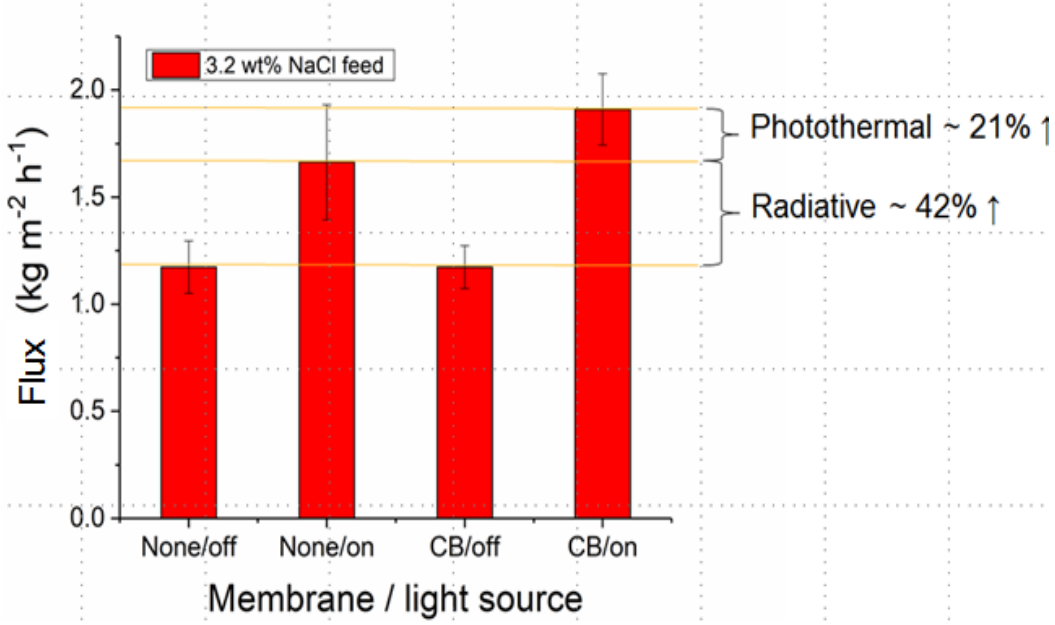

Figure 46: Pervaporation of 32 g L^{-1} NaCl feed waters.

The average result of three trials using a 32 g L^{-1} NaCl feed at room temperature is represented in Figure 46. The flux of the uncoated and carbon black coated membrane without exposure to the light source was about the same. The flux of the uncoated membrane with exposure to the light source was about 42% higher than the flux of the uncoated or coated membrane without exposure to the light source due to radiative heating of the feed by the light source. The flux of the carbon black coated membrane with exposure to the light source was about 21% higher than the flux of the uncoated membrane with exposure to the light source due to the photothermal effect and about 62% higher than the flux of the uncoated or coated membrane without exposure to the light source due to both radiative heating and the photothermal effect. All measured rejections for the membranes reported in are greater than 99.9%.

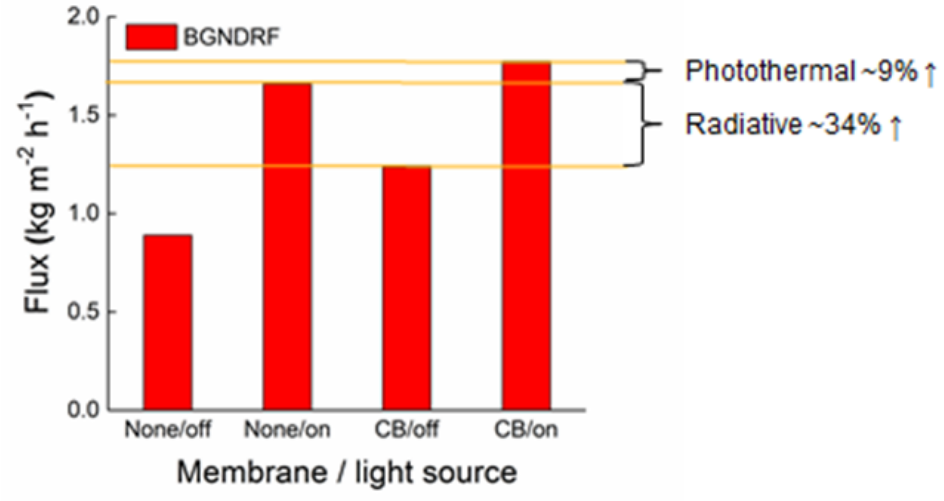

Figure 47: Pervaporation of simulated BGNDRF water (TDS 4,035 mg L^{-1}).

The result of a single trial using a simulated BGNDRF feed with a TDS of 4,035 mg L^{-1} (see) is shown in Figure 47. There is a difference between the flux of the uncoated and carbon black coated membrane without exposure to the light source. This difference is unexplained but may be mitigated by further trials. The flux of the uncoated membrane with exposure to the light source was about 34% higher than the flux of the carbon black coated membrane without exposure to the light source to radiative heating. The flux of the carbon black coated membrane with exposure to the light source was about 9% higher than the flux of the uncoated membrane with exposure to the light source due to the nanophotonic effect and about 43% higher than the carbon black coated membrane without exposure to the light source, due to both radiative heating and the photothermal effect.

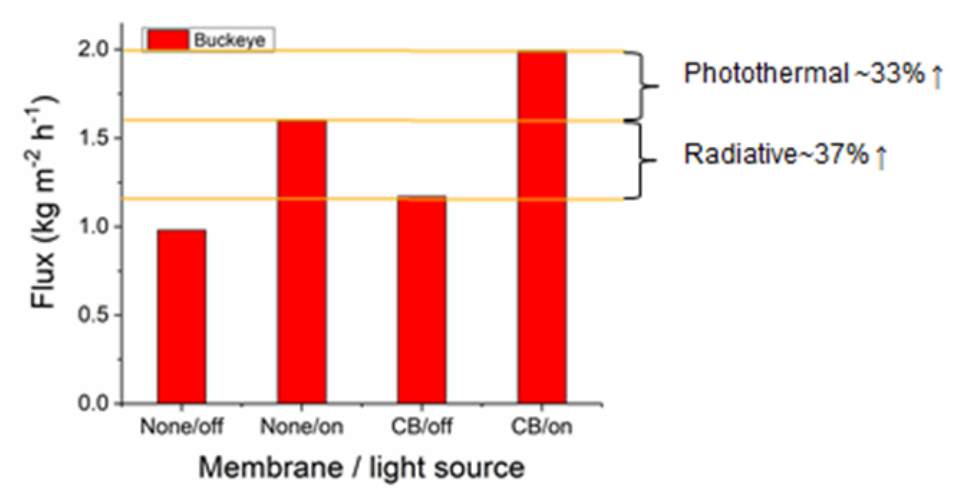

Figure 48: Pervaporation of simulated Buckeye water (TDS 1583 mg L^{-1}).

The result of a single trial using simulated Buckeye well water with a TDS of 1,583 mg L^{-1} is shown in Figure 48. The flux of the carbon black coated membrane without light exposure was about 10% higher than the flux of the uncoated membrane without light exposure. The flux of the uncoated membrane with light exposure was about 37% higher than the flux of the carbon black coated membrane without light exposure due to the radiative effect. The flux of the CB coated membrane with light exposure was about 37% higher than the flux of the uncoated membrane with light exposure due to the photothermal effect and about 70% higher than the carbon black coated membrane without light exposure due to both the radiative and photothermal effects.

The overall results show a high radiative heating effect. This is most likely due to the feed configuration. We did not use a feed reservoir. The solar cell (Figure 45) holds about 40.5 cc and the connecting tubing holds about 10 cm^3. This means than when the light source is on the feed is exposed to the light 40.5/50.5 percent of the time.

A significant photothermal effect was demonstrated in all cases. That is, a significant increase in flux beyond that obtained by irradiation of the feed was obtained by adding a nanophotonic (carbon black) layer to the membranes.

3.5 Conclusions for Chapter 3

The results suggest a significant flux enhancement by applying nanophotonic particles to pervaporation membranes. However, there is considerable overlap in the error bars in Figure 46 and no error bars, because of limited data for Figure 47 and Figure 48. The results should be regarded as preliminary but worthy of further investigation. It is difficult to compare the results obtained here for pervaporation with the results of the Dongare et al. study of DCMD due to the differences in experimental conditions. It is possible, based on the analysis of temperature polarization, that the application of nanophotonic photothermal heating will be more efficient in pervaporation than DCMD.

CHAPTER 4

THE MITIGATION OF CONCENTRATION POLARIZATION BY THE NANOPHOTONIC PHOTOTHERMAL EFFECT

The mitigation of concentration polarization is a simple theory. It is novel in that it has not been previously described.

As shown in Politano et al. and the experiments described in Chapter Three, the bulk feed is heated by the nanophotonic photothermal effect in excess of the irradiative heat supplied directly to the bulk feed by the light source. [112]

The solar cell used in the experiments described in Chapter Three is 4.5x4.5x2 cm, holding a volume of 40.5 cubic centimeters (cm^3).

The following are assumed conditions:

To start, assume pervaporation at 25 ℃ using dilute saline solution ($\rho \cong 1\ g/cm^3$) as a feed for one hour. The feed is circulated by a pump, and the volume of fluid in the tubing is negligible. The membrane is nanophotonic enhanced, and a solar source is employed. The nanophotonic heating of the membrane results in enhanced flux, and the heat also creates a boundary layer at the feed/membrane interface with a temperature of 27 ℃. The concentration polarization boundary layer thickness is 20 micrometers (μm). This assumption is the same as made by Baker (2012) in his chapter on concentration polarization (i.e., assume that the temperature polarization and concentration polarization layers have the same thickness.) This results in a boundary layer volume of 4.5x4.5x0.002 cm or 0.0405 cm^3. Assume that the temperature gradient that exists between the boundary layer and the bulk feed causes the bulk feed to rise in temperature by 1 ℃ due to convective heat transfer between the boundary layer and the

bulk feed. C_p of water is 4.1813 J g^{-1} K^{-1}. Then the enthalpy change of the bulk feed, ΔH [J], is shown in equation (127).

$$\Delta H = 4.1813 \frac{J}{gK} * 1°K * 40.5g \qquad (111)$$

(This neglects the loss of feed volume, 2-3 g, due to flux)

$$\Delta H = 169\, J$$

The heat flow to the bulk feed, Q [J s^{-1}], is:

$$Q = \frac{169\, J}{3600\, s}$$

$$Q = 0.047 \frac{J}{s}$$

The mass flow rate from the boundary layer, m [g s^{-1}] is shown in equation (112):

$$m = \frac{Q}{C_p \Delta T} \qquad (112)$$

$$m = \frac{0.047\ {}^{J}/_{s}}{4.1813\ {}^{J}/_{gK}\ 1°K}$$

$$m = 0.01125 \frac{g}{s}$$

The volumetric flow from the boundary layer, V [cm^3 s^{-1}] is:

$$V = 0.01125 \frac{cm^3}{s}$$

Therefore, the entire volume of the boundary layer is exchanged:

$$Boundary\ layer\ exchange\ rate = \frac{0.0405\ cm^3}{0.01125\ {}^{cm^3}/_{s}}$$

$$Boundary\ layer\ exchange\ rate = 3.6\ s$$

The entire boundary layer volume is exchanged by convection approximately every 3.6 seconds. This can be thought of as convectively stirring of the boundary layer. These concepts are illustrated in Figure 49.

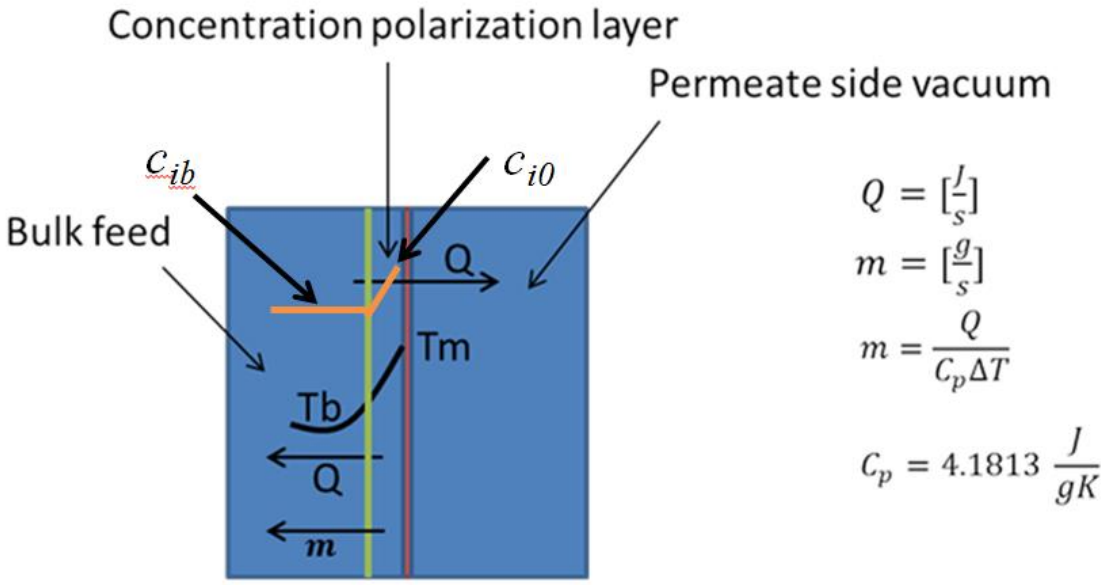

Figure 49: Reversal of temperature polarization results in heat and mass flow from the boundary layer to the bulk feed

As a result of mass flow from the boundary layer, the boundary layer is thinned as shown in Figure 50.

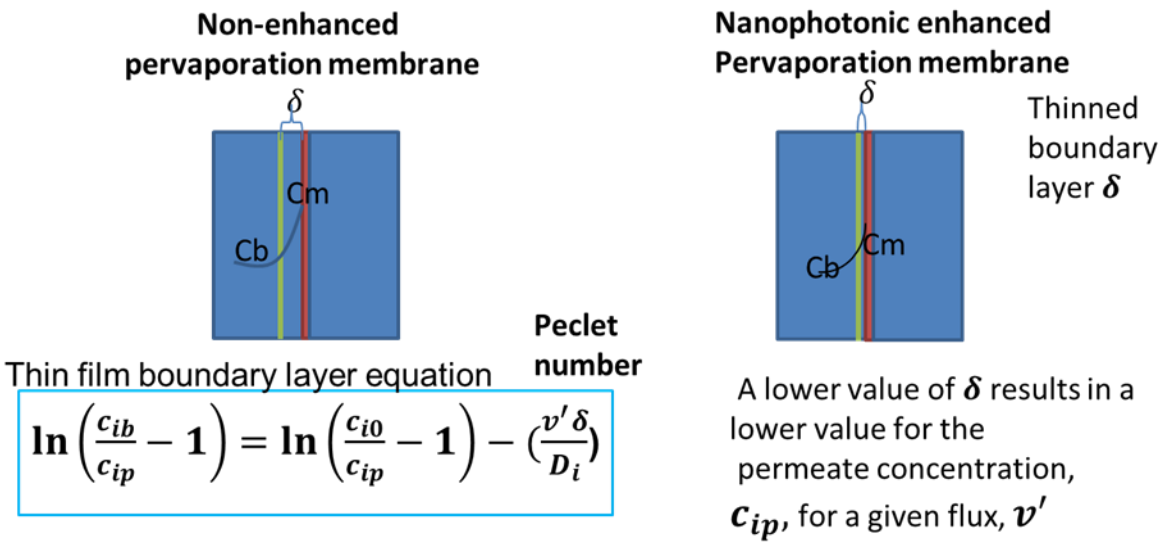

Figure 50: Thinning of the boundary layer by nanophotonic enhanced pervaporation membrane

As explained in Figure 50 a lower value of δ results in a lower value for the Peclet number, concentration polarization modulus (equation (38)), and solute permeate concentration (equation (64)) for a given flux.

If equation (64) were applicable in a pervaporation separation, desalination, organic dehydration, of VOC removal, then it would be possible to run experiments to illustrate the concentration polarization mitigation effect. Fluxes and rejections would be obtained at different feed temperatures using non-enhanced membranes. Then fluxes and rejections would be obtained with different distances of the solar source to the membrane surface using nanophotonic enhanced membranes. A hypothetical plot is presented in Figure 51. The nanophotonic enhanced membrane should have a slope closer to horizontal than the non-enhanced membrane representing a smaller value for δ.

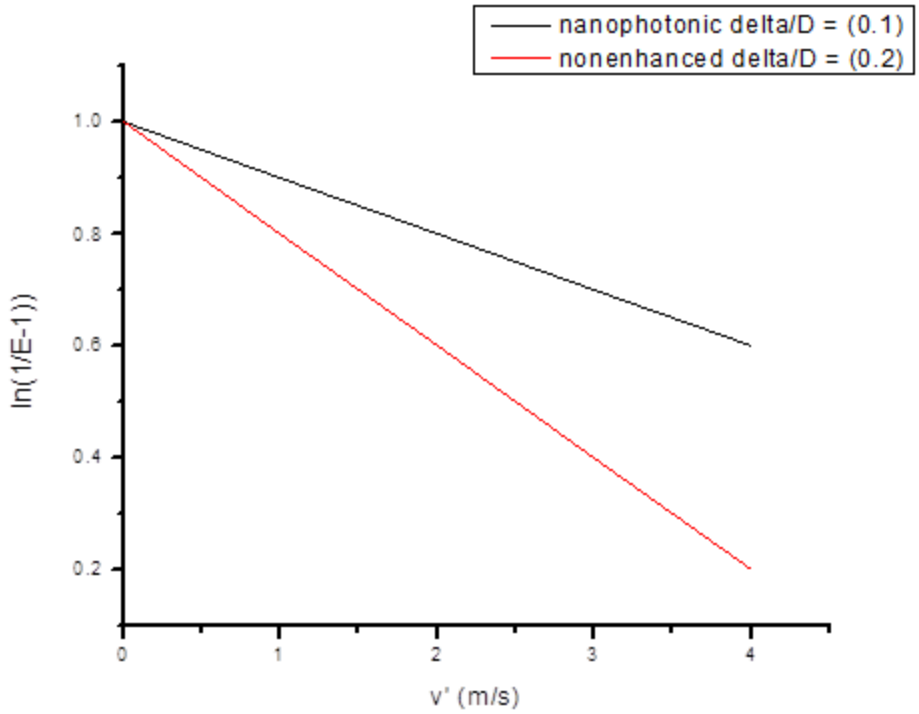

Figure 51: Hypothetical plot using equation (64) for nanophotonic enhanced and non-enhanced pervaporation membranes

In 2013 Li et al. reported the use of silver nanoparticles incorporated into a PDMS active layer to perform photothermal pervaporation VOC separation of a 5 wt% ethanol feed.[110] Li et al. reported an increase in selectivity of the membrane when under irradiation and hypothesized that the improved separation was due to the silver nanoparticles supplying extra enthalpy of vaporization to the ethanol. [110] It is also possible that the improved separation could represent the concentration polarization mitigation effect. Further experiments as described above are recommended.

Dissertation summary

Chapter 1 gave a brief description of membrane desalination and pervaporation desalination was described as occupying a niche for purification of high salinity feed waters such as RO concentrates. Transport through pervaporation membranes was discussed; the solution – diffusion model was discussed in detail. The solution – diffusion model does not provide a good description of sodium chloride transport through dense pervaporation membranes. Other transport models such as the Maxwell – Stefan model could be considered for describing sodium chloride transport through dense membranes. However the solution – diffusion model is the simplest to use and is appropriate for describing water transport. Materials for pervaporation membrane active layers were discussed, specifically the membranes used in the studies from which data extraction was performed as described in Chapter 2.

Chapter 2 gave a thorough discussion of the evaluation of concentration polarization in pervaporation desalination. The exponent of the Peclet number has been extensively used to quantify the concentration polarization modulus. The Peclet number in concentration polarization theory is the ratio of convective solute velocity to diffusive solute velocity in the boundary layer. To facilitate discussion with reference to TFBLT, fluxes were used instead of velocities; this is appropriate because volumetric flux and velocity have the same units. Semi – quantitative analysis showed that the Peclet number takes on a minimum value of 1 so that the concentration polarization modulus takes on a minimum value of 2.78 in pervaporation desalination. This conclusion represents one of the limitations of the steady state assumption underlying concentration polarization theory since the modulus may be overestimated. A second limitation is that the steady

state TFBLT and the indirect methods for obtaining the concentration polarization modulus, the RIS model, the method described by Baker, and Sherwood correlations, do not include the ability of the membrane to separate salt from water, despite the fact that the solute concentration profile in the boundary layer is a result of that separation. The underlying problem with all of the indirect methods for obtaining the concentration polarization modulus is the unavailability of direct methods to measure the concentration polarization modulus. It is suggested based on the analysis performed in Chapter 2 that the Reynolds number of the feed channels be considered when comparing the performance of pervaporation desalination membranes in different lab set-ups; higher turbulence in the feed channel will result in a lower value for the boundary layer thickness, less concentration polarization, and better membrane performance.

Chapter 3 discussed preliminary results showing flux enhancement by the nanophotonic photothermal effect in pervaporation desalination. The amount of data is limited so that further experiments are necessary to confirm the results.

Chapter 4 discussed a theory on the mitigation of concentration polarization by the nanophotonic photothermal effect. Concentration polarization is mitigated by convective stirring of the boundary layer consequent to nanophotonic heating of the membrane. Experiments were described which can confirm the theory.

REFERENCES

[[1] A. Subramani, J.G. Jacangelo, Treatment technologies for reverse osmosis concentrate volume minimization: A review, Separation and Purification Technology, 122 (2014) 472-489.

[2] C. Fritzmann, J. Löwenberg, T. Wintgens, T. Melin, State-of-the-art of reverse osmosis desalination, Desalination, 216 (2007) 1-76.

[3] Q. Wang, N. Li, B. Bolto, M. Hoang, Z. Xie, Desalination by pervaporation: A review, Desalination, 387 (2016) 46-60.

[4] B. Ashoor, S. Mansour, A. Giwa, V. Dufour, S. Hasan, Principles and applications of direct contact membrane distillation (DCMD): a comprehensive review, Desalination, 398 (2016) 222-246.

[5] W. An, X. Zhou, X. Liu, P. Chai, T. Kuznicki, S. Kuznicki, Natural zeolite clinoptilolite-phosphate composite membranes for water desalination by pervaporation, Journal of Membrane Science, 470 (2014) 431-438.

[6] M. Drobek, C. Yacou, J. Motuzas, A. Julbe, L. Ding, J.C.D. da Costa, Long term pervaporation desalination of tubular MFI zeolite membranes, Journal of Membrane Science, 415 (2012) 816-823.

[7] C.X.C. Lin, L.P. Ding, S. Smart, J.C.D. da Costa, Cobalt oxide silica membranes for desalination, Journal of colloid and interface science, 368 (2012) 70-76.

[8] A. Malekpour, A. Samadi-Maybodi, M. Sadati, Desalination of aqueous solutions by LTA and MFI zeolite membranes using pervaporation method, Brazilian Journal of Chemical Engineering, 28 (2011) 669-677.

[9] M. Naim, M. Elewa, A. El-Shafei, A. Moneer, Desalination of simulated seawater by purge-air pervaporation using an innovative fabricated membrane, Water Science and Technology, 72 (2015) 785-793.

[10] S. Burn, M. Hoang, D. Zarzo, F. Olewniak, E. Campos, B. Bolto, O. Barron, Desalination techniques—A review of the opportunities for desalination in agriculture, Desalination, 364 (2015) 2-16.

[11] E. Korngold, E. Korin, I. Ladizhensky, Water desalination by pervaporation with hollow fiber membranes, Desalination, 107 (1996) 121-129.
[12] B. Liang, W. Zhan, G. Qi, S. Lin, Q. Nan, Y. Liu, B. Cao, K. Pan, High performance graphene oxide/polyacrylonitrile composite pervaporation membranes for desalination applications, Journal of Materials Chemistry A, 3 (2015) 5140-5147.

[13] B. Liang, K. Pan, L. Li, E.P. Giannelis, B. Cao, High performance hydrophilic pervaporation composite membranes for water desalination, Desalination, 347 (2014) 199-206.

[14] M.C. Duke, J. O'Brien-Abraham, N. Milne, B. Zhu, J.Y. Lin, J.C.D. da Costa, Seawater desalination performance of MFI type membranes made by secondary growth, Separation and Purification Technology, 68 (2009) 343-350.

[15] E. Quinones-Bolanos, H. Zhou, R. Soundararajan, L. Otten, Water and solute transport in pervaporation hydrophilic membranes to reclaim contaminated water for micro-irrigation, Journal of Membrane Science, 252 (2005) 19-28.

[16] S.G. Chaudhri, B.H. Rajai, P.S. Singh, Preparation of ultra-thin poly (vinyl alcohol) membranes supported on polysulfone hollow fiber and their application for production of pure water from seawater, Desalination, 367 (2015) 272-284.

[17] C.H. Cho, K.Y. Oh, S.K. Kim, J.G. Yeo, P. Sharma, Pervaporative seawater desalination using NaA zeolite membrane: mechanisms of high water flux and high salt rejection, Journal of Membrane Science, 371 (2011) 226-238.

[18] M. Duke, S. Mee, J.D. da Costa, Performance of porous inorganic membranes in non-osmotic desalination, Water research, 41 (2007) 3998-4004.

[19] E. Huth, S. Muthu, L. Ruff, J.A. Brant, Feasibility assessment of pervaporation for desalinating high-salinity brines, Journal of Water Reuse and Desalination, 4 (2014) 109-124.

[20] S. Wijaya, M. Duke, J.D. da Costa, Carbonised template silica membranes for desalination, Desalination, 236 (2009) 291-298.

[21] Z. Xie, M. Hoang, T. Duong, D. Ng, B. Dao, S. Gray, Sol–gel derived poly (vinyl alcohol)/maleic acid/silica hybrid membrane for desalination by pervaporation, Journal of Membrane Science, 383 (2011) 96-103.

[22] P.S. Singh, S.G. Chaudhri, A.M. Kansara, W. Schwieger, T. Selvam, S. Reuss, V.K. Aswal, Cetyltrimethylammonium bromide–silica membrane for seawater desalination through pervaporation, Bulletin of Materials Science, 38 (2015) 565-572.

[23] Y.P. Kuznetsov, E. Kruchinina, Y.G. Baklagina, A. Khripunov, O. Tulupova, Deep desalination of water by evaporation through polymeric membranes, Russian Journal of Applied Chemistry, 80 (2007) 790-798.

[24] A. Subramani, J.G. Jacangelo, Emerging desalination technologies for water treatment: a critical review, Water research, 75 (2015) 164-187.

[25] R.W. Baker, Membrane technology and applications, John Wiley & Sons, 2012.

[26] J.S. Rowlinson, F. Swinton, Liquids and liquid mixtures: Butterworths monographs in chemistry, Butterworth-Heinemann, 2013.

[27] A. Criscuoli, M.C. Carnevale, E. Drioli, Evaluation of energy requirements in membrane distillation, Chemical Engineering and Processing: Process Intensification, 47 (2008) 1098-1105.

[28] A. Alkhudhiri, N. Darwish, N. Hilal, Membrane distillation: a comprehensive review, Desalination, 287 (2012) 2-18.

[29] L. Martínez-Díez, M.I. Vazquez-Gonzalez, Temperature and concentration polarization in membrane distillation of aqueous salt solutions, Journal of Membrane Science, 156 (1999) 265-273.

[30] P.D. Dongare, A. Alabastri, S. Pedersen, K.R. Zodrow, N.J. Hogan, O. Neumann, J. Wu, T. Wang, A. Deshmukh, M. Elimelech, Nanophotonics-enabled solar membrane distillation for off-grid water purification, Proceedings of the National Academy of Sciences, 114 (2017) 6936-6941.

[31] H. Zwijnenberg, G. Koops, M. Wessling, Solar driven membrane pervaporation for desalination processes, Journal of Membrane Science, 250 (2005) 235-246.

[32] P.A. Kober, PERVAPORATION, PERSTILLATION AND PERCRYSTALLIZATION, Journal of the American Chemical Society, 39 (1917) 944-948.

[33] D. Fedosov, A. Smirnov, E. Knyazeva, I. Ivanova, Zeolite membranes: synthesis, properties, and application, Petroleum Chemistry, 51 (2011) 657-667.

[34] M. Pina, R. Mallada, M. Arruebo, M. Urbiztondo, N. Navascués, O. De La Iglesia, J. Santamaria, Zeolite films and membranes. Emerging applications, Microporous and mesoporous materials, 144 (2011) 19-27.

[35] A. Khalid, M. Aslam, M.A. Qyyum, A. Faisal, A.L. Khan, F. Ahmed, M. Lee, J. Kim, N. Jang, I.S. Chang, Membrane separation processes for dehydration of bioethanol from fermentation broths: Recent developments, challenges, and prospects, Renewable and Sustainable Energy Reviews, 105 (2019) 427-443.

[36] J.G. Wijmans, R.W. Baker, The solution-diffusion model: a review, Journal of Membrane Science, 107 (1995) 1-21.

[37] J. Wijmans, R. Baker, A simple predictive treatment of the permeation process in pervaporation, Journal of Membrane Science, 79 (1993) 101-113.

[38] D.F. Sanders, Z.P. Smith, R. Guo, L.M. Robeson, J.E. McGrath, D.R. Paul, B.D. Freeman, Energy-efficient polymeric gas separation membranes for a sustainable future: A review, Polymer, 54 (2013) 4729-4761.

[39] J. Smith, Van ness, HC; Abbott, MW Introduction to Chemical Engineering Thermodynamics, McGraw-Hill, Boston, 329 (2001) 354.

[40] S. Bhattacharya, S.-T. Hwang, Concentration polarization, separation factor, and Peclet number in membrane processes, Journal of Membrane Science, 132 (1997) 73-90.

[41] D.D.B. www.ddbst.com, in, 2019.

[42] S. Mann, Modeling and Analysis on Pervaporation Separation of Composite Zeolite Membranes, Arizona State University, 2014.

[43] E. McLeary, J. Jansen, F. Kapteijn, Zeolite based films, membranes and membrane reactors: Progress and prospects, Microporous and mesoporous materials, 90 (2006) 198-220.

[44] L. Hesse, J. Mićović, P. Schmidt, A. Górak, G. Sadowski, Modelling of organic-solvent flux through a polyimide membrane, Journal of Membrane Science, 428 (2013) 554-561.

[45] F. Shokrian, K. Solaimani, G. Nematzadeh, P. Biparva, Removal of Nacl from aqueous solutions by using clinoptilolite, (2015).

[46] A. Costa-Corredor, Z. Pakowski, T. Lenczewski, P. Gou, Simulation of simultaneous water and salt diffusion in dry fermented sausages by the Stefan–Maxwell equation, Journal of Food Engineering, 97 (2010) 311-318.

[47] U. Beuscher, C.H. Gooding, The permeation of binary gas mixtures through support structures of composite membranes, Journal of Membrane Science, 150 (1998) 57-73.

[48] F. De Bruijn, L. Sun, Ž. Olujić, P. Jansens, F. Kapteijn, Influence of the support layer on the flux limitation in pervaporation, Journal of Membrane Science, 223 (2003) 141-156.

[49] L. Shan, J. Shao, Z. Wang, Y. Yan, Preparation of zeolite MFI membranes on alumina hollow fibers with high flux for pervaporation, Journal of Membrane Science, 378 (2011) 319-329.

[50] X. Lin, H. Kita, K.-i. Okamoto, Silicalite membrane preparation, characterization, and separation performance, Industrial & engineering chemistry research, 40 (2001) 4069-4078.

[51] V.A. Tuan, S. Li, J.L. Falconer, R.D. Noble, Separating organics from water by pervaporation with isomorphously-substituted MFI zeolite membranes, Journal of Membrane Science, 196 (2002) 111-123.

[52] R.W. van Gemert, F.P. Cuperus, Newly developed ceramic membranes for dehydration and separation of organic mixtures by pervaporation, Journal of Membrane Science, 105 (1995) 287-291.

[53] W.-J. Chen, C.R. Martin, Highly methanol-selective membranes for the pervaporation separation of methyl t-butyl ether/methanol mixtures, Journal of Membrane Science, 104 (1995) 101-108.

[54] B.N. Nair, K. Keizer, H. Suematsu, Y. Suma, N. Kaneko, S. Ono, T. Okubo, S.-I. Nakao, Synthesis of gas and vapor molecular sieving silica membranes and analysis of pore size and connectivity, Langmuir, 16 (2000) 4558-4562.

[55] M. Asaeda, J. Yang, Y. Sakou, Porous silica-zirconia (50%) membranes for pervaporation of iso-propyl alcohol (IPA)/water mixtures, Journal of chemical Engineering of Japan, 35 (2002) 365-371.

[56] T. Sano, M. Hasegawa, Y. Kawakami, H. Yanagishita, Separation of methanolrmmethyl-tert-butyl ether mixture by pervaporation using silicalite membrane, Journal of Membrane Science, 107 (1995) 193-196.

[57] C.J. Gump, X. Lin, J.L. Falconer, R.D. Noble, Experimental configuration and adsorption effects on the permeation of C4 isomers through ZSM-5 zeolite membranes, Journal of Membrane Science, 173 (2000) 35-52.

[58] M. Koukou, N. Papayannakos, N. Markatos, M. Bracht, H. Van Veen, A. Roskam, Performance of ceramic membranes at elevated pressure and temperature: effect of non-ideal flow conditions in a pilot scale membrane separator, Journal of Membrane Science, 155 (1999) 241-259.

[59] H. Van Veen, Y. Van Delft, C. Engelen, P. Pex, Dewatering of organics by pervaporation with silica membranes, Separation and Purification Technology, 22 (2001) 361-366.

[60] C.M. Braunbarth, L.C. Boudreau, M. Tsapatsis, Synthesis of ETS-4/TiO2 composite membranes and their pervaporation performance, Journal of Membrane Science, 174 (2000) 31-42.

[61] Y. Morigami, M. Kondo, J. Abe, H. Kita, K. Okamoto, The first large-scale pervaporation plant using tubular-type module with zeolite NaA membrane, Separation and Purification Technology, 25 (2001) 251-260.

[62] M. Kondo, M. Komori, H. Kita, K.-i. Okamoto, Tubular-type pervaporation module with zeolite NaA membrane, Journal of Membrane Science, 133 (1997) 133-141.

[63] K.-i. Okamoto, H. Kita, K. Horii, K.T. Kondo, Zeolite NaA membrane: preparation, single-gas permeation, and pervaporation and vapor permeation of water/organic liquid mixtures, Industrial & engineering chemistry research, 40 (2001) 163-175.

[64] A. Verkerk, P. Van Male, M. Vorstman, J. Keurentjes, Description of dehydration performance of amorphous silica pervaporation membranes, Journal of Membrane Science, 193 (2001) 227-238.

[65] P. Kölsch, M. Sziladi, M. Noack, J. Caro, L. Kotsis, I. Kotsis, I. Sieber, Ceramic membranes for water separation from organic solvents, Chemical engineering & technology, 25 (2002) 357-363.

[66] S. Li, V.A. Tuan, R.D. Noble, J.L. Falconer, Pervaporation of water/THF mixtures using zeolite membranes, Industrial & engineering chemistry research, 40 (2001) 4577-4585.

[67] C. Dawson, Zeolites: structural properties and benchmarks of feasibility, Arizona State University, 2013.

[68] I.z.a. http://www.iza-structure.org/databases/, International zeolite association, in.

[69] Y. Lin, I. Kumakiri, B. Nair, H. Alsyouri, Microporous inorganic membranes, Separation and Purification Methods, 31 (2002) 229-379.

[70] C.J. Brinker, G.W. Scherer, Sol-gel science: the physics and chemistry of sol-gel processing, Academic press, 2013.

[71] L.M. Vane, membrane materials for the removal of water from industrial solvents by pervaporation and vapor permeation, Journal of Chemical Technology & Biotechnology, 94 (2019) 343-365.

[72] D. Wong, J. Parasrampuria, Polyvinyl alcohol, in: Analytical profiles of drug substances and excipients, Elsevier, 1996, pp. 397-441.

[73] X. Ma, C. Hu, R. Guo, X. Fang, H. Wu, Z. Jiang, HZSM5-filled cellulose acetate membranes for pervaporation separation of methanol/MTBE mixtures, Separation and Purification Technology, 59 (2008) 34-42.

[74] J.G. Villaluenga, M. Khayet, P. Godino, B. Seoane, J. Mengual, Analysis of the membrane thickness effect on the pervaporation separation of methanol/methyl tertiary butyl ether mixtures, Separation and Purification Technology, 47 (2005) 80-87.

[75] L. Li, J. Hou, Y. Ye, J. Mansouri, V. Chen, Composite PVA/PVDF pervaporation membrane for concentrated brine desalination: Salt rejection, membrane fouling and defect control, Desalination, 422 (2017) 49-58.

[76] L. Li, J. Hou, Y. Ye, J. Mansouri, Y. Zhang, V. Chen, Suppressing salt transport through composite pervaporation membranes for brine desalination, Applied Sciences, 7 (2017) 856.

[77] Q. Wang, Y. Lu, N. Li, Preparation, characterization and performance of sulfonated poly (styrene-ethylene/butylene-styrene) block copolymer membranes for water desalination by pervaporation, Desalination, 390 (2016) 33-46.

[78] D. Wu, A. Gao, H. Zhao, X. Feng, Pervaporative desalination of high-salinity water, Chemical Engineering Research and Design, 136 (2018) 154-164.

[79] J. Wijmans, A. Athayde, R. Daniels, J. Ly, H. Kamaruddin, I. Pinnau, The role of boundary layers in the removal of volatile organic compounds from water by pervaporation, Journal of Membrane Science, 109 (1996) 135-146.

[80] Y. Winograd, A. Solan, M. Toren, Mass transfer in narrow channels in the presence of turbulence promoters, Desalination, 13 (1973) 171-186.

[81] E. Matthiasson, B. Sivik, Concentration polarization and fouling, Desalination, 35 (1980) 59-103.

[82] P. Cote, Mass transfer limitations in pervaporation for water and waste water treatment, in: Proceeding of Third International Conference on Pervaporation Processes, 1988, pp. 449-462.

[83] J.C. Crittenden, R.R. Trussell, D.W. Hand, K.J. Howe, G. Tchobanoglous, MWH's water treatment: principles and design, John Wiley & Sons, 2012
.
[84] B.J. Marinas, R.I. Urama, Modeling concentration-polarization in reverse osmosis spiral-wound elements, Journal of environmental engineering, 122 (1996) 292-298.

[85] B. Raghunath, Effect of boundary layer mass transfer resistance in the pervaporation of organic solutes from dilute aqueous solutions, (1993).

[86] B. Raghunath, S.-T. Hwang, Effect of boundary layer mass transfer resistance in the pervaporation of dilute organics, Journal of Membrane Science, 65 (1992) 147-161.

[87] M. She, S.-T. Hwang, Effects of concentration, temperature, and coupling on pervaporation of dilute flavor organics, Journal of Membrane Science, 271 (2006) 16-28.

[88] M. She, S.-T. Hwang, Concentration of dilute flavor compounds by pervaporation: permeate pressure effect and boundary layer resistance modeling, Journal of Membrane Science, 236 (2004) 193-202.

[89] A. Ali, F. Macedonio, E. Drioli, S. Aljlil, O. Alharbi, Experimental and theoretical evaluation of temperature polarization phenomenon in direct contact membrane distillation, Chemical Engineering Research and Design, 91 (2013) 1966-1977.

[90] E. Jang, S.-H. Nam, T.-M. Hwang, S. Lee, Y. Choi, Effect of operating parameters on temperature and concentration polarization in vacuum membrane distillation process, Desalination and Water Treatment, 54 (2015) 871-880.

[91] P.L.T. Brian, Concentration polar zation in reverse osmosis desalination with variable flux and incomplete salt rejection, Industrial & Engineering Chemistry Fundamentals, 4 (1965) 439-445.

[92] T. Sherwood, P. Brian, R. Fisher, Desalination by reverse osmosis, Industrial & Engineering Chemistry Fundamentals, 6 (1967) 2-12.

[93] M. Khayet, Membranes and theoretical modeling of membrane distillation: a review, Advances in colloid and interface science, 164 (2011) 56-88.

[94] L. Martinez, J.M. Rodriguez-Maroto, Membrane thickness reduction effects on direct contact membrane distillation performance, Journal of Membrane Science, 312 (2008) 143-156.

[95] K.W. Lawson, D.R. Lloyd, Membrane distillation. I. Module design and performance evaluation using vacuum membrane distillation, Journal of Membrane Science, 120 (1996) 111-121.

[96] K.W. Lawson, D.R. Lloyd, Membrane distillation, Journal of Membrane Science, 124 (1997) 1-25.

[97] T.K. Sherwood, R.L. Pigford, C.R. Wilke, Mass transfer, McGraw-Hill, 1975.

[98] V. Gekas, B. Hallström, Mass transfer in the membrane concentration polarization layer under turbulent cross flow: I. Critical literature review and adaptation of existing sherwood correlations to membrane operations, Journal of Membrane Science, 30 (1987) 153-170.

[99] R. Baker, J. Wijmans, A. Athayde, R. Daniels, J. Ly, M. Le, The effect of concentration polarization on the separation of volatile organic compounds from water by pervaporation, Journal of Membrane Science, 137 (1997) 159-172.

[100] E.A. Fouad, X. Feng, Use of pervaporation to separate butanol from dilute aqueous solutions: Effects of operating conditions and concentration polarization, Journal of Membrane Science, 323 (2008) 428-435.

[101] P. Gómez, R. Aldaco, R. Ibáñez, I. Ortiz, Modeling of pervaporation processes controlled by concentration polarization, Computers & Chemical Engineering, 31 (2007) 1326-1335.

[102] M.D.F. Rivers, Computational Modeling and Experimentation of Pervaporation Membrane Processes for Brackish Water Recovery, in: Chemical Engineering, Arizona State University, Tempe, AZ, 2018, pp. 18.

[103] O. Miyawaki, A. Saito, T. Matsuo, K. Nakamura, Activity and activity coefficient of water in aqueous solutions and their relationships with solution structure parameters, Bioscience, biotechnology, and biochemistry, 61 (1997) 466-469.

[104] E. Favre, Temperature polarization in pervaporation, Desalination, 154 (2003) 129-138.

[105] H.O. Karlsson, G. Trägårdh, Heat transfer in pervaporation, Journal of Membrane Science, 119 (1996) 295-306.

[106] J. Kuhn, R. Stemmer, F. Kapteijn, S. Kjelstrup, J. Gross, A non-equilibrium thermodynamics approach to model mass and heat transport for water pervaporation through a zeolite membrane, Journal of Membrane Science, 330 (2009) 388-398.

[107] A.S. Alsaadi, L. Francis, G.L. Amy, N. Ghaffour, Experimental and theoretical analyses of temperature polarization effect in vacuum membrane distillation, Journal of Membrane Science, 471 (2014) 138-148.

[108] R. Jiang, S. Cheng, L. Shao, Q. Ruan, J. Wang, Mass-based photothermal comparison among gold nanocrystals, PbS nanocrystals, organic dyes, and carbon black, The Journal of Physical Chemistry C, 117 (2013) 8909-8915.

[109] H. Chen, L. Shao, T. Ming, Z. Sun, C. Zhao, B. Yang, J. Wang, Understanding the photothermal conversion efficiency of gold nanocrystals, Small, 6 (2010) 2272-2280.

[110] Y. Li, T. Verbiest, R. Strobbe, I.F. Vankelecom, Improving the performance of pervaporation membranes via localized heating through incorporation of silver nanoparticles, Journal of Materials Chemistry A, 1 (2013) 15031-15038.

[111] A.A. Dongare P.D., S. Pedersen, et al. , Nanophotonic DCMD, in, El Paso, 2017.

[112] A. Politano, P. Argurio, G. Di Profio, V. Sanna, A. Cupolillo, S. Chakraborty, H.A. Arafat, E. Curcio, Photothermal membrane distillation for seawater desalination, Advanced Materials, 29 (2017) 1603504.